DLR
Deutsches Zentrum
für Luft- und Raumfahrt
German Aerospace Center

SFERA II

Work package 11, task 1

Calibration Procedures for Rotating Shadowband Irradiometers

Deliverable 11.5, public report

DLR, CIEMAT

Wilko Jessen, Stefan Wilbert, Luis Zarzalejo Tirado, Lourdes Ramirez Santigosa, Rita Valenzuela Balderrama, José Liria, Bijan Nouri, Natalie Hanrieder

Contents

Abbreviations

Term	Description
CIEMAT	Centro de Investigaciones Energéticas, Medioambientales y Tecnológicas
CL	calibration limits
CSP	Concentrated Solar Power
DLR	German Aerospace Center (Deutsches Zentrum für Luft- und Raumfahrt e.V.)
DLR-VigKing	DLR calibration method corresponding to functional corrections by King, Myers, Augustyn and Vignola
DLR2008	DLR calibration method corresponding to functional corrections by [Geuder et al., 2008]
IQR	interquartile range
Kern	RSI calibration method described in [Kern, 2010]
MAM	moving average method
PSA	Plataforma Solar de Almería
Q1	0.25-quantile (lower quartile)
Q2	0.5-quantile (median)
Q3	0.75-quantile (upper quartile)
RMSD	root mean square deviation
RSI	Rotating Shadowband Irradiometer
RSP4G	Rotating Shadowband Pyrheliometer by Reichert GmbH
RSR2	Rotating Shadowband Radiometer by Irradiance Inc.
STD	standard deviation
Twin-RSI	Twin-RSI by CSP Services GmbH
WMO	World Meteorological Organization
WRR	World Radiometric Reference

Greek symbols

Symbol	Description	Units
$\alpha_{\mathrm{L,G}}$	temperature dependence of Li-200 sensor [Geuder et al., 2008]	-
$\alpha_{\mathrm{L,K}}$	temperature dependence of LI-200 sensor [King and Myers, 1997]	-
α_{Pa}	temperature dependence of pyranometer	-
$\Delta DNI_{\mathrm{cal,rel}}$	conservative estimate of calibration uncertainty	%
$\Delta DNI_{\mathrm{ref,rel}}$	relative uncertainty of reference	%
Π_{DHI}	ratio of moving average of DHI_{Ref} / DHI_{RSI} to long-term mean of DHI_{Ref} / DHI_{RSI}	%
$\Pi_{DNI,max}$	maximum of Π_{DNI}	%
Π_{DNI}	ratio of moving average of DNI_{Ref} / DNI_{RSI} to long-term mean of DNI_{Ref} / DNI_{RSI}	%
Π_{GHI}	ratio of moving average of GHI_{Ref} / GHI_{RSI} to long-term mean of GHI_{Ref} / GHI_{RSI}	%
Π	ratio of moving average to long-term mean of reference measurement / calibrated RSI measurement	%
$\Pi_{\mathrm{cal,DNI}}$	mean ratio of short-term calibrated to long-term calibrated RSI DNI	%
Π_{spec}	spectral parameter for DHI correction	-
ϑ_{amb}	ambient temperature	°C
ϑ_{op}	expected ambient temperature in field operation	°C
ϑ_{ref}	reference temperature	25°C
ϑ_{RSI}	RSI sensor temperature	°C
$\Delta Soil_{\mathrm{ph}}$	uncertainty due to pyrheliometer soiling	%

Roman symbols

Symbol	Description	Units
AMF	air mass factor	-
AM	air mass	-
AOI	angle of incidence	°
CFd	DHI calibration factor in DLR-VigKing calibration	-
CFD_{longcal}	DHI calibration factor of long-term DLR2008 calibration	-
CFD_{shortcal}	DHI calibration factor of short-term DLR2008 calibration	-
CFD	DHI calibration factor in DLR2008 calibration	-
CFg	GHI calibration factor in DLR-VigKing calibration	-
CFG_{longcal}	GHI calibration factor of long-term DLR2008 calibration	-
CFG_{shortcal}	GHI calibration factor of short-term DLR2008 calibration	-
CFG	GHI calibration factor in DLR2008 calibration	-
CFn	DNI calibration factor in DLR-VigKing calibration	-
CF_{Licor}	LI-COR calibration factor for LI-200 sensor	$\mathrm{W \cdot A^{-1} \cdot m^{-2}}$
CF_{ph}	pyrheliometer calibration factor	$\mathrm{W \cdot V^{-1} \cdot m^{-2}}$
$CF_{\text{pa,a}}$	pyranometer calibration factor of the alternating sun- and shade method [ISO 9846]	$\mathrm{W \cdot V^{-1} \cdot m^{-2}}$
$CF_{\text{pa,c}}$	pyranometer calibration factor of the continuous sun- and shade method [ISO 9846]	$\mathrm{W \cdot V^{-1} \cdot m^{-2}}$
$CF_{\text{pa,Ia}}$	pyranometer calibration factor of pyranometer calibration method using a reference pyranometer [ISO 9847]	$\mathrm{W \cdot V^{-1} \cdot m^{-2}}$
DHI_{Ref}	reference DHI	$\mathrm{W \cdot m^{-2}}$
DHI_{RSI}	functionally corrected and calibrated RSI DHI	$\mathrm{W \cdot m^{-2}}$
DHI_{cor}	RSI DHI after functional correction	$\mathrm{W \cdot m^{-2}}$
DHI_{raw}	uncorrected DHI raw data	$\mathrm{W \cdot m^{-2}}$
DHI	diffuse horizontal irradiance	$\mathrm{W \cdot m^{-2}}$
DNI_{Ref}	reference DNI	$\mathrm{W \cdot m^{-2}}$
DNI_{RSI}	functionally corrected and calibrated RSI DNI	$\mathrm{W \cdot m^{-2}}$

Symbol	Description	Units
DNI_{cor}	RSI DNI after functional correction	$\text{W} \cdot \text{m}^{-2}$
DNI_{longcal}	DNI of RSI after long-therm calibration	$\text{W} \cdot \text{m}^{-2}$
DNI_{raw}	uncorrected DHI raw data	$\text{W} \cdot \text{m}^{-2}$
DNI_{shortcal}	DNI of RSI after short-therm calibration	$\text{W} \cdot \text{m}^{-2}$
DNI	direct normal irradiance	$\text{W} \cdot \text{m}^{-2}$
$E_{dir,hor}$	direct irradiance on a horizontal surface	$\text{W} \cdot \text{m}^{-2}$
F_{A}	spectral response parameter	-
F_{B}	cosine response (incidence angle) parameter	-
F_{C}	solar elevation angle (Cat Ear) parameter	-
$F_{\alpha,\text{Pa}}$	temperature correction coefficient during pyranometer calibration	-
F_{α}	temperature parameter	-
GHI_{Ref}	reference GHI	$\text{W} \cdot \text{m}^{-2}$
GHI_{RSI}	functionally corrected and calibrated RSI GHI	$\text{W} \cdot \text{m}^{-2}$
GHI_{cor}	RSI GHI after functional correction	$\text{W} \cdot \text{m}^{-2}$
GHI_{raw}	uncorrected GHI raw data	$\text{W} \cdot \text{m}^{-2}$
GHI	global horizontal irradiance	$\text{W} \cdot \text{m}^{-2}$
i	index for measurements in a series	-
$L_{\text{R,DHI}}$	Mean value of R_{DHI} over whole long-term duration	-
$L_{\text{R,DNI}}$	Mean value of R_{DNI} over whole long-term duration	-
$L_{\text{R,GHI}}$	Mean value of R_{GHI} over whole long-term duration	-
$M_{\text{R,DHI}}$	moving average of R_{DHI}	-
$M_{\text{R,DNI}}$	moving average of R_{DNI}	-
$M_{\text{R,GHI}}$	moving average of R_{GHI}	-
R_{DNI}	ratio of reference to corrected and calibrated RSI DNI	-
m	number of measurements	-
n	number of timestamps in short-term interval	-
$R_{\text{DHI,wd}}$	ratio of reference to corrected and calibrated RSI DHI before drift correction	-
R_{DHI}	ratio of reference to corrected and calibrated RSI DHI	-
$R_{\text{DNI,wd}}$	ratio of reference to corrected and calibrated RSI DNI before drift correction	-
$R_{\text{GHI,wd}}$	ratio of reference to corrected and calibrated RSI GHI before drift correction	-

Symbol	Description	Units
R_{GHI}	ratio of reference to corrected and calibrated RSI GHI	-
SEA	solar elevation angle	°
SZA	solar zenith angle	°
$S_{\mathrm{pr,a}}$	pyranometer responsivity in alternating sun- and shade method	$\mathrm{V} \cdot \mathrm{m}^2 \cdot \mathrm{W}^{-1}$
$S_{\mathrm{pr,c}}$	pyranometer responsivity in continuous sun- and shade method	$\mathrm{V} \cdot \mathrm{m}^2 \cdot \mathrm{W}^{-1}$
T	duration of short-term interval and calibration duration	days
t_d	12:00 pm timestamp	date
t	timestamp	date/hour/min
V_{D}	DHI voltage reading of test instrument	V
V_{G}	GHI voltage reading of test instrument	V
V_{I}	DNI voltage reading of test instrument	V

Preamble

This report was prepared within the SFERA II FP7 project, work package 11 task 1. We thank Prof. Frank Vignola from the University of Oregon for his comments on the draft version of this document.

1 Introduction

Concentrated Solar Power (CSP) projects require accurate assessment and monitoring of the available direct beam resource. To this end, ground measurements on site are inexpendable. Pyrheliometers with thermopile sensors as specified in [ISO 9060] are the standard instruments for field measurements of direct beam irradiance. During long-term deployment however, their comparatively high accuracy can only be maintained if the window through which the direct beam enters the instrument is cleaned frequently [Geuder and Quaschning, 2006]. In the case of long-term solar resource assessments on site this can pose a problem in terms of logistics and maintenance costs. This is particularly relevant, if the measuring site is in a remote location.

Rotating Shadowband Irradiometers (RSI) on the other hand have a lower accuracy to start with due to systematic errors of its photodiode sensor. However, they are less affected by soiling [Geuder and Quaschning, 2006] and provide higher accuracy in long-term measuring campaigns at sites where cleaning is not possible on a daily basis. Furthermore, they are comparatively inexpensive and do not require as much additional equipment i.e. a tracking system. A solar panel is sufficient for power supply.

The systematic errors of the sensor used in RSIs are caused by cosine and temperature effects and its spectral non-uniform responsivity. A number of correction functions can be employed to reduce these errors significantly. Additionally, a thorough calibration of the sensor with application of the correction functions can further improve the quality of measurements.

The calibration procedures of thermopile pyranometers and pyrheliometers are well documented in standards such as [ISO 9059], [ISO 9846] and [ISO 9847]. Because these standards are not applicable to RSIs due to their inherent characteristics specific calibration procedures for this type of instrument were developed. This work shall discuss the differences between calibration procedures for thermopile irradiometers and RSI and aspects which can be transferred from the existing standards to RSI calibration.

Some of the existing calibration methods have been successfully employed for a number of years. However, a thorough assessment of the necessary calibration duration with multiple measurements from several instruments has not been carried out before this project. Therefore, besides the comparison of calibration methods this work examines to which extend the RSI calibration results fluctuate in dependence on the duration of the calibration measuring period and furthermore provide a basis on which to choose the most suitable duration.

2 Radiometers

2.1 General remarks on thermopile and silicon sensors

Both, thermopiles and photodiodes (silicon sensors) are commonly used in irradiometers. However, while [ISO 9060] defines the specification and classification of pyranometers and pyrheliometers with thermopile sensors, it explicitly excludes so called silicon-pyranometers (short, Si-pyranometers) due to their specific attributes. ISO working groups are discussing an update could overcome this restriction. The following will point out the differing characteristics of silicon sensors and thermopile sensors.
A thermopile is a serial circuit of thermocouples. Thermocouples are connecting points between wires from different materials which generate an electric potential upon exposure to temperature differences between one connecting point and another. The materials can be two metals such as antimony and bismuth. Combining a number of thermocouples into a thermopile increases the generated voltage signal [Pedrotti et al., 2008]. Other possible material combinations are bismuth-silver, silver-palladium and differently doped semiconductors [Naumann et al., 2014].
For measurement of solar flux by thermopiles the temperature difference between the thermocouples is induced by a black absorber surface which is exposed to solar irradiance and a thermally insulated reference [Pedrotti et al., 2008]. Usually the absorber surface is a thin layer of black metal or a semiconductor material that uniformly absorbs the full range of wavelengths in natural light. Thus, typical thermopile radiometers respond uniformly to the whole spectral range of solar irradiance as depicted in figure 2.1.

Silicon sensors on the other hand are based on the photoelectric effect only respond to a limited spectral range from 400 nm to 1100 nm (see figure 2.1) which does not cover the whole spectrum of irradiance (250 to approx. 2500 nm). Furthermore, its responsivity varies for different wavelengths. Because of the influence of the air mass (AM) on the spectral composition of the irradiance this results in significant inaccuracy during low solar elevation angles [Augustyn et al., 2004].

Nonetheless, Si-pyranometers like the LI-COR LI-200 (figure 2.2) are widely used for their lower acquisition costs, fast response time and ease of maintenance. Silicon sensors respond within microseconds [Stoffel et al., 2010]. Thermopiles usually need 1 - 5 seconds to reach 95 % of their final value. Instruments that use thermopile sensors i.e. pyranometers and pyrhe-

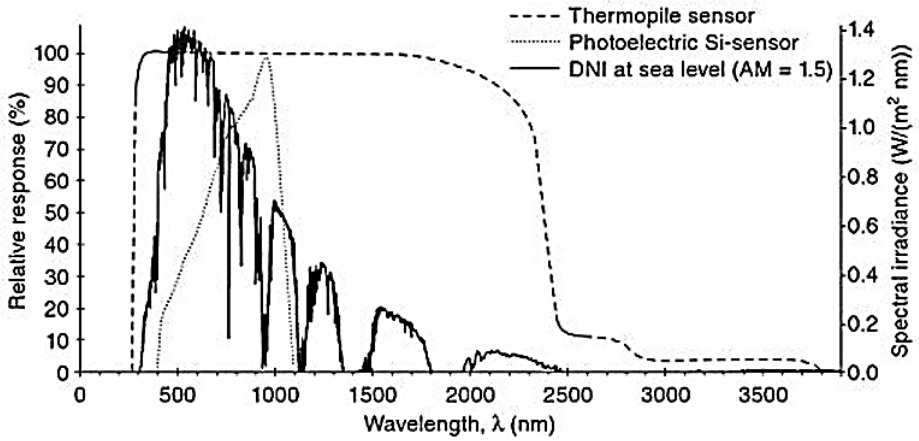

Figure 2.1: Spectral responsivity of thermopile and silicon sensors with energy density per nm wavelength of DNI at sea level. [Lovegrove and Stein, 2012]

Figure 2.2: LI-COR LI-200SA Silicon-Pyranometer [LI-COR, 2005].

liometers react strongly to soiling of their protective window or glass dome while the Li-200 with its photodiode under a diffusor lense is only slightly affected [Geuder and Quaschning, 2006]. This amounts to a tangible difference in maintenance costs and is the foremost argument for using Si-pyranometers at remote measurement sites. All LI-COR LI-200 sensors are delivered precalibrated for global horizontal irradiance (GHI) measurements with an uncertainty of 5 % (see specifications in Appendix table E.1).

2.2 Pyranometers

Pyranometers as defined in [ISO 9060] use thermopile sensors and can be classified as second standard, first class and second class for GHI measurement. Besides GHI they can also be applied for diffuse horizontal irradiance (DHI) measurements in combination with a tracked shading device such as a shadow ball or disc (see upper right in figure 2.3).
Essential for the correct operation of pyranometers is the exact horizontal alignment which can be achieved through its adjustable feet. This is most relevant for measurement of GHI due to the cosine effect of the angle of incidence (AOI) on the direct irradiance reaching the sensor. Measurements of DHI on the other hand are less affected by misalignment, since the diffuse irradiance has almost uniform intensity from all directions.

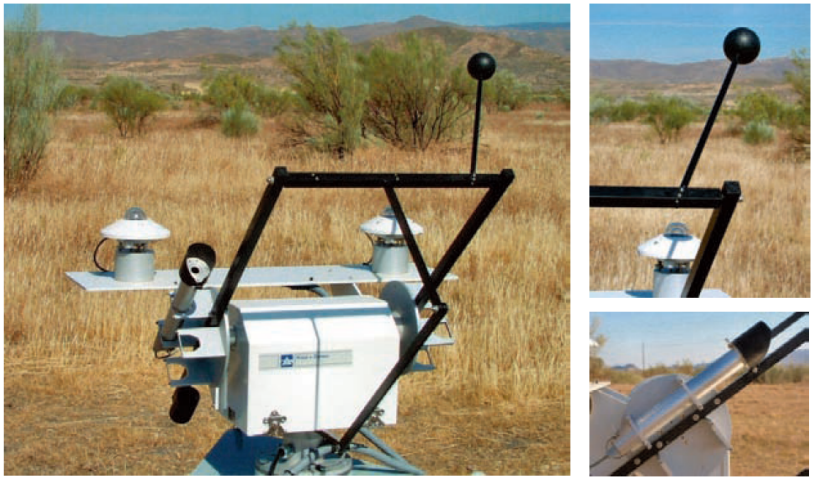

Figure 2.3: DLR reference measurement system for RSI calibration. Upper right: pyranometer with shadow ball. Lower right: pyrheliometer. [Quaschning, 2011]

Pyranometers are equipped with a double glass dome which protects the sensor from convection and usually have a build in bubble for leveling. In most models a white plastic cover (sun shield) protects the metal body from heating up and reduces reflection. Furthermore silicon granules absorb humidity which eventually enters the sealed off instrument over time. Because thermopiles are temperature dependent in their responsivity, some of the high end models incorporate temperature sensors. This allows an increased accuracy through linear temperature correction functions. Commonly used temperature sensors are thermistors and PT100. Figure 2.4 depicts the typical build of Kipp & Zonen pyranometers.

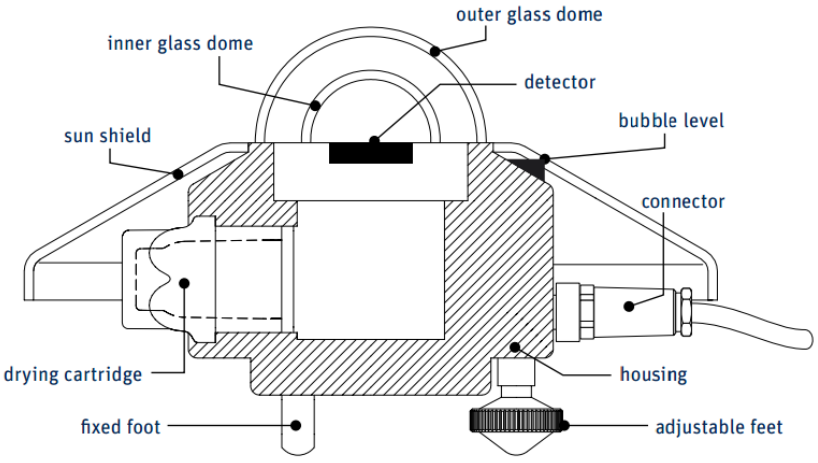

Figure 2.4: Pyranometer (here Kipp & Zonen models CMP6, CMP11, CMP21 and CMP22). [Kipp&Zonen, 2013]

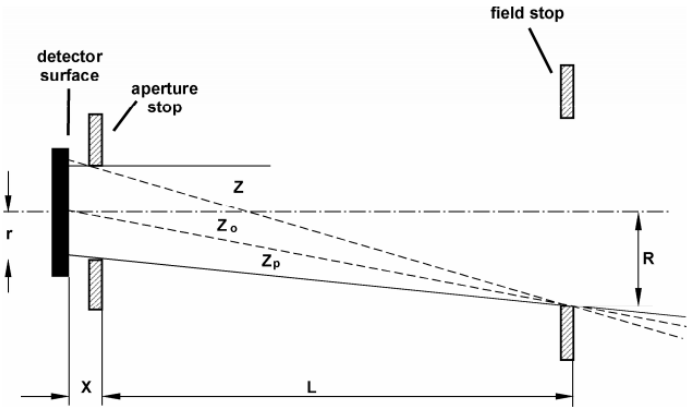

Figure 2.5: Optical construction of a pyrheliometer. [Kipp&Zonen, 2008]

2.3 Pyrheliometers

The most common pyrheliometers have thermopile sensors and are used for measurement of *DNI*. One example is the Kipp & Zonen CHP1 depicted in figures 2.3 and 2.5. Their [ISO 9060] classification goes from second standard to second class in dependence on not only the instruments individual specifications and calibration procedure but also its traceability to the World Meteorological Organization (WMO).
Pyrheliometers resemble a tube with the thermopile sensor in its back end. By this design the diffuse irradiance is shaded off while a small window at the front of the tube allows the direct beam to reach the detectors surface. Essential for its correct operation is its alignment towards the sun for which permanent tracking is required.
In the calibration of pyrheliometers an absolute cavity pyrheliometer is often used as the reference instrument. Only this variation of pyrheliometers qualifies for the highest classification as first standard [ISO 9060]. Their operational principle is not based on thermopiles. The instrument's tube is alternately exposed to and shaded from irradiance. In one common variation of absolute cavity irradiometers the measurements are taken by monitoring the electric current which is necessary to compensate the absence of heat flux from solar irradiance during the shaded phase. Further details on absolute cavity pyrheliometers can be found in [ISO 9060] and [WRC, 2001].

2.4 Rotating Shadowband Irradiometers

Manufacturers use varying names for their RSI models. Three examples of commercially available models are the Rotating Shadowband Radiometer by Irradiance Inc. (RSR2), the Rotating Shadowband Pyrheliometer by Reichert GmbH (RSP4G) and the Twin-RSI by CSP Services GmbH (Twin-RSI) (see figure 2.6) The three models were compared to the same ref-

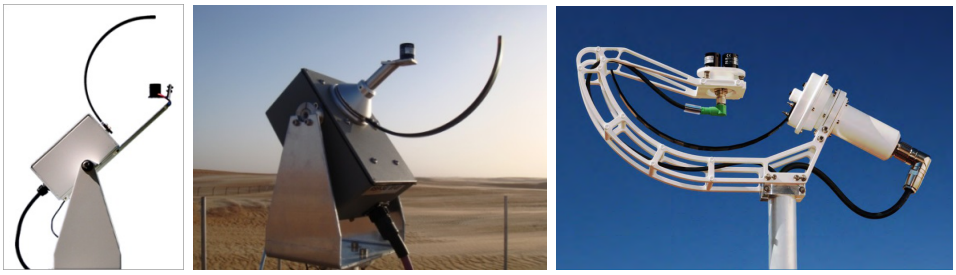

Figure 2.6: Rotating Shadowband Irradiometers. Left: RSR2, center: RSP4G, right: Twin-RSI. [Wilbert et al., 2014]

erence data set in [Vuilleumier et al., 2017]. In this work the term RSI is used to refer to the instrument type and a specific instrument of this instrument type independent of the exact model (RSR2, RSP4G and Twin-RSI).
All presently existing variations of RSI use the LI-200 sensor. This is owed primarily to its fast response which is a prerequisite for the RSI's principle of operation [Kern, 2010].
Depending on the model, a shadowband rotates about once or twice per minute around the horizontally mounted Si-pyranometer. During the shadowbands rotation the signal of the photodiode is recorded. While the sensor is unshaded, thus fully exposed, GHI measurements take place. During the instance in which the sensor is completely shaded by the shadowband, only DHI can reach the sensors surface. This results in a sudden drop of the measured value as represented by the burst in figure 2.7. The lowest value is less than the DHI because the shadowband shades off a portion of the sky and thus not only blocks direct irradiance from reaching the sensor but also a small fraction of diffuse irradiance. Therefore, shoulder values as depicted in figure 2.7 are determined for DHI measurements and its difference to the GHI is added to the minimum [Wilbert et al., 2014]. With the GHI and DHI measurements the DNI can be calculated by the sun position along equation 2.1.

$$DNI = \frac{GHI - DHI}{\cos(SZA)} \tag{2.1}$$

Besides not needing a tracking system for the determination of DNI RSI also profit from the silicon sensors advantages over thermopile irradiometers in regards to costs of acquisition and maintenance (see section 2.1). This makes it possible to leave the instrument unattended for longer periods of time than alternative instruments such as pyrheliometers.
During field deployment the measured data of the RSI is stored in one minute averages. The mode of data sampling differs among the three models in accordance to table 2.1.

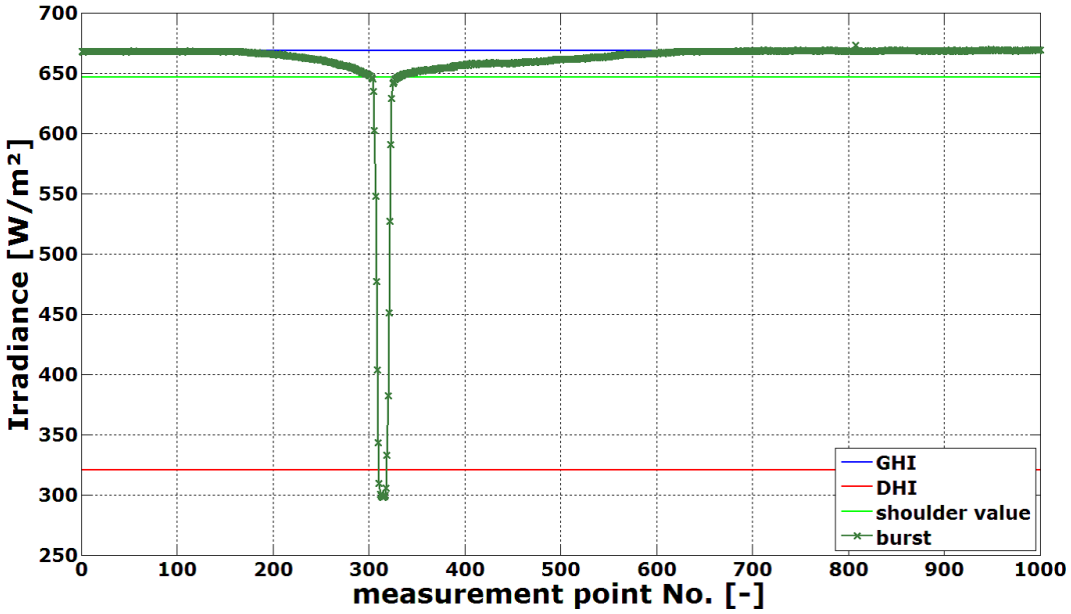

Figure 2.7: Irradiance signal logged during a rotation of the shadowband and derived irradiances. [Wilbert, 2014]

Table 2.1: Mode of data sampling for three types of RSIs [Wilbert et al., 2014]

Rotation frequency	*GHI*	*DHI*	*DNI*
		Twin RSI	
1 / (30 sec) alternating for both sensors	1 / sec	Shadowband correction averaged with previous value	Calculated from *GHI*, *DHI* and solar position as 1 min average with correction for *DHI* drift
		RSR2	
at least 1 / (30 sec) up to 1/(5 sec) if 20 W/m² change in *GHI*	1 / (5 sec)	Averaged for each rotation	Averaged for each rotation
		RSP4G	
1 / (60 sec)	1 / sec	Calculated once per minute as average of two rotations	Calculated every second from 1 second *GHI* samples and 1 minute *DHI* samples. Averaged every 60 seconds

3 Correction functions for Rotating Shadowband Irradiometers

Irradiance measurements by RSI are affected by a number of systematic errors. Correctional functions use correlations to environmental parameters for error reduction. This section introduces several sets of correction functions.

3.1 Correction functions by King, Myers, Augustyn and Vignola

This set of corrections is the outcome of a number of publications by King and Myers, Augustyn et al. and Vignola. In some cases the correction functions have been published in different versions. The version presented here will describe the functions as used at DLR. Prof. Vignola confirmed that these are the correct formulas.
The functional parameters are sensor temperature, SZA, the AM, GHI and DHI. In this method the GHI is corrected first since its corrected value is used for calculating the corrected DHI. The DNI is determined from both corrected values as described along equation 2.1.

The GHI correction as fomulated in [Augustyn et al., 2004]:

$$GHI_{\mathrm{cor}} = GHI_{\mathrm{raw}} \cdot \frac{F_\alpha}{F_{\mathrm{A}} \cdot F_{\mathrm{B}} \cdot F_{\mathrm{C}}} \tag{3.1}$$

where:	GHI_{raw}	:	Uncorrected GHI value
	F_α	:	Temperature parameter
	F_{A}	:	Spectral response parameter (AM correction)
	F_{B}	:	Cosine response parameter
	F_{C}	:	Solar height (Cat ear) parameter

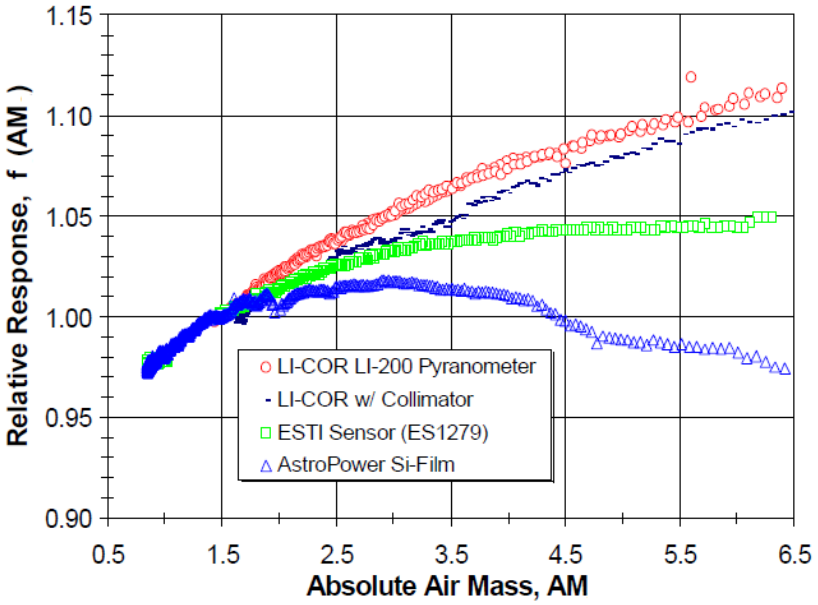

Figure 3.1: Course of sensor response F_A in correlation to AM [King et al., 1998].

1. **Temperature correction**
   [King and Myers, 1997] determined a temperature coefficient of $\alpha_{L,K} = 8.2 \cdot 10^{-4}$ by evaluating seven LI-COR sensors with a method that is commonly used for photovoltaic reference cells. Equation 3.2 is used to calculate the temperature correction parameter in dependence on the sensor temperature ϑ_{RSI} with a reference of $\vartheta_{ref} = 25°C$.

$$F_\alpha = 1 - \alpha_{L,K} \cdot (\vartheta_{RSI} - \vartheta_{ref}) \tag{3.2}$$

   Where ϑ_{RSI} can not be measured inside the sensor it can be substituted by an estimate using the ambient temperature ϑ_{amb}:

$$\vartheta_{RSI} = \vartheta_{amb} + (-4.883 \cdot 10^{-6} \cdot {GHI_{raw}}^2 + 0.00953 \cdot GHI_{raw} - 0.5) \tag{3.3}$$

2. **Spectral response correction**
   In [King et al., 1998] the changing spectrum of the solar irradiance was determined to be correlated to the change of AM. It is compensated by an empirically developed cubic function (equation 3.4 and figure 3.1) which uses AM as parameter. It proved to be applicable at a wide range of sites during clear sky conditions.

$$F_A = 2.631 * 10^{-4} \cdot AM^3 - 6.319 \cdot 10^{-3} \cdot AM^2 + 5.401 \cdot 10^{-2} \cdot AM + 0.932 \tag{3.4}$$

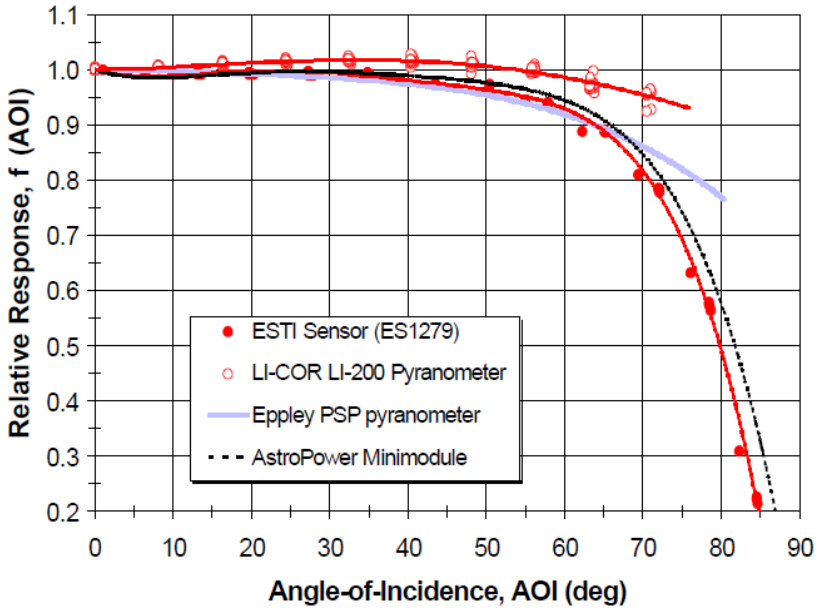

Figure 3.2: Course of sensor response F_B in correlation to the AOI in degree. [King et al., 1998]

3. **Cosine response correction**

   The cosine response in [King et al., 1998] has also been characterized by an empirical derived function (equation 3.5) in accordance to figure 3.2. Since RSI are mounted in horizontal position the sensors AOI is identical with the SZA.

$$F_B = -4.504 \cdot 10^{-7} \cdot SZA^3 + 1.357 \cdot 10^{-5} \cdot SZA^2 + 6.074 \cdot 10^{-4} \cdot SZA + 1 \tag{3.5}$$

   This function has been published in contradictory versions. In [King et al., 1997] the last coefficient is given as $6.074 \cdot 10^{-5}$. At DLR this is assumed to be by error and the definition in [King and Myers, 1997] is used since it is consistent with [King et al., 1998] and [Vignola, 2006].

4. **Cat ear correction**

   [Augustyn et al., 2004] introduces the term cat ear for the increased inaccuracy (figure 3.3) of the sensor during $SZA > 75°$ which peaks at $SZA = 81°$. In [Vignola, 2006] this function is stated with differing coefficients. After comparison of available sources at DLR this is assumed to be by error [Wilbert et al., 2014]. Figure 3.4 shows the respective correction as given in [Augustyn et al., 2004] which is defined by three functions depending on the SZA (see equation 3.6).

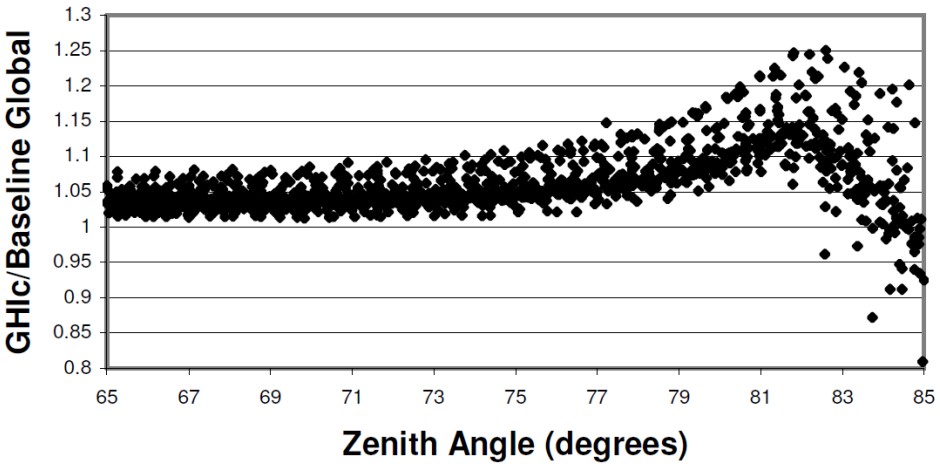

Figure 3.3: The cat ear error: GHI_{cor} (before cat ear correction) / GHI reference. SZA from 65 to 85°[Augustyn et al., 2004]

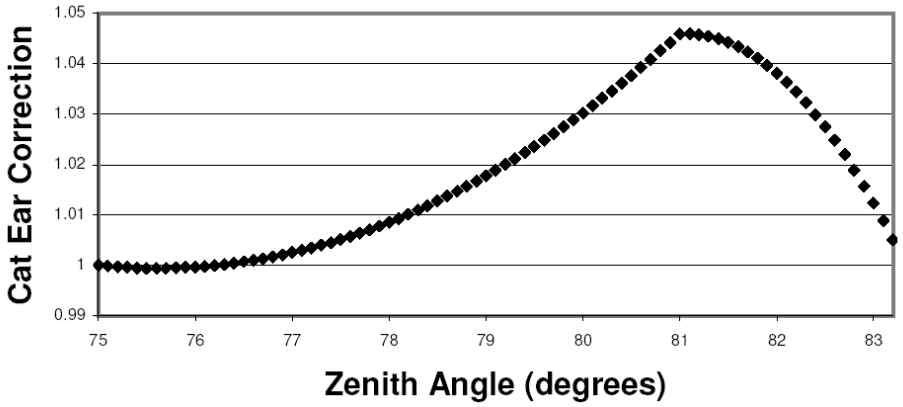

Figure 3.4: Cat ear correction [Augustyn et al., 2004]

$$F_C = \begin{cases} 10.164664 - 0.24242 \cdot SZA + 1.603 \cdot 10^{-3} \cdot SZA^2 & \text{if} \quad 75° < SZA < 81° \\ -58.03442 + 1.457577 \cdot SZA - 8.99 \cdot 10^{-3} \cdot SZA^2 & \text{if} \quad 81° \leq SZA < 83.2° \\ 1 & \text{if} \quad 0° \leq SZA \leq 75° \vee SZA \geq 83.2° \end{cases} \tag{3.6}$$

5. DHI **correction**

   DHI under clear sky conditions contains a great contribution from short wavelength (blue) and the Si-pyranometers are not very sensitvy to these wavelengths. Therefore DHI is measured too low during clear days and [Vignola, 2006] formulated a DHI correction (figure 3.5 and equations 3.7 and 3.8). The correction uses the already corrected GHI_{cor} as a parameter.

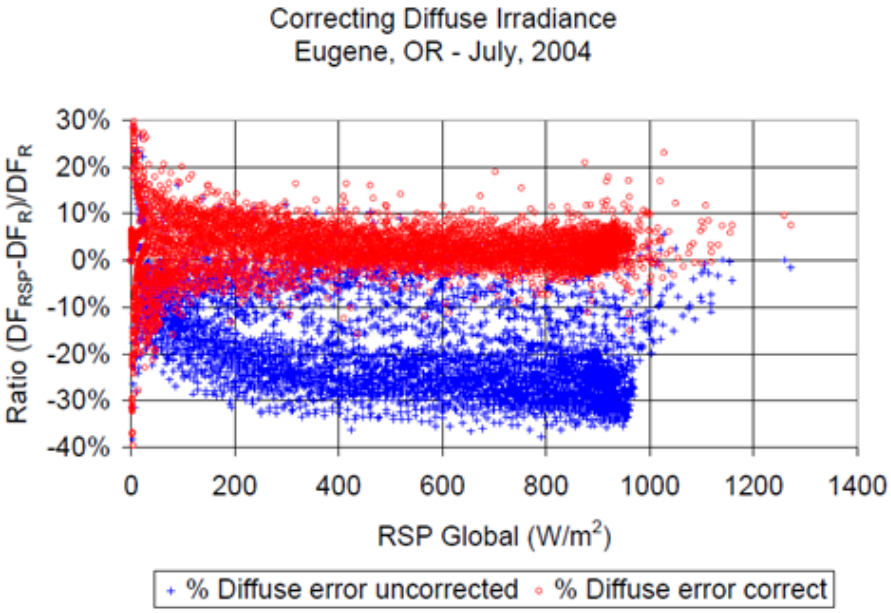

Figure 3.5: Comparison of DHI_{raw} (here DF_{RSP}) and DHI_{cor} (here DF_{R}) against GHI_{raw} (here RSP Global)[Vignola, 2006]

For $GHI_{\text{cor}} \leq 865.2$ W/m^2:

$$DHI_{\text{cor}} = DHI_{\text{raw}} + GHI_{\text{cor}} \cdot (-9.1 \cdot 10^{-11} \cdot {GHI_{\text{cor}}}^3 + 2.3978 \cdot 10^{-7} \cdot {GHI_{\text{cor}}}^2 - 2.31329234 \cdot 10^{-4} \cdot GHI_{\text{cor}} + 0.11067578794) \tag{3.7}$$

and for $GHI_{\text{cor}} > 865.2$ W/m^2:

$$DHI_{\text{cor}} = DHI_{\text{raw}} + GHI_{\text{cor}} \cdot (0.0359 - 5.54 \cdot 10^{-6} \cdot GHI_{\text{cor}} \tag{3.8}$$

3.2 Correction functions by Geuder et al.

Another set of correction functions is presented in [Geuder et al., 2003]. An improved update was given in [Geuder et al., 2008]. Correctional functions are applied to account for the parameters ambient air temperature, sensor temperature, AM, ambient pressure, solar elevation angle (SEA), the intensities of DNI and DHI and a spectral parameter which is calculated from the intensities of the three irradiance components i.e. GHI, DNI and DHI. Most of these functions have not been fully published for which they can not be elucidated in the same detail as done in section 3.1.

1. **Temperature correction**

   [King and Myers, 1997] introduced a temperature dependence which differed from the

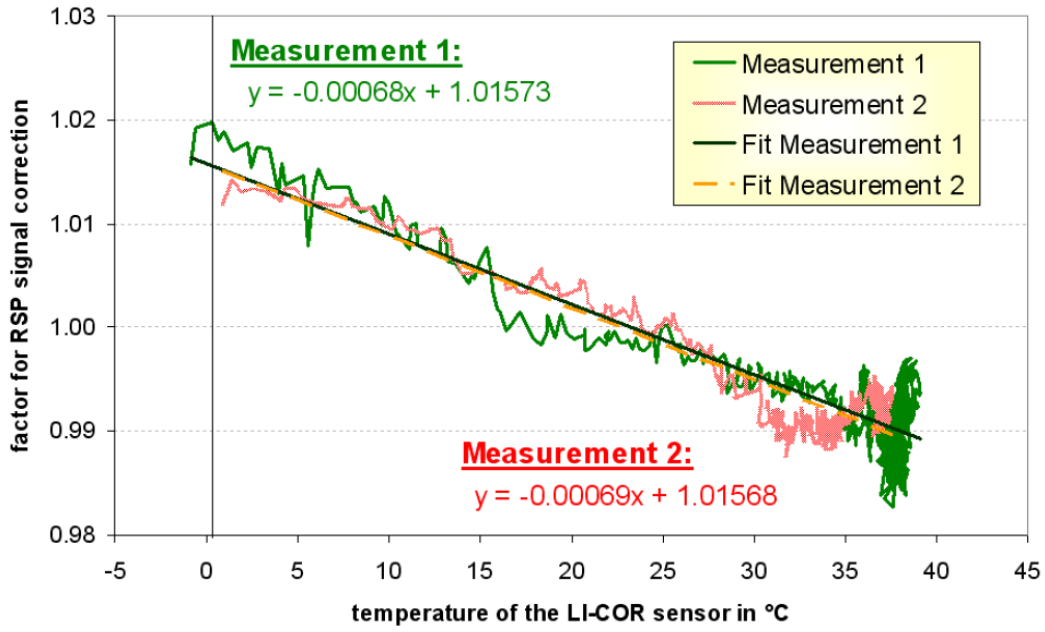

Figure 3.6: Dependence of the LI-COR sensors responsivity on temperature. [Geuder et al., 2008]

   one given by the sensor manufacturer (see equation 3.2 and table E.1 for comparison). Therefore another independent investigation was undertaken by DLR. The outcome was a temperature dependence of $\alpha_{L,G} = 7 \cdot 10^{-4}$ for deviations from a reference temperature of $\vartheta_{ref} = 25°C$ [Geuder et al., 2008]. Using this α the temperature correction factor is calculated along equation 3.2. Missing temperature measurements can be substituted by an estimate along equation 3.3, using $\alpha_{L,G}$ instead of $\alpha_{L,K}$.

2. **Spectral influence on measurement of diffuse irradiance**

   Because of the LI-200 sensors non-uniform spectral responsivity (see section 2.1) the DHI measurement is affected especially during clear deep blue skies and could be underestimated by up to 50% under these conditions [Geuder et al., 2008]. Therefore a spectral parameter Π_{spec} was found for a functional correction (see figure 3.7) including an ambient temperature coefficient. The parameter Π_{spec} is calculated along:

$$\Pi_{spec} = \frac{DNI \cdot GHI}{DHI^2} \tag{3.9}$$

3. **Air mass correction**

   In [Geuder et al., 2008] both, GHI and DHI measurements undergo a functional air mass correction. Its main parameter is the air mass factor (AMF) as defined in [Young, 1994]. It is calculated with the true SZA in accordance to an algorithm from [Michalsky, 1988] and

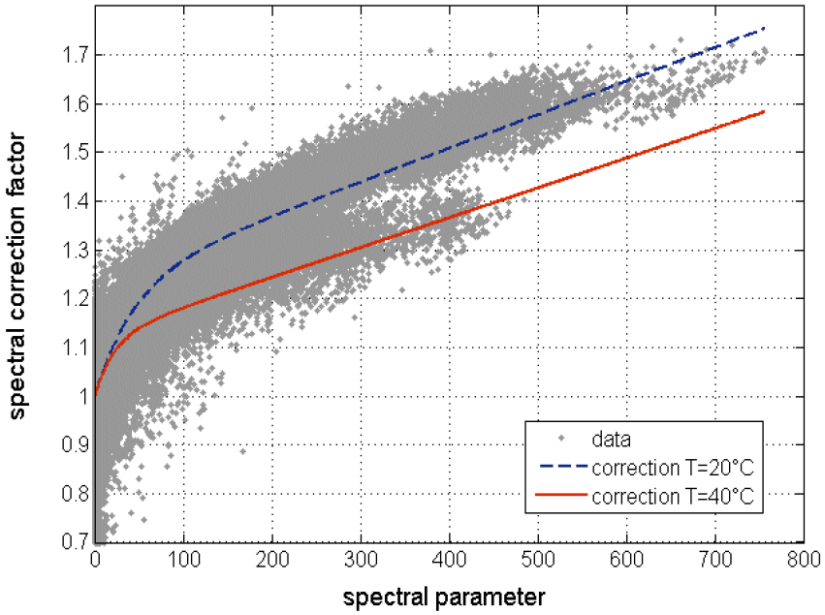

Figure 3.7: Correlation between the spectral correction factor for DHI and the spectral parameter Π_{spec} in dependence on the ambient temperature. [Geuder et al., 2008]

corrected for ambient pressure. Figure 3.8 visualizes the correction function in dependence on the pressure corrected AMF.

4. **The solar elevation angle influence on measurements of** GHI
   As described in section 3.1 the so called cat ear effect is the increase of inaccuracy at low SEA. [Geuder et al., 2008] introduced two correction functions for SEA below and above 3° to reduce this influence from the already AMF corrected GHI. Figure 3.9 displays the corrections factors course in dependence on the elevation angle.
5. **Irradiance intensity correction**
   Finally the remaining deviations of DHI and DNI from their reference values are reduced by a cubic and a linear function respectively. The functions parameter are the intensities of irradiance. A logarithmic correction for DNI was introduced in a later publication [Geuder et al., 2016].

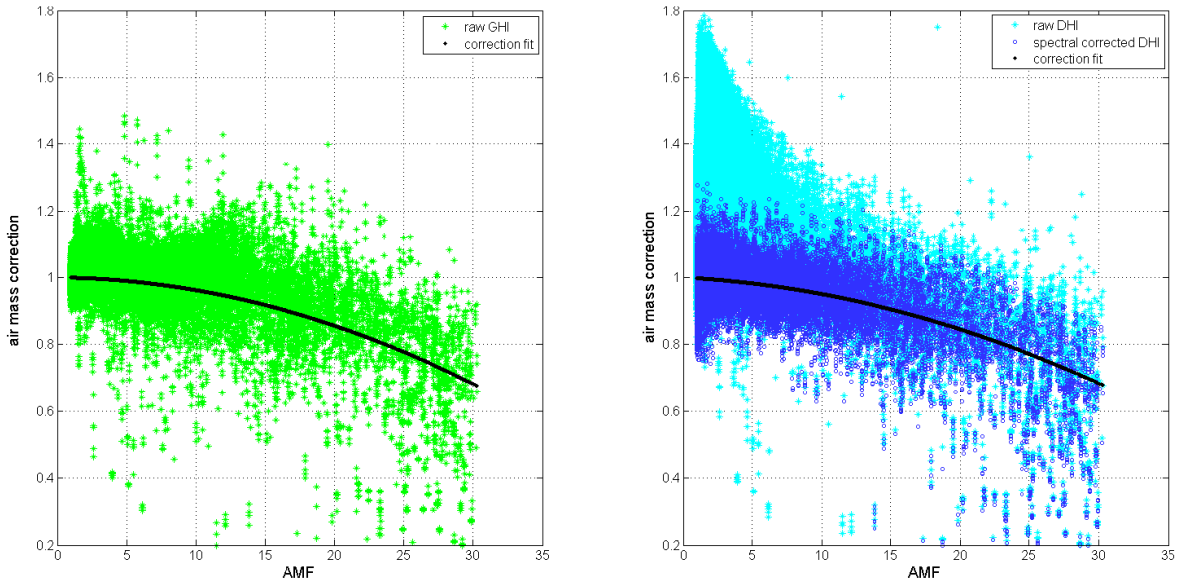

Figure 3.8: Correction for pressure corrected *AMF*. Left: *GHI* correction. Right: *DHI* correction with and without spectral correction. [Geuder et al., 2008]

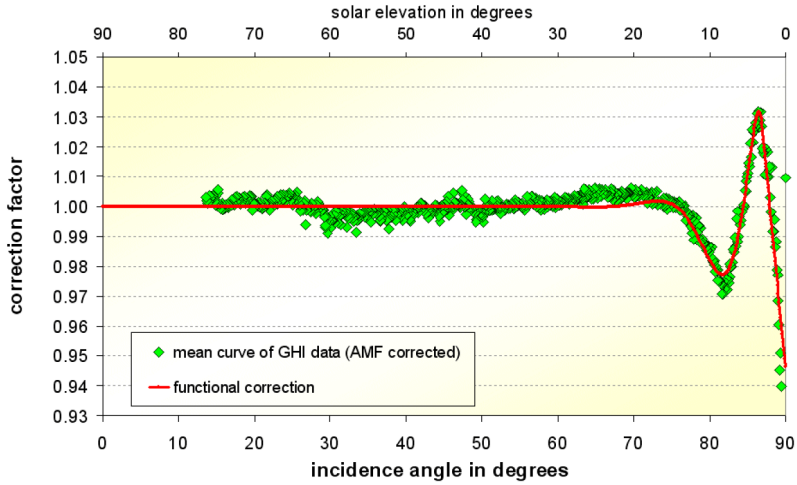

Figure 3.9: Mean curve of (*AMF* corrected) correction factor for *GHI* in dependence on the *SEA* [Geuder et al., 2008]

3.3 Correction functions by Hanussek

Based on the correction functions from [Geuder et al., 2008], Hanussek contributed a new correction function to [Geuder et al., 2011]. The most noteable change is that the incidence angle correction is only applied on the direct component of the irradiance and not on the global irradiance including the diffuse irradiance as in the case of [Geuder et al., 2008]. The correction functions used the same spectral correction. A small reduction of measurement errors was found compared to [Geuder et al., 2008]. However, the functions are currently not used to the knowledge of the authors of this report.

3.4 Correction functions by Vignola et al., 2017

In [Vignola et al., 2017] a new set of correction functions and the corresponding calibration is presented. In a first step the temperature correction is performed for DNI and DHI components. Then a spectral correction is applied for DNI and DHI. The spectral correction for DHI is different for clear sky and cloudy sky cases which is a main difference to other correction functions. The spectral adjustment factors are derived based on the spectral response data of the pyranometer and spectra created for the expected atmospheric conditions at the site using a clear sky model. For cloudy conditions the DHI correction also includes an additional empirical correction term. For skies with some or total cloud cover, the DHI correction factor is adjusted by the mix of diffuse and DNI values. This comes from the assumption that under totally cloudy skies, the DHI responsivity will be very close to the direct horizontal irradiance responsivity and the mix of clear sky responsivity and total cloud cover responsivity is obtained by fitting to the DHI reference data. An incidence angle correction finalizes the DNI correction and then GHI is calculated from DNI and DHI. The incidence angle correction is derived from the remaining error after the temperature correction and spectral correction of DNI. Because this new method uses the spectral irradiance data adapted to the site it has the potential to reduce the site dependence of the measurement uncertainty and the calibration.

4 Calibration of thermopile sensors

4.1 Calibration of field pyrheliometers - using a reference pyrheliometer

This calibration method uses a reference pyrheliometer for comparison and is described in detail in [ISO 9059]. The following will outline this method for the purpose of comparison to RSI calibration. For further details and practical instructions the reader is referred to the standard.
The DNI is measured by a reference pyrheliometer and one or more field pyrheliometers. Calibration takes place by comparing the field instruments to the reference. Around 20 data series are taken over the course of at least three days. In each series 1 integrated or 10 instantaneous readings are recorded. From each reading and each series a preliminary calibration factor is calculated. After statistical data treatment the final calibration factor can be calculated as the average value of the remaining preliminary factors.

Measuring equipment

1. Field pyrheliometer to be calibrated
2. Reference pyrheliometer
   Has to be of the same or higher category than the test pyrheliometer. A reference of the same classification category is only acceptable for field pyrheliometers (first class and second class instruments, also see [ISO 9060]).
3. Sun tracker
4. Data acquisition system with a resolution of at least 0.05 % of the maximum pyrheliometer reading and at least four channels. Measurements should be in synchronicity within one second.

Meteorological and site variables

1. If pyrheliometers with open aperture are used, the wind speed should be low (also see 6.3).
2. Ideally, clouds should cover less than 12.5 % of the sky. In any case their angular distance from the sun has to be greater than 15° in order not to obstruct direct irradiation from reaching the instruments (also see [ISO 9060]).
3. Atmospheric turbidity should be similar to intended field deployment conditions. High turbidity is problematic for pyrheliometers with wide aperture angles since it causes too high measurements due to scattering towards the instrument (also see [ISO 9060]).

4. DNI ideally should have values of 700 W/m^2 and higher. The acceptable minimum is 300 W/m^2. Low irradiance may require longer measuring periods.

Preparation

1. The distance between separately mounted measuring instruments has to be less than 20 meters
2. The measuring system is started and tested at least 30 minutes prior the measurements.
3. Alignment of the instruments to the sun needs to be checked immediately before beginning a measurement series.
4. The instrument windows needs to be cleaned before each series.
5. A log-book has to be prepared. This is used to report important occurrences.

Data sampling

1. Data is taken in 20 series of 10 to 20 minutes in length.
2. In each series at least 1 integrated or 10 instantaneous measurements are taken.
3. The sampling rate has to be at least 1 per second.
4. Meteorological conditions like the mean SEA and mean ambient temperature are documented for each series.

Data treatment

1. Data from all pyrheliometers aquired during operational problems noted in the log-book is rejected.
2. Calculation of the preliminary calibration factors $CF_{\mathrm{ph}}(i)$ for each reading i:

$$CF_{\mathrm{ph}}(i) = \frac{DNI_{\mathrm{Ref}}(i)}{V_{\mathrm{I}}(i)} \tag{4.1}$$

where: DNI_{Ref} : DNI value of the reference pyrheliometer
V_{I} : DNI voltage signal of the field pyrheliometer

3. All $CF_{\mathrm{ph}}(i)$ which deviate by more than 2 % from the mean of their respective series are rejected.
4. The final calibration factor is calculated as the mean of the remaining $CF_{\mathrm{ph}}(i)$ with m as the number of remaining readings:

$$CF_{\mathrm{ph}} = \frac{1}{m} \cdot \sum_{i}^{m} CF_{\mathrm{ph}}(i) \tag{4.2}$$

5. The STD of the $CF_{\mathrm{ph}}(i)$ is calculated separately per series. The STD of the individual means of each series is calculated as well. Both indicate the stability of measurements.

Documentation

The calibration certificate or protocol has to include the following information:

1. Calibration method
2. Field pyrheliometer: manufacturer, type, model and serial number.
3. Reference pyrheliometer: manufacturer, type, model and serial number.
4. Calibration of the reference and thus the test instrument has to be traceable to the World Radiometric Reference (WRR).
5. Final calibration factor for the field pyrheliometer as well as the STD.
6. Meteorological conditions during calibration.
7. Number of evaluated single measurements and the number of measuring days.
8. The calibration data needs to be stored for at least 5 years

4.2 Calibration of field pyranometers

[ISO 9846] and [ISO 9847] give instructions for the calibration of pyranometers. [ISO 9060] is often referenced for further details. This section is intended to give the reader the necessary background for understanding the differences to RSI calibration. For further details and practical instructions the reader is referred to the respective norm.

4.2.1 Using a reference pyrheliometer

[ISO 9846] refers to this outdoor calibration method as the alternating sun- and shade method. Due to its more complicated procedure it is usually only applied for calibrating the first pyranometer. Once calibrated it can be used as a reference in the procedures described in section 4.2.2 and section 4.2.3 for calibrating multiple pyranometers at once. While DLR applies annex D of [ISO 9846] for improved accuracy the following summary will refer to the basic version of this method.
The pyranometer is equally shaded and exposed in turns while comparing it to a reference pyrheliometer. At the end of each shaded state the DHI is recorded from the pyranometer. At the end of the exposed state the pyranometer records the GHI. Simultaneously, the pyrheliometer measures and writes the DNI values. By taking the difference of the DHI and GHI values and comparing it to the DNI value the calibration factor for the pyranometer is calculated. At least 3 intervals (shaded + exposed + shaded = 3 intervals) need to be measured per series. This has to be repeated for at least 10 series.

Measuring equipment

1. Pyranometer to be calibrated
2. Reference pyrheliometer with at least first class classification (see [ISO 9060] for classification and recalibration requirements).
3. Sun tracker
   The necessary accuracy of the sun tracker depends on the slope angle of the pyrheliometer.
4. Shadowball/disc
   The radius of the shadowball/disc must be larger than the outer radius of the pyranometers glass dome by a minimum of its distance times $\tan(0.5°)$.
5. Data aquisition system with an uncertainty of 0.1 % of the pyranometers calculated output at 1100 W/m^2 is required. All data needs to be read simultaneously.

Meteorological and site variables

1. Clear sky conditions. Clouds are tolerable if they are at a far distance from the sun, i.e. more than 45°.
2. Strong winds towards the pyrheliometers window are to be avoided (see section 4.1 and 6.3).
3. Obstacles on the horizon seen from the pyranometer should not obscure the sun or cause specular reflections.

Preparation

1. The radiometers and the data acquisition system shall commence operation at least 30 minutes before the start of the measurements.
2. The tilt angle of the pyranometer is 0°.
3. The distance between separately mounted measuring instruments has to be less than 30 meters.
4. Zero-point, polarity and nominal strength of signals need to be checked for all irradiometers.
5. Windows and glass domes of the instruments shall be cleaned before measurements.

Data sampling

1. Data sampling is performed in at least 10 measurement series. The measurements should be taken over the course of at least 3 days and during AOI that deviate less than ±5 % from the later intended operation conditions.
2. Each series has to start and end with a shaded interval.
3. Each series should include at least 3 intervals (i.e. shaded, exposed, shaded) but should not take longer than 36 minutes.
4. The interval duration t_0 is is the response time in which the pyranometer signal achieves 99.7 % of its final theoretical value. The norm allows to choose t_0 up to 20 % longer, if wind or dust conditions are unstable.
5. Method of signal reading (see figure 4.1)
   At the end of the shaded interval a DHI voltage signal V_D is read.
   At the end of the shaded interval a GHI voltage signal V_G is read, as well as one integrated DNI reference signal DNI_Ref by the pyrheliometer which corresponds to the same time span.
   The ambient temperature ϑ_amb needs to be measured at least once prior to and once after each series.

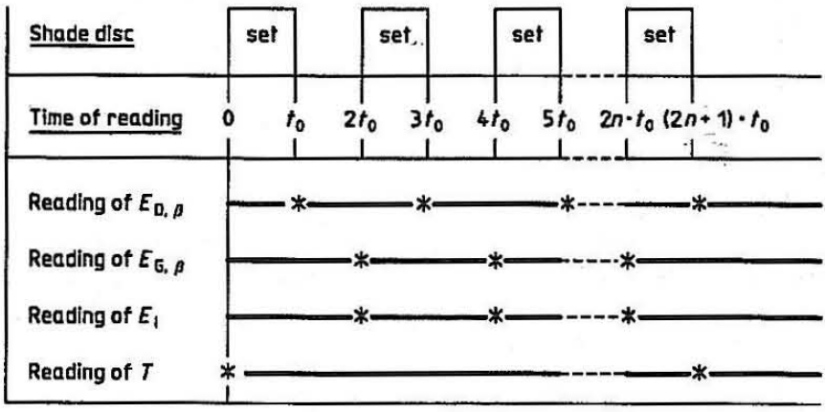

Figure 4.1: Data sampling scheme for one series. $E_{D,\beta}$ = DHI, $E_{G,\beta}$ = GHI and E_I = DNI reading. [ISO 9846]

Mathematical treatment

1. Calculate the responsivity $S_{\mathrm{pr,a}}(i)$ for each set i of measurements (1 set = shaded, exposed, shaded) separately for each a series along:

$$S_{\mathrm{pr,a}}(i) = \frac{V_{\mathrm{G}}(2i) - 0.5 \cdot [V_{\mathrm{D}}(2i-1) + V_{\mathrm{D}}(2i+1)]}{DNI_{\mathrm{Ref}}(2i) \cdot sin[SEA(2i)]} \tag{4.3}$$

2. Reject those $S_{\mathrm{pr,a}}(i)$ of each series which deviate by more than 1 % from the series mean responsivity. If more than half of the $S_{\mathrm{pr,a}}$ of a series are rejected, the whole series is excluded.
3. The remaining data is then used to calculate the final responsivity $S_{\mathrm{pr,a}}$ as the mean value of all remaining $S_{\mathrm{pr,a}}(i)$. The calibration factor $CF_{\mathrm{pa,a}}$ is defined by its reciprocal:

$$S_{\mathrm{pr,a}} = \frac{1}{m} \cdot \sum_{i}^{m} S_{\mathrm{pr,a}}(i) \tag{4.4}$$

$$CF_{\mathrm{pa,a}} = \frac{1}{S_{\mathrm{pr,a}}} \tag{4.5}$$

Where the ambient temperature ϑ_{amb} during a set of measurements i deviates significantly from the intended operation temperature ϑ_{op} and the pyranometer has a specified temperature coefficient a temperature correction factor $F_{\alpha,\mathrm{Pa}}$ is applied to the respective $S_{\mathrm{pr,a}}(i)$ before calculating $S_{\mathrm{pr,c}}$:

$$F_{\alpha,\mathrm{Pa}}(i) = 1 - \alpha_{\mathrm{Pa}} \cdot (\vartheta_{\mathrm{amb}}(i) - \vartheta_{\mathrm{op}}) \tag{4.6}$$

Documentation

See pyrheliometer calibration (section 4.1).
Additional requirements:

1. The pyranometers serial number and position angles.
2. Date and time of calibration, calibration site (latitude, longitude and altitude), special remarks.
3. Shadow ball/disc geometry.
4. Final resonsivity and calibration factor for the pyranometer as well as the responsivities STD.
5. Range of parameters in which the the calibration results are valid (e.g. SEA, Temperature etc.)
6. Data storage is not required.

4.2.2 Using a reference pyrheliometer and a reference pyranometer

In [ISO 9846] the following calibration procedure is referred to as the continuous sun- and shade method. It can be used as soon as one has a calibrated pyrheliometer and a calibrated pyranometer. This method allows the simultaneous calibration of multiple pyranometers. The reference pyrheliometer and the shaded reference pyranometer are continuously collecting data for DNI and DHI measurements respectively, which is then summed up and compared to the GHI measured by the field pyranometers under calibration.

Measuring equipment
See alternating sun- and shade method (section 4.2.1).
The reference pyranometer has to be of a higher class (see [ISO 9060] for classification) than the field pyranometer's and with documented calibration history. The last outdoor calibration by the alternating sun- and shade method (section 4.2.1) has been within less than 12 months and under conditions similar to those during the field pyranometer calibration (not further specified). Furthermore, it should exhibit a high long-therm stability (not further specified). These requirements are listed in [ISO 9847] to which [ISO 9846] refers.

Meteorological and site variables
See alternating sun- and shade method (section 4.2.1).
A higher degree of cloudiness is tolerable, if clouds move slowly without obstructing the sun or causing more than 1 % DHI variation within 10 seconds.

Preparation

See alternating sun- and shade method (section 4.2.1).

Data sampling

1. Each series consists of 10 to 20 sets of measurements.
   At least 10 series have to be recorded in the course of at least 3 days.
2. Each series should spread over 10 to 30 minutes.
3. Each set consists of a GHI signal V_{G} from the test pyranometer
   a DHI reference signal DHI_{Ref} from the shaded pyranometer
   a DNI reference signal DNI_{Ref} from the pyrheliometer
   the corresponding time and temperature.
4. Measurements should take place during the most stable periods.
5. Each measurement has to be completed within 1 second and at a sampling rate between 0.5 to 2 sets per minute (The lower sampling rates refer to the use of an absolute cavity pyrheliometer).

Mathematical treatment

1. All measurements which deviate by more than 5 % from the average of their series are excluded. A whole series is canceled if more than 50 % of its values have been eliminated.
2. From the filtered data the responsitivities $S_{\mathrm{pr,c}}(i)$ for all sets of measurement are calculated:

$$S_{\mathrm{pr,c}}(i) = \frac{V_{\mathrm{G}}(i)}{DNI_{\mathrm{Ref}}(i) \cdot sin\,[SEA(i)] + DHI_{\mathrm{Ref}}(i)} \tag{4.7}$$

3. The final responsivity $S_{\mathrm{pr,c}}$ is defined by their mean and the calibration factor $CF_{\mathrm{pa,c}}$ by its reciprocal. They are calculated along equations 4.4 to 4.6 while using $S_{\mathrm{pr,c}}$ instead of $S_{\mathrm{pr,a}}$.

Documentation

See alternating sun- and shade method (section 4.2.1).

4.2.3 Using a reference pyranometer

[ISO 9847] describes outdoor and indoor calibration methods for field pyranometers in horizontal and tilted angles which use only a pyranometer as reference. Since RSI are always operated in horizontal alignment this section will describe the outdoor calibration for horizontal positioning to which the norm refers to as outdoor calibration method Ia.
The reference pyranometer must have been calibrated through comparison to a pyrheliometer in accordance to the alternating sun- and shade method in section 4.2.1. The necessary

duration of data sampling varies depending on the overall sky conditions. While during clear sky two to three days are sufficient, for continuous cloudy sky conditions a minimum duration of 10 days is required. This long-term characteristic requires careful monitoring of data sampling conditions and data consistency in order to eliminate influences by operational problems.

Measuring equipment

1. Field pyranometers to be calibrated
2. Reference pyranometer
   same as in the continuous sun- and shade method (section 4.2.2).
3. Precision calibration table at 0° horizontal tilt.
4. Data acquisition system
   The data logger has to be capable of recording three separate channels (also see section 4.2.1).

Meteorological and site variables

1. Objects on the horizon should not exceed an elevation angle of 5° and must not cause specular reflection onto the instruments.
2. If the field pyranometer is to be applied for solar resource monitoring, the *GHI* should consist by at least 80 % of $E_{dir,hor}$. Also an angular cloud distance from the sun of at least 30° is required. *Note: The last criteria can be replaced by an irradiation threshold which indicates obstruction by clouds.*

Preparation

1. All pyranometers are installed on a common calibration table at 0° tilt angle.
2. Checks for zero-point, polarity and nominal strength and stability of signals are carried out.
3. The instruments domes get cleaned.
4. Equal influence of foreground reflections is tested by switching the instrument positions.
5. Tilt angles need to be rechecked during calibration in dependence on the tables mechanical and thermal stability.

Data sampling

All voltage readings are taken simultaneously.
The procedure differs in dependence on the sky conditions:

1. **Stable cloudless sky conditions:**
   The data is sampled from a period of 2 to 3 days (longer periods are optional). It has

to be obtained at varying solar elevation angles > 20°. The solar noon must be included. Measurements are taken in at least 15 series of which each includes at least 21 voltage readings within 10 to 20 minutes.

2. **Unstable sky conditions** (clouds at > 30° distance from the sun):
   The data is sampled from a period of 5 to 14 days. It has to be obtained at varying solar elevation angles > 20°. The solar noon must be included. Measurements are taken in at least 15 series of which each includes at least 21 continuous voltage readings within 1 to 5 minutes and under steady irradiation conditions. Alternatively each series can be integrated over 1 to 5 minutes.
3. **Cloudy sky conditions:**
   If the field pyranometers are to be used for solar resource monitoring, cloudy sky conditions are not suitable for calibration.
   The data is sampled for at least 10 days. The obtained data has to be taken at different solar elevation angles and varying cloudiness. Its hourly mean GHI has to be greater than 100 W/m^2. At least 50 integrated 1 hour measurement intervals are taken.

Mathematical treatment

1. Reject all data which has been subject to operational problems.
2. The ratio $CF_{\mathrm{pa,Ia}}(i)$ is calculated for each reading:

$$CF_{\mathrm{pa,Ia}}(i) = \frac{GHI_{\mathrm{Ref}}(i)}{V_{\mathrm{G}}(i)} \tag{4.8}$$

   In either of the following three cases the GHI_{Ref} needs to be fitted to the calibration conditions (e.g. temperature) before calculating the $CF_{\mathrm{pa,Ia}}(i)$:

   a) Reference and field pyranometer are not of the same model
   b) Reference and field pyranometer do not have the same temperature response
   c) The reference pyranometer has not been calibrated for the intended field operation conditions (e.g. temperature ϑ_{op}).

3. Reject measurements for which $CF_{\mathrm{pa,Ia}}(i)$ deviates by more than 2 % from the mean of its respective series.
4. The final calibration factor $CF_{\mathrm{pa,Ia}}$ is calculated as the mean of the remaining $CF_{\mathrm{pa,Ia}}(i)$.

$$CF_{\mathrm{pa,Ia}} = \frac{1}{m} \cdot \sum_{i}^{m} CF_{\mathrm{pa,Ia}}(i) \tag{4.9}$$

   If the ϑ_{amb} during calibration deviates strongly from ϑ_{op} and the temperature responsivity of the field pyranometers from the reference, a temperature correction in accordance to equation 4.6 needs to be applied to the $CF_{\mathrm{pa,Ia}}(i)$ before calculating $CF_{\mathrm{pa,Ia}}$.
5. The STD of the mean $CF_{\mathrm{pa,Ia}}(i)$ per series from the final calibration factor represents the

stability of the calibration and should be less than ± 0.5 %.

Documentation

See alternating sun- and shade method (section 4.1).
Additional requirements:

1. Reference and field pyranometer instead of pyrheliometers.
2. pyranometer positioning and tilt angles during calibration.
3. Results should also include the absolute uncertainty.
4. Range of validity (parameters: SEA, temperature, etc.)
5. Data storage is not required.

5 Calibration of Rotating Shadowband Irradiometers

This section will outline four calibration methods for RSIs. Two of them are developed and performed by DLR at CIEMAT's Plataforma Solar de Almería (PSA). Each of the method refers to one of the two sets of correction functions introduced in section 3. Therefore, this section differentiates between the DLR calibration method corresponding to functional corrections by [Geuder et al., 2008] (DLR2008) and the DLR calibration method corresponding to functional corrections by King, Myers, Augustyn and Vignola (DLR-VigKing). In addition the RSI calibration method described in [Kern, 2010] (Kern) as practiced by Irradiance Inc. and Vignola et al., 2017 will be briefly introduced.
While the Kern method only calibrates for GHI the other methods assign specific calibration factors to different types of irradiance. In both DLR methods and in the Vignola et al., 2017 method the RSI is compared to a reference DNI (DNI_{Ref}) and a reference DHI (DHI_{Ref}) measured with a pyrheliometer and a pyranometer shaded with a shadowball. The reference GHI (GHI_{Ref}) is calculated from both reference instruments since this yields higher accuracy than GHI measurement by a pyranometer (see [ISO 9060]). Nonetheless a second pyranometer is used to monitor the quality of reference measurements by redundancy.
Data collection at PSA usually takes place continuously over the course of 30 to 120 days. Due to the manifold environmental and operational influences that can occur during this time span the raw data needs to be screened and manually reviewed for errors and temporary system failures. At DLR the calculation of calibration factors is based on minimizing the root mean square deviation (RMSD) but differs for both methods.
An examination presented in [Geuder et al., 2011] compared the RMSD of RSI measurements from the reference for different calibration methods as well as the bias of their annual sum of irradiation. It was found that the Kern method improved measurements of GHI and more so DHI. In comparison to the other methods under examination the Kern method brought the least reduction in RMSD of DNI measurements. DLR-VigKing whilst using data from a wider range of meteorological conditions and assigning three separate calibration factors (see section 5.2) performed better in regard to DNI while using the same set of correction functions (section 3.1). Yet better results in all three irradiance components were achieved by using the DLR2008 method. Only little experience has been collected so far with the Vignola et al., 2017 method, but this method is promising as it is more physical and includes means to reduce site dependence.
The description of the DLR calibration methods have been extracted from DLR's RSI calibration software. Other references than these are cited in the text below.

5.1 Calibration method DLR2008

This calibration method assigns two calibration factors: CFG for GHI and CFD for DHI. Since both GHI and DHI have different spectral compositions the sensor's responsivity differs among the two. The difference in responsivity was incorporated into the correction functions and hence the correction refers to the mean among the group of instruments used for the development of the correction functions. However, the difference in responsivity for GHI and DHI is specific to each individual sensor. Thus, better results are achieved by using separate calibration factors [Geuder et al., 2008].
Because DNI is the desired measurand, CFG is optimized for determination of the DNI as further explained in the following. The corrected and calibrated DNI, DNI_{cor} is determined from the corrected and calibrated GHI_{cor} and DHI_{cor}.
The calibration method for DLR2008 was also adapted to the Hannusek correction functions and the version of the DLR2008 corrections with the logarithmic corrections from [Geuder et al., 2016].

Measuring equipment

1. The RSI to be calibrated
2. Table 5.1 lists all other instruments presently used at the PSA for RSI calibration as they appear on the calibration protocol. For specifications of the reference irradiometers, sun tracker and data logger see Appendix E.

Table 5.1: Instruments for RSI calibration as used in Q3 2014 (source: DLR)

Manufacturer	Model	Serial Number	Functionality/ Measurand	Calibration/Test remarks		
				constant	by	date
Kipp&Zonen	CMP21	90281	GHI	9.47 µV/(W/m²)	Kipp&Zonen	May-2013
Kipp&Zonen	CV 2	70990	Ventilation unit, GHI			
Kipp&Zonen	CMP21	90292	DHI	8.30 µV/(W/m²)	Kipp&Zonen	May-2013
Kipp&Zonen	CV 2	70992	Ventilation unit, DHI			
Kipp&Zonen	CHP1	90163	DNI	7.98 µV/(W/m²)	Kipp&Zonen	May-2014
Campbell Scientific	CS215	E1839	Air temp. and rel. humidity		Sensirion	
Campbell Scientific	CS100	3696476	Air pressure		Setra	Aug-2008
Kipp&Zonen	2AP-BD	10186	Sun tracking		Kipp&Zonen	Mar-2002
Kipp&Zonen	2AP Sun Sensor	60207	Sun tracking		Kipp&Zonen	Dec-2006
Campbell Scientific	CR1000	7916	Data logger for precise sensors			

Meteorological and site variables

1. Various weather conditions should occur during the measuring period (see [Geuder et al., 2011]).
2. No objects in the vicinity or on the horizon cause shade or reflections on any of the instruments.

Preparation

This overview refers to the measuring site at the PSA where all reference instruments are already set up and are continuously operated and monitored regardless of RSI calibration.

1. All instruments are operated in close vicinity to each other (< 10 meters).
2. RSIs are mounted in horizontal position with their shadowbands towards $\pm 5°$ from the geographical north [Wilbert et al., 2014]. Horizontal misalignment of the LICOR sensor should be within $\pm 0.1°$ and needs to be monitored during the measuring period.
3. The RSIs are connected to the data logger and registered in the calibration database.

Data sampling

1. GHI_{Ref}, DHI_{Ref} and DNI_{Ref} are sampled every second and recorded as one minute average values as well as the ambient pressure and temperature.
2. The RSI values for GHI, DHI and DNI are averaged and recorded once per minute. The sampling rate before calculation of one minute values differs for RSR2, RSP4G and Twin-RSI as detailed in table 2.1. In RSP4G and Twin-RSI the sensor temperature is recorded as well.
3. Monitoring the measurements:
   In order to identify and resolve operational problems the recorded data of all instruments is scrutinized at least once per weekday by manually reviewing the course of GHI, DNI and DHI of RSI and reference instruments. Furthermore, the instruments are inspected in situ for anomalies. The redundant GHI measurement is used to confirm correct operation of the reference instruments. Operational errors are documented in the calibration database.
4. Instrument cleaning during the measuring period:
   The window of the pyrheliometer, the glass domes of the pyranometers as well as the diffusor disks of the RSI are cleaned daily except for weekends. The exact time of each cleaning event is documented.
5. All relevant events in the vicinity (e.g. construction works, maintenance of nearby instruments) are documented.

Data treatment

1. For each data channel 10 minutes mean values are calculated.

2. A screening algorithm performs a quality check of all recorded channels as recently presented in [Geuder et al., 2015]. Among others, the quality check screens if measured values are physically possible, if their fluctuation (or lack of it) is realistic and excludes data which has been manually flagged during the measuring period.
3. A soiling correction algorithm is applied to DNI_{Ref} in accordance to the documented cleaning events (see [Geuder and Quaschning, 2006]).
4. The LI-COR calibration factor CF_{Licor} is applied to the RSI data.
5. The RSI and reference data is compared for consistency:
   If a time stamp or one of its respective irradiance measurements is missing, it is removed in both reference and RSI.
6. For RSI without temperature sensor (e.g. RSR2) the sensor temperature is estimated by an algorithm based on GHI and ambient temperature. Another estimation algorithm substitutes missing pressure measurements in all RSI using the barometric formula.
7. GHI_{Ref} is calculated from DHI, DNI and the sun height angle using the apparent sun height at the middle of each 10 minutes interval.
8. The irradiance data is manually reviewed:
   First, the GHI_{raw}, DHI_{raw} and DNI_{raw} (RSI data with applied CF_{Licor}) and the reference data are checked for plausibility by comparison. Irradiance data which has been flagged by the screening algorithm is excluded as well. In a second check the deviation of RSI data from the reference data before and after application of the functional corrections (specific to the calibration method, here DLR2008) are compared to each other. Erroneous data is marked for exclusion and a comment is saved in the database.
9. All data exclusions are applied.
10. Calculation of calibration factors

    a) GHI_{Ref} and DHI_{Ref} as well as their deviation from the corrected RSI measurements GHI_{cor} and DHI_{cor} are screened for the calibration limits (CL) as defined in table 5.2.

Table 5.2: Calibration limits used at DLR [Geuder et al., 2011]

Reference DNI **[W/m²]**	> 300
Reference GHI **[W/m²]**	> 10
Reference DHI **[W/m²]**	> 10
SEA [°]	> 5
Max deviation between corrected RSI and reference [%]	$\pm$ 25

    b) The screened data is used to determine the DHI calibration factor CFD by an algorithm which minimizes the RMSD of the corrected and calibrated DHI_{RSI} from DHI_{Ref} through variation of CFD [Geuder et al., 2011]. Further information concerning the application of CFD is given in the next paragraph.
    c) While ignoring the previous GHI and DHI data screening the DNI_{Ref} and its deviation

from the corrected RSI measurement DNI_{cor} is screened for CL (table 5.2).

d) With applied CFD the screened data is used to determine the calibration factor CFG for GHI by an algorithm which minimizes the RMSD of DNI_{cor} from DNI_{Ref} by variation of CFG [Geuder et al., 2011]. Further information concerning the application of CFG is given in the next paragraph.

11. Calibration results are manually reviewed:
    Deviation of RSI data from the reference before an after calibration is compared. If further erroneous data is found it can be marked for exclusion and steps 9 to 11 are repeated.
12. Bias, STD and RMSD of the corrected and calibrated RSI data from the reference are calculated.

Application of the calibration factors to the RSI data

1. The functionally corrected and calibrated GHI is obtained by multiplying the calibration factor to the functionally corrected GHI_{cor}:

$$GHI_{\mathrm{RSI}} = CFG \cdot GHI_{\mathrm{cor}} \tag{5.1}$$

2. The functionally corrected and calibrated DHI is determined with the functionally corrected DHI_{cor} and the DHI calibration factor.
   If $DNI_{\mathrm{raw}} \geq 2\,\mathrm{W/m^2}$:

$$DHI_{\mathrm{RSI}} = CFD \cdot DHI_{\mathrm{cor}} \tag{5.2}$$

   In case of $DNI_{\mathrm{raw}} < 2\ \mathrm{W/m^2}$:

$$DHI_{\mathrm{RSI}} = CFD \cdot GHI_{\mathrm{RSI}} \tag{5.3}$$

3. The corrected and calibrated DNI is determined as:

$$DNI_{\mathrm{RSI}} = \frac{GHI_{\mathrm{RSI}} - DHI_{\mathrm{RSI}}}{\cos(SZA)} \tag{5.4}$$

Documentation

1. RSI and LI-200 serial number
2. Details of reference instruments including last calibration (table 5.1).
3. Calibration factors
4. RMSD of GHI_{cor} and DNI_{cor} from the reference.
5. Calibration period and effective period after data exclusions.
6. Summary of the calibration procedure (e.g. temporal resolution (10 min) and CL applied during calibration)
7. The calibration data and all data exclusions are stored at DLR for future reference.

5.2 Calibration method VigKing

DLR-VigKing determines three separate calibration factors CFg, CFd and CFn for GHI, DHI and DNI respectively [Geuder et al., 2011]. In DLR2008 the GHI error is slightly increased by optimizing its calibration factor for determination of DNI. The assignment of three separate factors in DLR-VigKing avoids this effect. Each calibration factor is optimized for RMSD of the measurand it is applied to.
In all aspects other than the correction functions, the assignment of calibration factors and the application thereof this method is identical to DLR2008 (see 5.1 for reference). The following will elucidate the differences by, replacing step no. 10 of the data treatment in DLR2008 and clarifying how the calibration factors are to be applied. In deviation from the account given in [Geuder et al., 2011] in todays practice the same CL (table 5.2) are used in both calibration methods.

Data treatment

10. Calculation of calibration factors
    a) GHI_{Ref} and DHI_{Ref} as well as their deviation from the corrected RSI measurements GHI_{cor} and DHI_{cor} are screened for the CL as defined in table 5.2.
    b) The screened data is used to determine the GHI calibration factor CFg by an algorithm which minimizes the RMSD of the corrected and calibrated GHI_{RSI} from GHI_{Ref}.
    c) The previous data screening for CL is repeated with applied CFg [Geuder et al., 2011].
    d) The screened data is used to determine the DHI calibration factor CFd by an algorithm which minimizes the RMSD of the corrected and calibrated DHI_{RSI} from DHI_{Ref} [Geuder et al., 2011].
    e) CFg and CFd are applied successively. While ignoring the previous data screenings the DNI_{Ref} and its deviation from the corrected RSI measurement DNI_{cor} is screened for CL (table 5.2).
    f) with applied CFg and CFd the screened data is used to determine the DNI calibration factors CFn by an algorithm which minimizes the RMSD of the corrected and calibrated DNI_{RSI} from DNI_{Ref} [Geuder et al., 2011].

Application of the calibration factors to the RSI data

1. The functionally corrected and calibrated GHI is obtained by multiplying the calibration factor to the functionally corrected GHI_{cor}:

$$GHI_{\mathrm{RSI}} = CFg \cdot GHI_{\mathrm{cor}} \tag{5.5}$$

2. The functionally corrected and calibrated DHI (DHI_{RSI}) is determined along equations 3.7 and 3.8 with GHI_{RSI} instead of GHI_{cor} and multiplication with the calibration factors for DHI:
   For $GHI_{\mathrm{RSI}} \leq 865.2$ W/m^2

$$\begin{aligned} DHI_{\mathrm{RSI}} = CFd \cdot \big[DHI_{\mathrm{raw}} + GHI_{\mathrm{RSI}} \cdot (&-9.1 \cdot 10^{-11} \cdot {GHI_{\mathrm{RSI}}}^3 + 2.3978 \cdot 10^{-7} \cdot {GHI_{\mathrm{RSI}}}^2 \\ &-2.31329234 \cdot 10^{-4} \cdot GHI_{\mathrm{RSI}} + 0.11067578794) \big] \end{aligned} \tag{5.6}$$

   and for $GHI_{\mathrm{RSI}} > 865.2$ W/m^2

$$DHI_{\mathrm{RSI}} = CFd \cdot \left[DHI_{\mathrm{raw}} + GHI_{\mathrm{RSI}} \cdot (0.0359 - 5.54 \cdot 10^{-6} \cdot GHI_{\mathrm{RSI}} \right] \tag{5.7}$$

3. The corrected and calibrated DNI (DNI_{RSI}) is determined as:

$$DNI_{\mathrm{RSI}} = CFn \cdot \frac{GHI_{\mathrm{RSI}} - DHI_{\mathrm{RSI}}}{\cos(SZA)} \tag{5.8}$$

5.3 Calibration method Kern

Another calibration method is practiced by Irradiance Inc. and has been examined by [Kern, 2010]. This method calibrates for GHI only and replaces the sensor manufacturers calibration factor CF_{Licor}. Therefore, this calibrations can be performed without mounting the sensor on a RSI since no DHI measurement and thus no shadowband is required.
The method applies GHI correction functions (Temperature, spectral response and cosine response) which were published in [King et al., 1998] (see section 3.1). The calibration factor is determined by averaging the ratios between RSI and a reference. The following will outline a brief overview of the procedure:

1. The reference instruments and data logger are of the same class as in the DLR methods (sections 5.1 and 5.2). The reference GHI is calculated from a pyrheliometer and a shaded pyranometer.
2. The LI-200 sensors are horizontally mounted on a calibration table in close proximity of the reference.
3. Data is continuously collected over a period of 12 to 49 days and divided into 7 to 33 series.

4. Test GHI is sampled in 3 second intervals and recorded as 1 minute averages.
5. GHI_{Ref} is also recorded as 1 minute means.
6. Operational problems and relevant events are recorded in a log-book.
7. The data treatment includes an automatic check for validity of the measurements using the Data Quality Management System by Augustyn & Company.
8. Measurements are filtered for following requirements:
   $10\ \text{W/m}^2 < GHI < 1500\ \text{W/m}^2$, and $AM \approx 1.5$ (at the measuring site in [Kern, 2010] the AM requirement translated into $56.8° < SEA < 58.8°$). Additionally a GHI fluctuation of less than 10 W/m^2 per minute is required. Clear sky conditions are ensured by using the DNI and the [Bird, 1984] model (see [Kern, 2010]).
9. Preliminary calibration factors are calculated as the ratio between corrected GHI_{cor} and GHI_{Ref} and reviewed by the operator.
10. Those series whose preliminary calibration factors deviate by more than 5 % from the mean are excluded.
11. The final calibration factor is calculated as the mean of the remaining preliminary factors.

5.4 Calibration method Vignola et al., 2017

The most recent and most physical correction functions from [Vignola et al., 2017] are described already together with an appropriate calibration method. The method uses a reference station with thermal pyranometers and pyrheliometers and determines a DNI and a DHI calibration factor. In addition also the SZA dependency is determined for each sensor. The procedure for DNI calibration is summarized as follows:

1. Determine a preliminary calibration factor to obtain a DNI as close as possible to the reference DNI from the RSI's DNI
2. After adjusting for the temperature dependence of the pyranometer, determine the DNI responsivity as a function of the SZA and normalize these correction factors to 1 at SZA=45°
3. Calculate clear sky DNI spectra a a function of the SZA for the expected conditions during the calibration and, using the typical spectral response of the pyranometer, determine the spectral error and the appropriate correction factor. Normalize these correction factors to 1 at SZA=45°.
4. Multiply the instrument DNI values that are temperature adjusted by the spectral correction factor and obtain a cosine correction function as a function of SZA by dividing the spectrally corrected DNI values by the measurements of the reference pyrheliometer.

For DHI the following procedure is used:

1. Determine a preliminary calibration factor under clear sky conditions to obtain a DHI as close as possible to the reference DHI from the RSI's DHI
2. After adjusting for the temperature dependence of the pyranometer, determine the DHI responsivity as a function of the SZA and normalize these correction factors to 1 at SZA=45°
3. Calculate clear sky DHI spectra as a function of SZA for the expected conditions during the calibration and, using the typical spectral response of the pyranometer, determine the spectral error and appropriate correction factor. Normalize these correction factors to 1 at SZA=45°.
4. The DHI correction factor for totally and partially cloudy skies is a function of the clear sky DHI adjustment factor and the clear sky DNI adjustment factor depending on the cloudiness. If data are available, a fit to local data can be determined. Otherwise use the generic fit in [Vignola et al., 2017].
5. If the sensor is used at a site with different climate the spectral correction factors can be derived for the local clear sky spectra and applied instead of those for the conditions during the calibration.

If the sensor is used at a site with different climate the spectral correction factors can be derived for the according clear sky spectra and applied instead of those for the conditions during the calibration.

6 Comparison of RSI calibration to calibration of thermopile sensors

As elaborated in section 2 there are distinct differences between thermopile sensors and the LI-200 Si-pyranometer. Additionally, RSIs are used to determine three irradiance components virtually at once while pyranometers and pyrheliometers measure only one component (or at least one at a time in the case of pyranometers). Due to its attributes the RSI requires very specific calibration procedures (section 5) which also involve correction of its systematic errors (section 3).
All calibration methods for pyranometers and pyrheliometers with thermopiles use similar modes of data collection and the same basic principles of data treatment. While the Kern method is orientated along these principles, the RSI calibration methods performed by DLR and the Vignola et al., 2017 method differ in both areas. The duration of data acquisition, the data rejection process and calculation of calibration factors are fundamentally different.
In the following the calibration methods are compared in regards to the measuring equipment, measuring site, mode of data acquisition and data treatment. The different requirements in these categories are summarized in table 6.1.

6.1 Measuring equipment

All calibration methods under discussion except pyranometer calibration with a reference pyranometer (section 4.2.3) involve the use of a tracking system for either field or reference instruments or both. Pyranometer calibration with pyrheliometers and RSI calibration require a tracked shading device. All calibration methods involve sensors for measurements of ambient temperature and where possible temperature of the irradiance sensors.
Besides the RSI itself the RSI calibration methods by DLR employ the same setup of equipment as the continuous sun- and shade method (section 4.2.2) for measurement of DNI, DHI and GHI.
Since the photodiode sensor has a higher uncertainty than thermopile pyranometers the instructions in regard to tracking and installation of the measuring system given in [ISO 9846] are downward compatible and can be transferred to RSI calibration.
The requirements for the data logger's voltage measurement from the existing calibration standards are also applicable to RSI calibration.

Table 6.1: Comparison of selected requirements in RSI and thermopile sensor calibration

Calibration method	Data sampling	Duration	Irradiance	SEA	cloud conditions
Pyrheliometer					
[ISO 9059]	20 series of 10 to 20 min	≥ 3 days	$DNI \geq 300$ W/m^2 better: $DNI \geq 700$W/m^2	intended field $SEA \pm 5°$	<12 % of sky >15° distance from sun
Pyranometer					
[ISO 9846], alternating sun/shade	≥ 10 series of ≤ 36 min	≥ 3 days	-	-	>45° distance from sun
[ISO 9846], continuous sun/shade	10 to 20 series of 10 to 30 min	≥ 3 days	-	-	>45° distance from sun
[ISO 9847], cloudless sky	≥ 15 series of 10 to 20 min	2 to 3 days	$DNI \geq 0.8 \cdot$GHI	>20°	clear sky
[ISO 9847], unstable sky	≥ 15 series of 1 to 5 min	5 to 14 days	$DNI \geq 0.8 \cdot GHI$	>20°	>30° distance from sun
[ISO 9847], cloudy sky	≥ 50 integrated intervals of 1 hour each	≥ 10 days	mean $GHI > 100$ W/m^2	-	-
RSI					
Both DLR methods	continuous	30 to 120 days	$GHI > 10$ W/m^2 $DHI > 10$ W/m^2 $DNI > 300$ W/m^2	>5°	-
Kern	continuous, division into 7 - 33 series	12 to 49 days	$GHI > 10$ W/m^2 GHI changes < 10 W/(m$^2 \cdot$min)	- 56.8°to 58.8°	clear sky

6.2 Site variables

Due to pyranometers 360° field of view angle all calibration methods which involve this type of instrument require the absence of reflections from objects in the vicinity above the sensor as well as on the horizon. Such reflections can cause additional irradiance on the sensor and thus affect the measured value. Also objects on the horizon should not obscure the sun. The LI-COR Si-pyranometer has a 360° field of view angle as well and its calibration involves thermopile pyranometers. Thus, these aspects need to be considered in RSI calibration. In pyrheliometer calibration this is not the case since the pyrheliometer's field of view is restricted by its aperture. While in [ISO 9846] for pyranometer calibration with a pyrheliometer this requirement is not further quantified [ISO 9847] (pyranometer calibration using a reference pyranometer) limits the elevation angle of objects on the horizon to <5°. This limit also occurs in RSI calibration since only measurements taken during SEA>5° are used (see table 5.2).

6.3 Data acquisition and treatment

Data aquisition

In calibration of pyranometers and pyrheliometers measurements are taken in 10 to 20 series of up to 36 minutes each. Exception to this rule is a variation of the outdoor calibration method for cloudy sky conditions as defined in [ISO 9847] (calibration of pyranometer using a pyranometer, see section 4.2.3) where measurements are taken in sets of one hour duration over a period of at least 10 days. In terms of duration this method is the closest to RSI calibration methods.

However, the RSI calibration methods require substantially longer measuring periods in order to include a sufficient variety of spectral composition of irradiance. This is owed to the nonuniform responsivity of the LI-COR sensor. In order to produce accurate measurements with a calibrated RSI during varying conditions the calibration needs to cover a similar variety.

Both [ISO 9059] and [ISO 9846] require low wind speeds (not further specified) and directions other than towards the pyrheliometers aperture. As stated in [ISO 9059], this is relevant only where a pyrheliometer with an open aperture (e.g. an absolute cavity pyrheliometer) is involved. If field pyrheliometers are used as a reference instrument or if the test sensors's uncertainty is significantly higher than the uncertainty caused by the wind, this restriction is not required. Both is the case in RSI calibration and hence the wind speed is not relevant.

Furthermore, calibration methods for thermopile sensors have varying individual requirements in regards to aspects such as overall cloudiness and position of clouds and turbidity. Clouds reduce the overall GHI as well as and especially the DNI if they mask the sun. Clouds can

also reflect radiation if they are close to the sun and hence increase GHI. Since these are the measurands for pyranometers and pyrheliometers respectively a high energy flux in each is desirable during calibration. In pyrheliometer calibration the required angular cloud distance from the sun is half as much as in pyranometer calibration due to the pyrheliometers narrower field of view. On the other hand, pyrheliometer calibration requires a very low overall cloudiness. For turbidity related requirements in pyrheliometer calibration see section 4.1.
Similarly, also the Kern method only calibrates with data collected during very specific meteorological conditions. Clear sky conditions at an $AM1.5$ are desired.

Data rejection

All methods reject measurements which took place during documented operational problems. In other aspects the data rejection in DLR methods for calibration of RSI differs from Kern and thermopile calibration. The rejection criteria for Vignola et al, 2017 are currently not published.
DLR2008 and DLR-VigKing: Data rejection takes place in three ways. First, an automated screening for quality of the recorded measurements is applied [Geuder et al., 2015]. Second, rejection is done by an experienced operator who identifies erroneous data by visually comparing the course of measurements and if necessary, by investigating documented records and collected data from other instruments in the vicinity. And ultimately, by automated screening for CL in dependence which calibration factor is calculated (see section 5.1). This includes rejecting all RSI measurements which deviate by more than 25 % from the reference.
The CL include thresholds for the acceptable minimum irradiance and SEA. While the CL threshold for GHI and DHI lower than a limit given in [ISO 9847] for pyranometer calibration with pyranometers and cloudy conditions the DNI threshold matches the minimum tolerable DNI during pyrheliometer calibration. The DNI and SEA requirements in DLR2008 and DLR-VigKing are owed to the purpose of solar resource monitoring since CSP plants only operate during these conditions.
Thermopile sensors and Kern: The deviation of preliminary calibration factors is used as a common criteria for rejecting individual measurements. For each measurement it is compared to the mean of all preliminary calibration factors in its respective series. The threshold differs between the methods and ranges from 1 % to 5 %. For example, in pyranometer calibration methods a whole series is discharged once half of its measurements has been rejected.

Correction functions

In all RSI calibration methods functional corrections are applied for a range of parameters. Calibration of thermopile sensors only have temperature corrections (and in some pyranometers incidence angle correction) in common with RSI calibration. However, such corrections during thermopile calibration are applied only on a case to case basis since they influence the

measured irradiance less than for RSIs. These differences are a direct result of the LI-200 sensor's systematic errors.

Calculation of calibration factors

Calibration methods for pyranometers and pyrheliometers as well as the Kern method calculate a single calibration factor by determining the mean value of the ratio between reference and field instrument measurements. RSI calibrations by DLR or the Vignola et al., 2017 method on the other hand determine two or three separate calibration factors. Additionally, the LI-200 sensors calibration factor assigned by the manufacturer is used during calibration and needs to be applied along with the new calibration factors during field deployment of the calibrated instrument. The SZA dependence can be added to the calibration result for thermopile sensors and this is also the case for the Vignola et al. 2017 method.

Statistical analysis

The quality of calibration of thermopile sensors and RSI calibration by Kern is evaluated by using the STD. Only in the outdoor calibration method described in [ISO 9847] (section 4.2.3) a clear limit is given for acceptable STD. In RSI calibration at DLR bias, STD and RMSD of the RSI from the reference are reviewed. Bias can occur for RSI calibration with these methods due to the minimization of the RMSD. The optimization parameters for Vignola et al, 2017 are currently not published.

6.4 Summary

It was found that the requirements and instructions in regard to tracking and set up of the measuring system in the continuous sun- and shade method [ISO 9846] as well as the limit of an elevation angle of 5 °for objects on the horizon from [ISO 9847] have been transferred to RSI calibration. Other than these two aspects the RSI calibration has different requirements and procedures. Table 6.1 lists an excerpt of the discussed aspects for comparison.
Since RSI are used for determination of three measurands with different spectral compositions the assignment of multiple calibration factors is one of the most apparent advantages of the DLR and Vignola et al., 2017 methods in comparison to Kern (see section 5). For this purpose the test measurements are taken while the RSI's Si-pyranometer is mounted in an operational RSI instead of on a calibration table without the rotating shadowband. Furthermore, the data used in DLR calibrations includes a variety of spectral and other meteorological conditions as they occur during the operation of a CSP plant. All RSI calibration methods use correctional functions to compensate the LI-COR sensor's systematic errors.
Calibration of thermopile sensors on the other hand uses data with preferably high intensity of the measurand. Under such conditions a smaller amount of data is required. As seen in

[ISO 9847] (section 4.2.3), the lower the irradiance conditions are the longer the measuring period has to be.
The range of calibration duration presently used for RSI calibrations at DLR (see table 6.1) is rather wide. It is desirable to either narrow the range or to clarify the specific conditions under which a longer or shorter duration is required. This will be addressed in chapter 7.

7 Evaluation of RSI calibration duration

7.1 Introduction

Since the RSI calibration at DLR is optimized for determination of *DNI* the same should be the case for its duration. In general the measuring period should include all relevant weather conditions. Its necessary duration can vary in dependence on the location [Geuder et al., 2014]. Furthermore, some sites may not be suitable for calibration measurements during certain times of the year. At the PSA however, calibrations are assumed to be possible throughout the year.

Since timely delivery of the calibrated instruments is important to the end user, this aspect needs to be taken into consideration. Nonetheless, the calibration duration should be long enough to keep the fluctuation of results of individual calibrations within acceptable limits. In addition to evaluating the calibration duration in terms of stability of results the possibility of seasonal influences shall be investigated as well.

To both ends, results of multiple short-term calibrations need to be compared to the result of a calibration with the longest possible measuring duration which is assumed to deliver the best result. For technical reasons the direct comparison was substituted by an alternative method which is expected to provide equivalent conclusions as will be elaborated in section 7.2.

A total of seven long-term data sets from five instruments (see table 7.1 and figure 7.1) has been evaluated in regard to *DNI* for durations from 1 day up to 180 days duration.

The majority of these data sets was courteously provided by Suntrace GmbH for which the authors wish to express their gratitude.

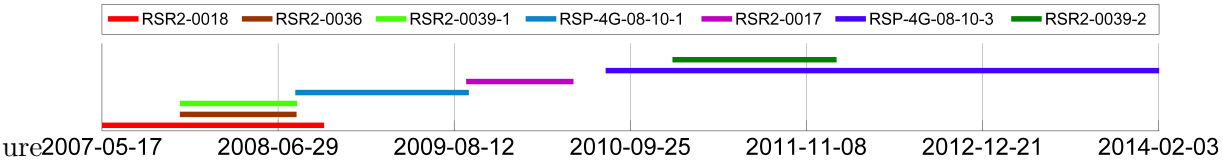

Figure 7.1: Evaluated data sets. Total period covered (including the gap between RSR2-0017 and RSP-4G-08-10-3): 2342 days or ~6.5 years

Table 7.1: Evaluated data sets

Instrument	from	to	Duration [days]
RSP-4G-08-10-1	2008-08-08	2009-09-16	404
RSP-4G-08-10-3	2010-07-29	2014-02-07	1289
RSR2-0017	2009-09-09	2010-05-16	251
RSR2-0018	2007-05-17	2008-10-15	517
RSR2-0036	2007-11-12	2008-08-12	274
RSR2-0039-1	2007-11-12	2008-08-13	292
RSR2-0039-2	2011-01-01	2012-01-18	382
Total (with overlapping)			3391
Total (without overlapping)			2342

7.2 Evaluation method

In order to compare the results of short-term calibrations to the results of long-term calibrations, a large number of calibrations would be necessary to derive statistically sound conclusions. Although in the course of this project a modification of the calibration software was programmed to produce calibrations of moving intervals with varying duration this method has been given up due to the excessive time consumption of calculations and its workspace memory issues in Matlab. Therefore, a different method has been applied which was already used in [Geuder et al., 2014].
The following sections 7.2.1, 7.2.2 and 7.2.3 line out the chosen method of data treatment and its validation. These sections refer to DLR2008 but the method was also applied to DLR-VigKing with its respective correction functions and calibration factors.

7.2.1 Moving average method

For differentiation from an evaluation based on actual short-term calibration results this evaluation method as outlined in the following shall be referred to as the moving average method (MAM). An instrument is calibrated for a long-term measuring period. The thereby derived calibration factors CFG_{longcal} and CFD_{longcal} are applied to the functionally corrected RSI raw data. This produces functionally corrected and calibrated 10 minute mean values of the RSI measurements from the calibration period. The same manual and automatic data exclusion including CL as applied during the calibration process is kept in place while calculating the ratios of reference to RSI irradiance $R_{\text{GHI,wd}}$, $R_{\text{DNI,wd}}$ and $R_{\text{DHI,wd}}$ along equations 7.1 to 7.3.

$$R_{\text{GHI,wd}}(t) = \frac{GHI_{\text{Ref}}(t)}{GHI_{\text{RSI}}(t)} \tag{7.1}$$

$$R_{\mathrm{DNI,wd}}(t) = \frac{DNI_{\mathrm{Ref}}(t)}{DNI_{\mathrm{RSI}}(t)} \tag{7.2}$$

$$R_{\mathrm{DHI,wd}}(t) = \frac{DHI_{\mathrm{Ref}}(t)}{DHI_{\mathrm{RSI}}(t)} \tag{7.3}$$

where:	GHI_{RSI}	:	corrected and calibrated RSI GHI
	DNI_{RSI}	:	corrected and calibrated RSI DNI
	DHI_{RSI}	:	corrected and calibrated RSI DHI
	t	:	timestamp

In the next step the data needs to be checked for sensor drift as elaborated in section 7.2.2. Thereafter the (if necessary) drift corrected ratios R_{GHI}, R_{DNI} and R_{DHI} are used to calculate their moving average (here: moving in steps of 24 hours) values for moving short-term intervals of duration T:

$$M_{\mathrm{R,GHI}}(T, t_d) = \frac{1}{n} \cdot \sum_t R_{\mathrm{GHI}}(t) \quad \text{with} \quad t \in \left[t_d - \frac{T}{2} \quad , \quad t_d + \frac{T}{2} \right] \tag{7.4}$$

$$M_{\mathrm{R,DNI}}(T, t_d) = \frac{1}{n} \cdot \sum_t R_{\mathrm{DNI}}(t) \quad \text{with} \quad t \in \left[t_d - \frac{T}{2} \quad , \quad t_d + \frac{T}{2} \right] \tag{7.5}$$

$$M_{\mathrm{R,DHI}}(T, t_d) = \frac{1}{n} \cdot \sum_t R_{\mathrm{DHI}}(t) \quad \text{with} \quad t \in \left[t_d - \frac{T}{2} \quad , \quad t_d + \frac{T}{2} \right] \tag{7.6}$$

where:	t_d	:	12:00 pm timestamps within long-term period
	n	:	Number of timestamps in short-term interval

Thereafter, the ratio Π of the moving short-term means to the long-term mean of the whole measuring period is calculated. Π represents the deviation of daily short-term calibrations from the long-term calibration with sufficient accuracy as will be shown in section 7.2.3. All further statistical analysis for calibration duration represented by T will be based on its respective course of Π.

$$\Pi_{\mathrm{GHI}}(T, t_d) = \frac{M_{\mathrm{R,GHI}}(T, t_d)}{L_{\mathrm{R,GHI}}} \tag{7.7}$$

$$\Pi_{\mathrm{DNI}}(T, t_d) = \frac{M_{\mathrm{R,DNI}}(T, t_d)}{L_{\mathrm{R,DNI}}} \tag{7.8}$$

$$\Pi_{\mathrm{DHI}}(T, t_d) = \frac{M_{\mathrm{R,DHI}}(T, t_d)}{L_{\mathrm{R,DHI}}} \tag{7.9}$$

where:	$L_{\mathrm{R,GHI}}$	:	Mean value of R_{GHI} over whole long-term duration

$L_{R,DNI}$	:	Mean value of R_{DNI} over whole long-term duration
$L_{R,DHI}$	:	Mean value of R_{DHI} over whole long-term duration

7.2.2 Elimination of sensor drift

In some data sets a significant drift of the sensor's responsivity was observed. In [Geuder et al., 2014] it was stated that in rare cases the drift of a sensor can exceed the ±2 % per year (see [LI-COR, 2011]) specified by the manufacturer. However, most of the sensors examined in [Geuder et al., 2014] exhibited a drift of less than 1 % per year.
The RSI calibration software for the DLR2008 and DLR-VigKing methods as well as the Kern method do not take drift into account. Since drift occurs over time its effect on short-term calibrations is relatively small. However, in regards to long-term calibrations drift needs to be addressed because the derived calibration factors will refer to the mean of the sensors responsivity during the calibration period. The irradiance before and after the point of time when the mean responsivity occurs will either be under- or overestimated.

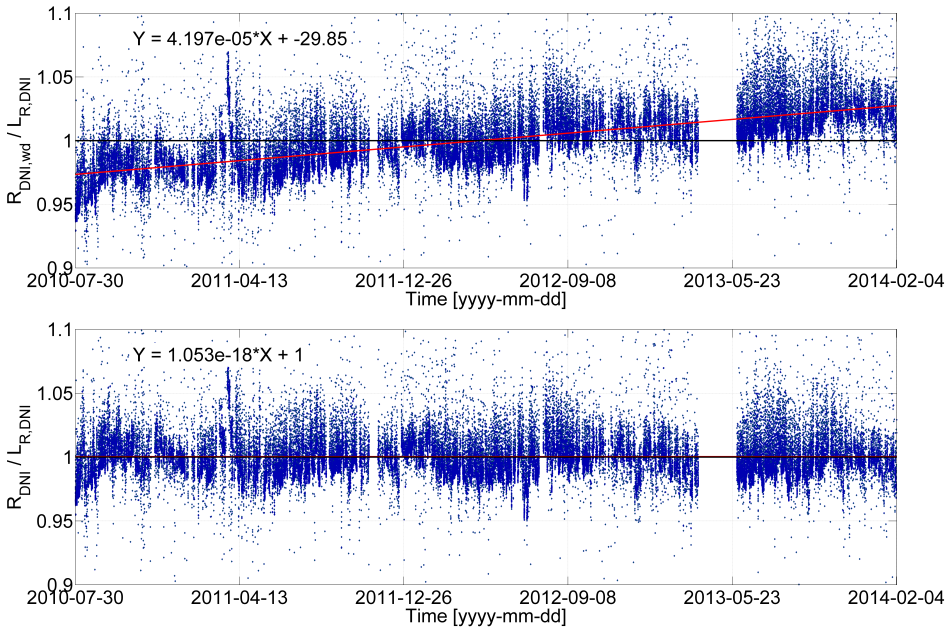

Figure 7.2: Course of R_{DNI} / $L_{R,DNI}$ in 10 min values for RSP-4G-08-10-3. The upper graph is before (subscript "wd": with drift) and the lower graph is after drift elimination.

Therefore, the drift affects the ratios of reference to RSI irradiance which subsequently causes a rotation of the Π course. Figure A.3 in the Appendix shows a clear example of this for a 3.5 years calibration.
Without removing the influence of drift from strongly affected data any statistical evaluation of Π in regards to fluctuation of calibration results will be inherently flawed due to its extreme values towards the beginning and end of the period.

It was found that the influence of drift can be removed from the Π_{DNI} by correcting the data after calibration took place. To this end a linear fitting function is placed through the ratio of $R_{\mathrm{DNI,wd}}$ to $L_{\mathrm{R,DNI}}$ (see upper graph in figure 7.2). As defined in section 7.2.1 the $R_{\mathrm{DNI,wd}}$ are the 10 min averages of the ratio between the reference and the corrected and calibrated RSI DNI. Since $L_{\mathrm{R,DNI}}$ is the mean of $R_{\mathrm{DNI,wd}}$ the average of the ratio between the two is 1. The drift is removed by dividing the $R_{\mathrm{DNI,wd}}$ by the linear fitting function. Thereafter, in order to check the result the ratio of the corrected R_{DNI} to the original $L_{\mathrm{R,DNI}}$ is plotted anew (lower graph in figure 7.2). Due to inaccuracy of the fitting function in some cases this process may cause an offset of the now horizontally aligned graph. In such cases the process is repeated (the new fitting function is a horizontal line representing the offset) until the mean of the corrected R_{DNI} is identical to the original $L_{\mathrm{R,DNI}}$.
Similarly, this process is carried out for GHI and DHI as well.

Even though this process is required in some cases it has to be used with care since the algorithm can not differentiate between seasonal changes and sensor drift. Therefore, this data treatment was only applied where the fitting function represents a clear non-seasonal drift (see section A).

7.2.3 Validation of the moving average method

In order to verify that the moving mean method is a valid strategy for the purpose of this evaluation the following calculations have been performed in regard to DNI.
First, a number of short-term calibrations was carried out for a given set of raw data (RSR2-0018 in the examples below) from a long-term measuring period.
For each short-term calibration the obtained calibration factors CFG_{shortcal} and CFD_{shortcal} depend on its period of time which is defined by its interval duration T and its middle timestamp t_d. The calibration factors were applied to the corresponding data set which produced a separate set of calibrated DNI_{shortcal} for each combination of T and t_d. DNI_{longcal} is defined similarly, using the results of the long-term calibration CFG_{longcal} and CFD_{longcal}.
The DNI_{shortcal} and DNI_{longcal} were then put in relation by calculating $\Pi_{\mathrm{cal,DNI}}$, the mean of the ratio of the former to the latter for the time period that corresponds to the respective short-term calibration.

$$\Pi_{\mathrm{cal,DNI}}(T, t_d) = \frac{1}{n} \cdot \sum_{t} \frac{DNI_{\mathrm{shortcal}}(T, t_d, t)}{DNI_{\mathrm{longcal}}(t)} \qquad \text{with} \qquad t \in \left[t_d - \frac{T}{2} \quad , \quad t_d + \frac{T}{2} \right] \tag{7.10}$$

Finally, $\Pi_{\mathrm{cal,DNI}}$ was compared to the Π_{DNI} for each short-term interval in respect to coincidence. In this way it is possible to estimate if the results of the MAM are sufficiently representative for the deviation of actual short-term calibration results from a long-term calibration.

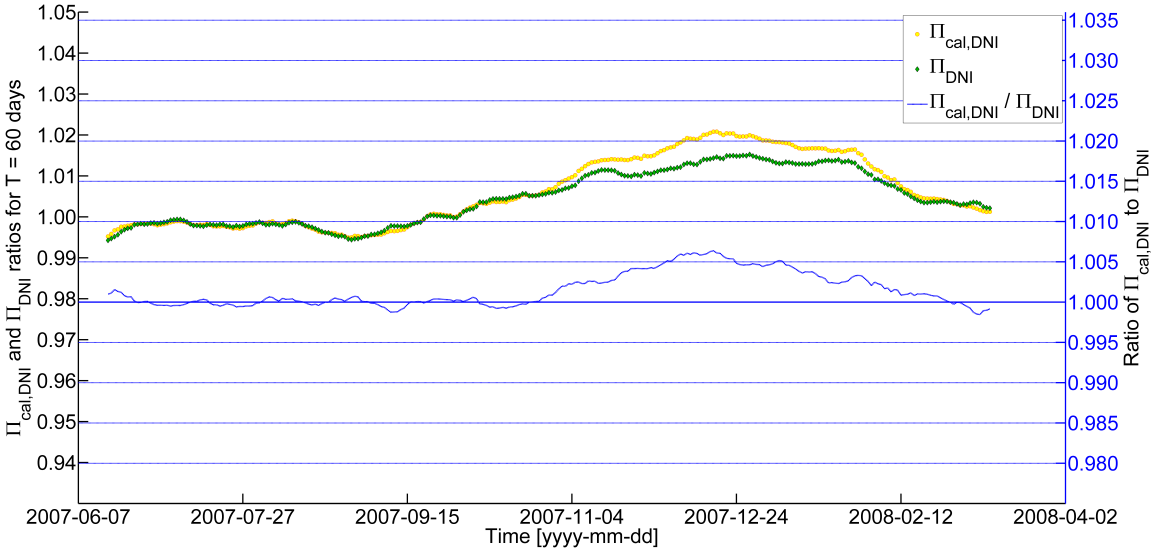

Figure 7.3: Comparison of course of Π_{DNI} and $\Pi_{cal,DNI}$ for 270 calibrations with T=60 days. Evaluated data set: RSR2-0018.

Figures 7.3 and 7.4 show the correlation between Π_{DNI} and $\Pi_{cal,DNI}$ for 270 calibrations of 60 days duration and for 428 calibrations of 90 days duration. These examples exhibit a maximum deviation of the Π_{DNI} from the $\Pi_{cal,DNI}$ of about ±0.5 %. However, during most of the examined periods the coincidence is within ±0.2 %. Further exemplary comparisons have been performed with similar outcome. Therefore, within it's limitations the MAM can be considered sufficiently accurate for the purpose of investigating general tendencies of short-term calibrations in comparison to long-term calibrations.

7.2.4 Comparison to data treatment in [Geuder et al., 2014]

The starting point of this investigation was the work presented in [Geuder et al., 2014] where the data set RSR2-0018 was evaluated in regard to calibration duration by using the MAM. Π_{DNI} was plotted for a period of six months from a 17 month data set for one day, one week and one month calibrations. This was accomplished by using an Excel-sheet with implemented visual basics code which used to be the standard for RSI calibrations at DLR before the presently used software was developed. It was found that at the PSA a site specific minimum duration of one month should be sufficient for satisfactory calibration results [Geuder et al., 2014].
In the course of this present work the RSR2-0018 data set has now been reevaluated for the whole 17 months. Additionally, the original plot (figure 7.5) has been reproduced in order to ensure correct understanding of the previous work and to address eventual differences.
The new calculations show a similar result. However, they differ from the original ones which

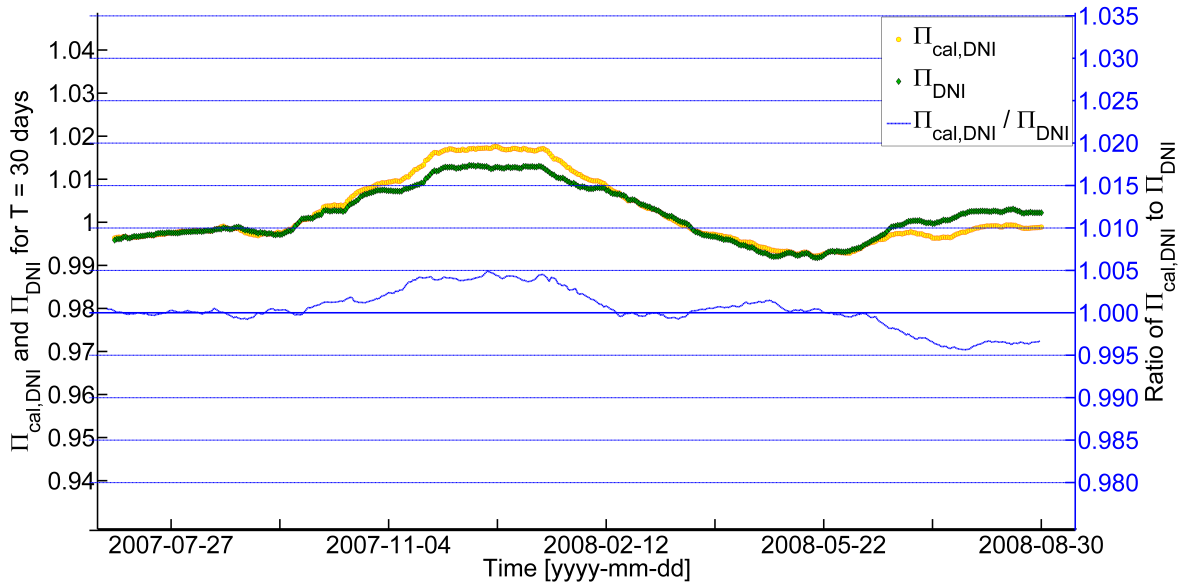

Figure 7.4: Same as figure 7.3 for 428 calibrations with T=90 days.

Table 7.5: Calibration limits used in [Geuder et al., 2014] plot for RSR2-0018

Reference *DNI* **[W/m²]**	> 250
Reference *GHI* **[W/m²]**	> 10
Reference *DHI* **[W/m²]**	> 10
Sun height angle [°]	> 5
Max deviation of RSI raw data from reference [%]	± 15

can be compared by the plots in figures 7.5 and 7.6. Since the original calculation's data files and programs were available, the origin of these differences was investigated by step by step comparison. First of all, it has to be noted that the original plot from [Geuder et al., 2014] was done for DLR-VigKing calibration (section 5.2) with the exception of using different definitions for the correction functions F_B [King et al., 1997] and F_C [Vignola, 2006]. For further details on varying definitions of correction functions the reader is referred section 3.1. Secondly, the calibration limits for data exclusion used at the time (see table 7.5) differ from those in table 5.2 which are used today. In the case of the RSR2-0018 data set only negligible drift was present. This was already stated in [Geuder et al., 2014]. Thus, neither in the previous nor in the present work drift correction was considered necessary.

Another minor difference is that the presently used calibration software substitutes missing ambient pressure measurements by an estimated value while the Excel-sheet didn't perform a calculation in such cases. Additionally, the plot by [Geuder et al., 2014] associated the Π_{DNI} values to the first timestamp of their intervals while the new plots presented in this work place

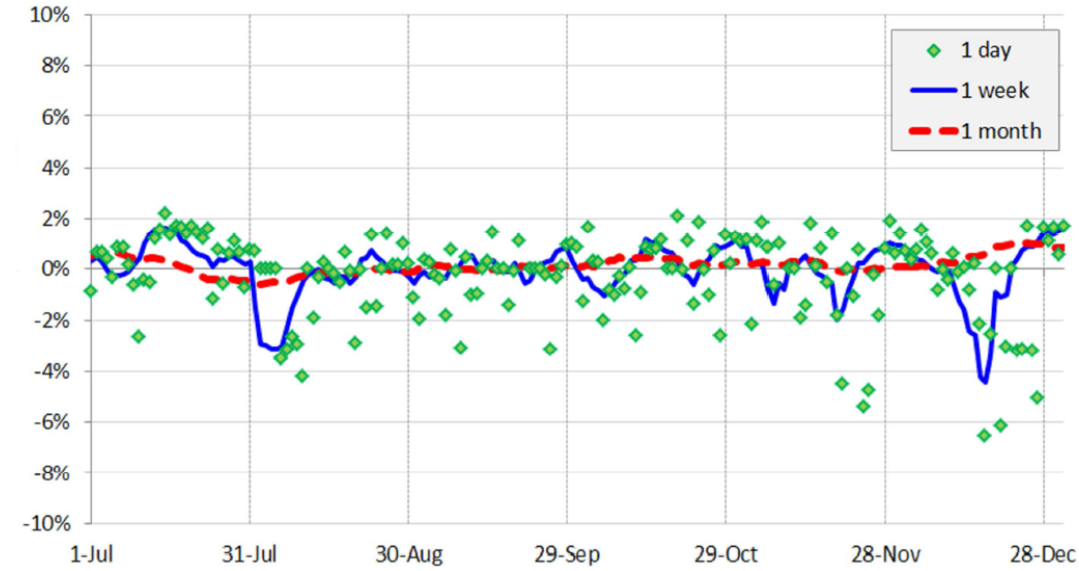

Figure 7.5: Course of Π_{DNI} in RSR2-0018 data set of 2007 as presented in [Geuder et al., 2014]; based on DLR-VigKing calibration with definitions for F_B and F_C as given in [King et al., 1997] and [Vignola, 2006]. The vertical axis refers to Π_{DNI}. The horizontal axis refers to the date.

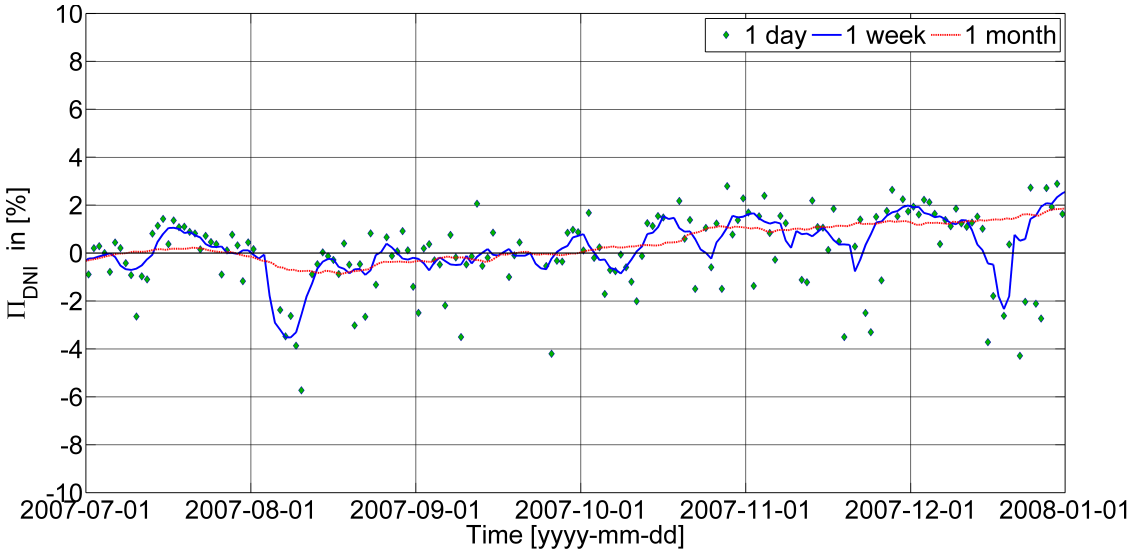

Figure 7.6: Same as 7.5 with definitions for F_B and F_C as specified in section 3

them in middle of their intervals. This causes a horizontal shift of the curves which represent moving mean intervals of more than one day.
In detail comparison revealed that the greater part of the differences between the graphs in both figures 7.5 and 7.6 was caused by the differing definitions of F_B and F_C. Subsequently, in both the Excel-sheet and the software used in the present work it was possible to reproduce the result of the other by adjusting the definitions of F_B and F_C. Therefore, both evaluation tools have the same validity with respect to the definitions they use.

7.3 Data analysis

In the following the data sets which were introduced in section 7.1 will be evaluated in regard to the influence of calibration duration on calibration results based on Π_{DNI} (see MAM in section 7.2.1). As elucidated in section 7.2.2 it was necessary to remove sensor drift from some data sets. This was the case for RSP-4G-08-10-1, RSP-4G-08-10-3 and RSR2-0039-2. A discussion of the presence of drift in individual data sets can be found in Appendix A.

7.3.1 Calibration duration - DLR2008

Figure 7.7 displays the distribution of Π_{DNI} for each data set (table 7.1) for varying calibration duration in form of boxplots. The equivalent plots for Π_{GHI} and Π_{DHI} can be found in the Appendix (figures B.7 and B.8).
Boxplots visualize a number of statistical parameters which help to characterize the distribution of values in a set of data. Since some readers might not be familiar with boxplots the following provides a brief summary. See table 7.6 for reference.
The upper and lower edges of the box itself are defined by the 0.25-quantile (lower quartile, Q1) and the 0.75-quantile (upper quartile, Q3). The difference between both defines the interquartile range (IQR) which therefore includes half of all values. The 0.5-quantile (median, Q2) is represented by the horizontal line within the box. The boxplots used here also include the arithmetic mean which is represented by a circle. For the outer whiskers different definitions can be used. In this version the whiskers are defined as the lowest value greater than Q1$-1.5\cdot$IQR and the highest value smaller than Q3$+1.5\cdot$IQR. In the case of normal distribution they include 99.3 % of all values. The values outside the whiskers are shown as individual data points and considered as potential outliers. By the whiskers the reader can identify the maximum deviation from zero.

Generally, for short durations T the data sets are symmetrically distributed around zero. With increasing T the range of distribution of Π_{DNI} values narrows. As the interval duration T increases the whiskers get closer to zero while the symmetry is reduced. In most data sets

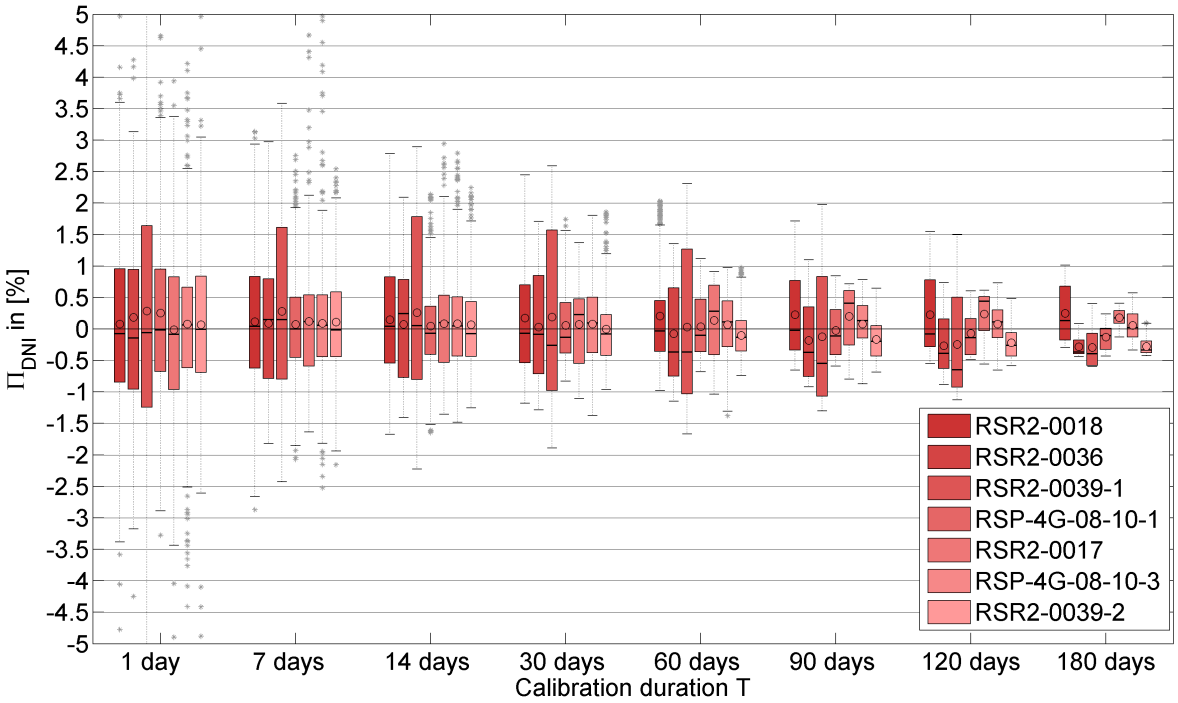

Figure 7.7: Π_{DNI} in dependence on calibration duration for seven data sets.

Table 7.6: Boxplot definitions

Q1	Lower quartile or 0.25-quartile. 25% of all values ≤ Q1
Q2	Median or 0.5-quartile. 50% of all values ≤ Q2
Q3	Upper quartile or 0.75-quartile. 75% of all values ≤ Q3
IQR	Interquartile range. IQR=Q3−Q1
Lower whisker	lowest value > Q1−1.5·IQR
Upper whisker	highest value < Q3+1.5·IQR
Lower potential outliers	All values < lower whisker
Upper potential outliers	All values > upper whisker
Mean	Arithmetic mean of all values

zero is outside the IQR for $T = 180$ days.
In figure 7.7 it can be observed that all evaluated T including single day calibrations produce in about half of all data sets $M_{R,DNI}$ within ±1 % their respective $L_{R,DNI}$. However, the rest of the single day moving averages reach deviations in the range of ±15 % from the respective long-term mean. Similar behavior was observed for duration of up to seven days with slight reductions of scatter.
A significant reduction of scatter was reached with increasing the duration to 14 days. For $T = 14$ days all Π_{DNI} stayed within the range of ±3 %. Scatter keeps reducing with increasing calibration duration.
Comparing the results of $T = 30$ to $T = 60$, for all data sets in figure 7.7 except RSR2-0039-1 the range of Π_{DNI} reduced from ±2.5 % to ±1.75 % and less. Except for RSR2-0039-1 all upper whiskers reduced their value by at least 0.5 %.
Further increase of duration T from 60 days to 90 days yields reduction of Π_{DNI} whiskers by less than 0.25 % for the cost of increasing the measurement period by its half. Longer durations than $T = 90$ days are rarely considered practicable due to time consumption. Therefore, up to this point the sighting of distributions of Π_{DNI} confirm DLR's general preference of a $T = 60$ days calibration duration. However, evaluation of seasonal tendencies as discussed in the following section 7.3.2 implicated an alternative approach to calibration duration.

7.3.2 Calibration duration: seasonal influences - DLR2008

In order to identify seasonal tendencies the Π_{DNI} for $T = 14$ days, $T = 60$ days, $T = 90$ days and $T = 180$ days were plotted over the time span of the long-term calibration measuring period for various RSIs. While evaluating the timelines it needs to be considered that each plotted data point refers to the middle timestamp of its interval (see section 7.2.1).
Out of all available data sets the RSP-4G-08-10-3 covers the longest time span and is therefore most useful to observe seasonal changes although a two month period of erroneous data (2013-04-01 to 2013-05-30) had to be excluded from calibration.
The horizontal axis in figure 7.8 indicates the date. The first day of each month is represented by a grey vertical line. The left vertical axis displays Π_{DNI}. The second vertical axis provides the daily number of timestamps which where usable for calibration.
The number of usable timestamps per day clearly coincides with the seasons, reaching its peak around solstice in middle of June and its minimum around solstice in middle of December while spring and autumn behave similar to each other. This is common to all data sets (table 7.1) at hand and is a clear correlation to the daily hours of daylight. Therefore, a calibration of the same duration differs in the amount of usable data in dependence on the time of the year it is performed in. For detailed Π_{DNI} curves of each individual data set introduced in table 7.1 see figure 7.8 and in the Appendix figures B.1 to B.6.

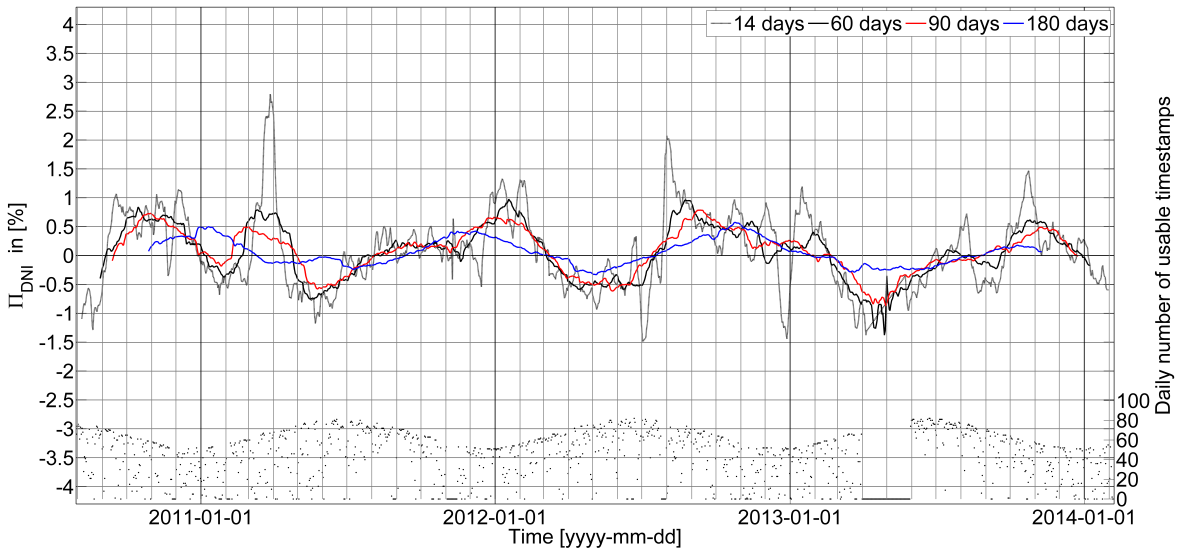

Figure 7.8: Course of Π_{DNI} for varying calibration duration for RSP-4G-08-10-3 with daily number of usable timestamps. The vertical gridlines indicate the first day of each month.

Because the RSP-4G-80-10-3 data set begins in summer and ends in winter, all seasons are equally represented in the long-term mean $L_{\mathrm{R,DNI}}$ of the reference/RSI ratio. Around early summer Π_{DNI} often reaches a negative percentage for all $T \geq 14$ days which indicates that RSI calibrations during such times tend to underestimate the DNI in comparison to the long-term calibration. During winter the tendency is to overestimate the DNI (see section 7.2.1 and 7.2.3 for definition and correlation of Π_{DNI} and $\Pi_{\mathrm{cal,DNI}}$).
Figure 7.9 displays the course of Π_{DNI} for $T = 120$ days for the seven (table 7.1) evaluated data sets. This duration was chosen because moving averages of the interval length $T = 120$ days result in fluctuations of Π_{DNI} which are steady enough to recognize reoccurring seasonal tendencies in this form of visualization. In this graph during summer the greatest deviations of $M_{\mathrm{R,DNI}}$ from $L_{\mathrm{R,DNI}}$ occur before solstice. In winter the greatest deviation occurs between October and first of January which coincides with the low number of usable timestamps as seen in figure 7.8. However, the most apparent observation taken from figure 7.9 is the extraordinary amplitude of $\Pi_{\mathrm{DNI}}(T{=}120$ days) on the first of January 2008 and in April 2008. Since three data sets from that period were available (all three taken by different instruments) and all three show the same characteristics in Π_{DNI}, Π_{GHI} and Π_{DNI} (see Appendix C) it is save to attribute the high amplitudes to the extraordinary irradiance conditions at the time.

Distributions by duration and starting month

In order to derive recommendations in regard to the necessary calibration duration for different times of the year the Π_{DNI} of the seven data sets (table 7.1) was sorted by calibration starting

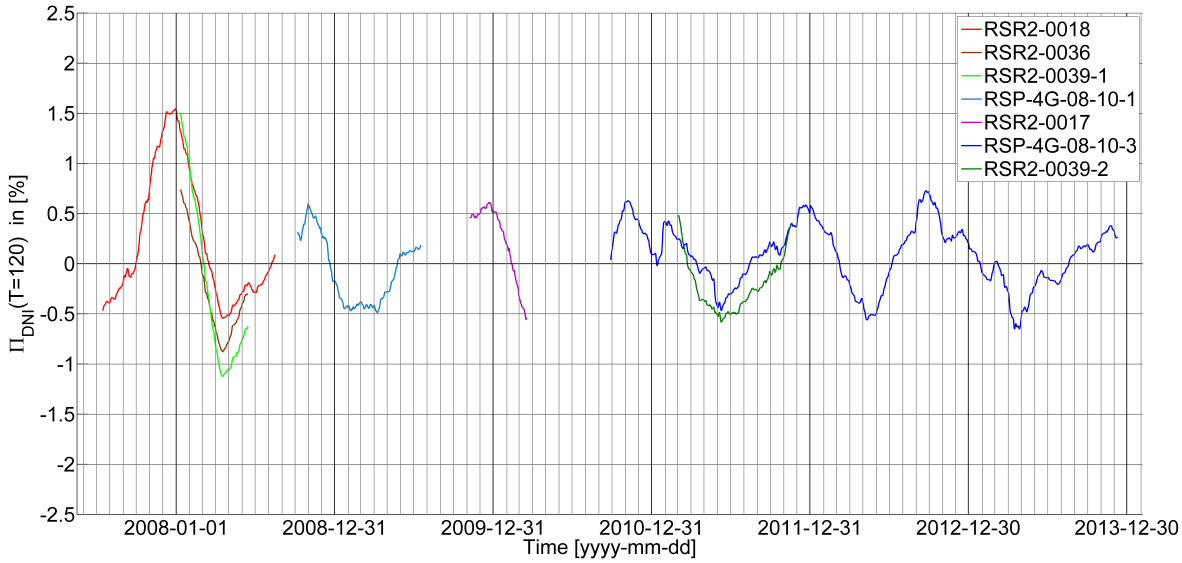

Figure 7.9: Π_{DNI}(T=120 days) from seven evaluated data sets (table 7.1).

month and the combined distribution thereof was visualized in boxplots as presented in figure 7.10. This allows the reader to choose the required duration in dependence on the starting time of measurements and the acceptable distribution of Π_{DNI}. The same was done for Π_{GHI} and Π_{DHI} in figures 7.11 and 7.12. Since most of the time the greater part of *GHI* is due to *DNI* the seasonal course of Π_{GHI} distributions displays more similarities with the seasonal course of distributions of Π_{DNI} than of Π_{DHI}. Among the three types of Π pertaining to the three components of irradiance the widest range is present in the distribution of $M_{R,DHI}$ / $L_{R,DHI}$ ratios.

Most boxes in figure 7.10 are well centered around their mean. The course of the Π_{DNI} reaches its peaks between November and January and between March and May. This was to be expected after the observations made in figure 7.9 and indicates that a shorter calibration duration suffices during most part of the year in order to produce calibration results of uncertainty similar to calibrations which start during the mentioned periods with a longer measuring duration. Since the data in figure 7.10 is sorted by calibration starting month the highest mean values of Π_{DNI} occur earlier for longer durations T than for shorter durations.

The comparatively high Q3 and upper whiskers in November and December as well as the lower outliers in April and May are due to the unusual meteorological conditions during the period from the end of 2007 to late spring in 2008. This period not only exhibits strong fluctuations of calibration results, but it is also over-represented by its three data sets. In comparison among the monthly Π_{DNI} distributions from individual data sets for $T = 60$ days (figure 7.13) this is recognizable. However, removing the RSR2-0036 and the RSR2-0039-1 data sets from the evaluation (thus representing the period with only one data set) would

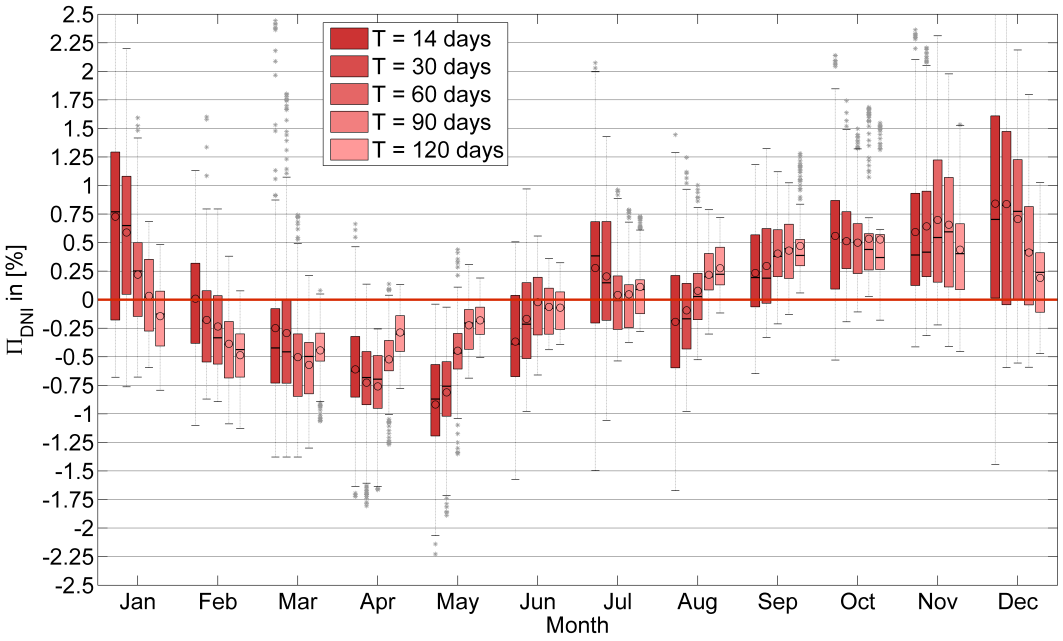

Figure 7.10: Π_{DNI} for T=14 days, 30 days, 60 days, 90 days and 120 days sorted by calibration starting month.

only bring marginal changes to the visualization of Π_{DNI} distributions in figure 7.10.
The upper outliers for starting dates in March are caused by the unusual behavior of the RSP-4G-08-10-3 data set during March 2011 (see figure 7.8).

With DLR2008 calibration the determined *DNI* values are a direct function of *GHI* and *DHI* measurements (section 5.1). Consideration of the distributions of Π_{GHI} and Π_{DHI} (figures 7.11 and 7.12) allows to interpret some of the Π_{DNI} distributions characteristics. For example, for a calibration duration of $T = 30$ days the positive Π_{DNI} from November to January (figure 7.10) coincide with negative Π_{DHI} (figure 7.12) and Π_{GHI} close to zero (figure 7.11). Therefore, it appears that in this example the seasonal tendency is to produce calibrations which (in comparison to a long-term calibration) overestimate *DNI* as a result of underestimation of *DHI* (see equation 5.4).
Similarly, the Π_{DNI} values of $T = 30$ days decrease with the month of the year for calibration starting dates from March to May for a relatively constant low range of Π_{GHI} values (figure 7.11) and increase of Π_{DHI} from negative values towards positive values (figure 7.12). This indicates that calibrations tend to produce increasing *DHI* calibration factors (*CFD*) as the calibration starting date progresses from March through May and thus measure increasingly low *DNI* values (relative to a long-term calibration).
The described effects (as in above example for T=30 days) are due to the meteorological conditions during these periods which influence the Π_{DNI} of all calibration durations alike. However, with increased duration T (e.g. T=120 days) the effects can be reduced significantly.

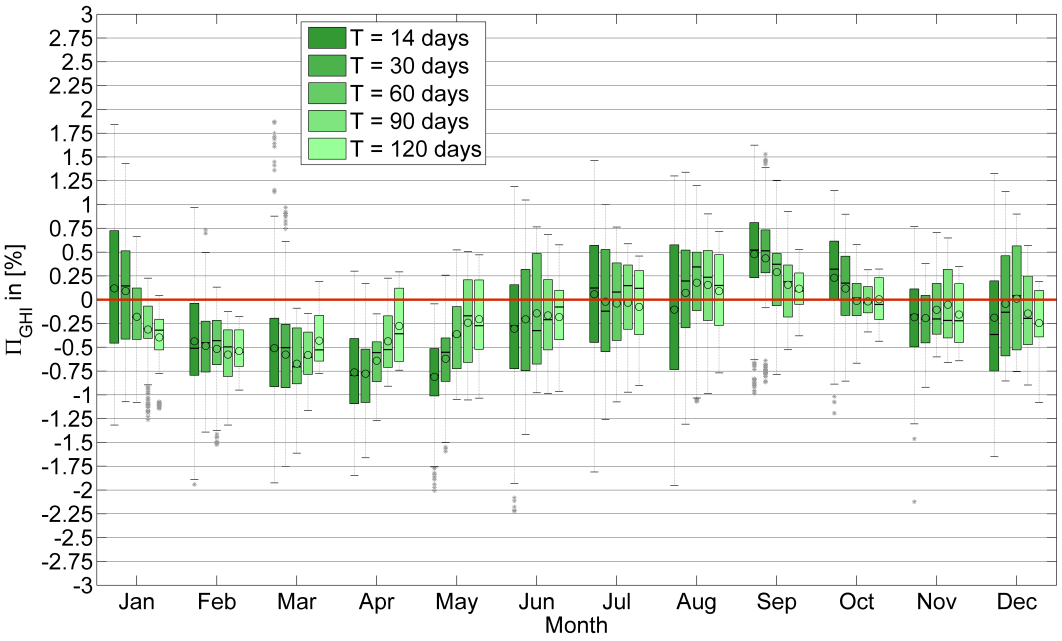

Figure 7.11: Same as figure 7.10 for Π_{GHI}.

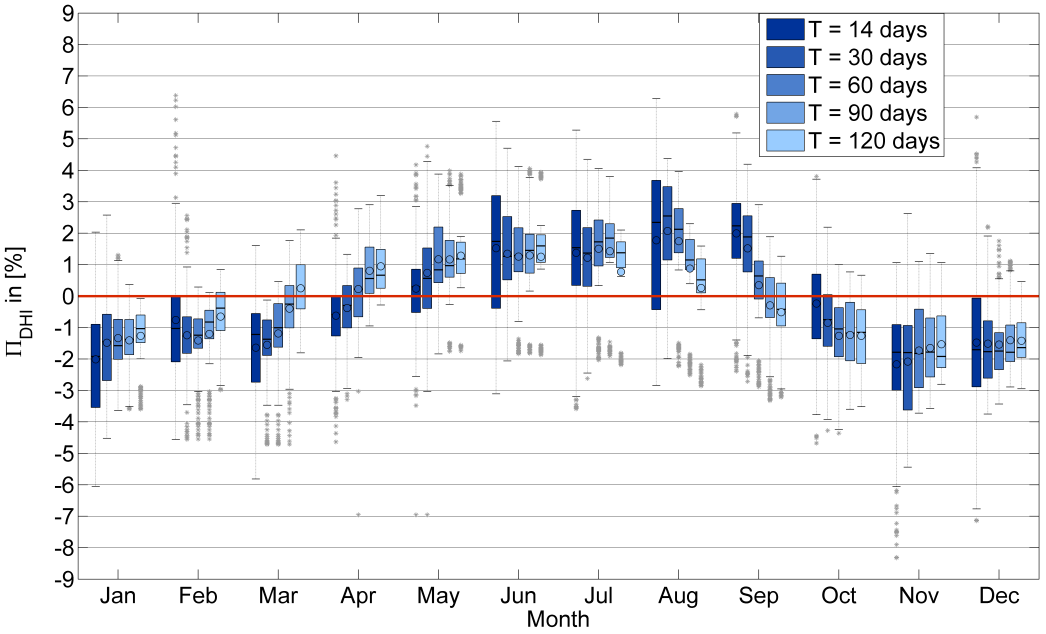

Figure 7.12: Same as figure 7.10 for Π_{DHI}.

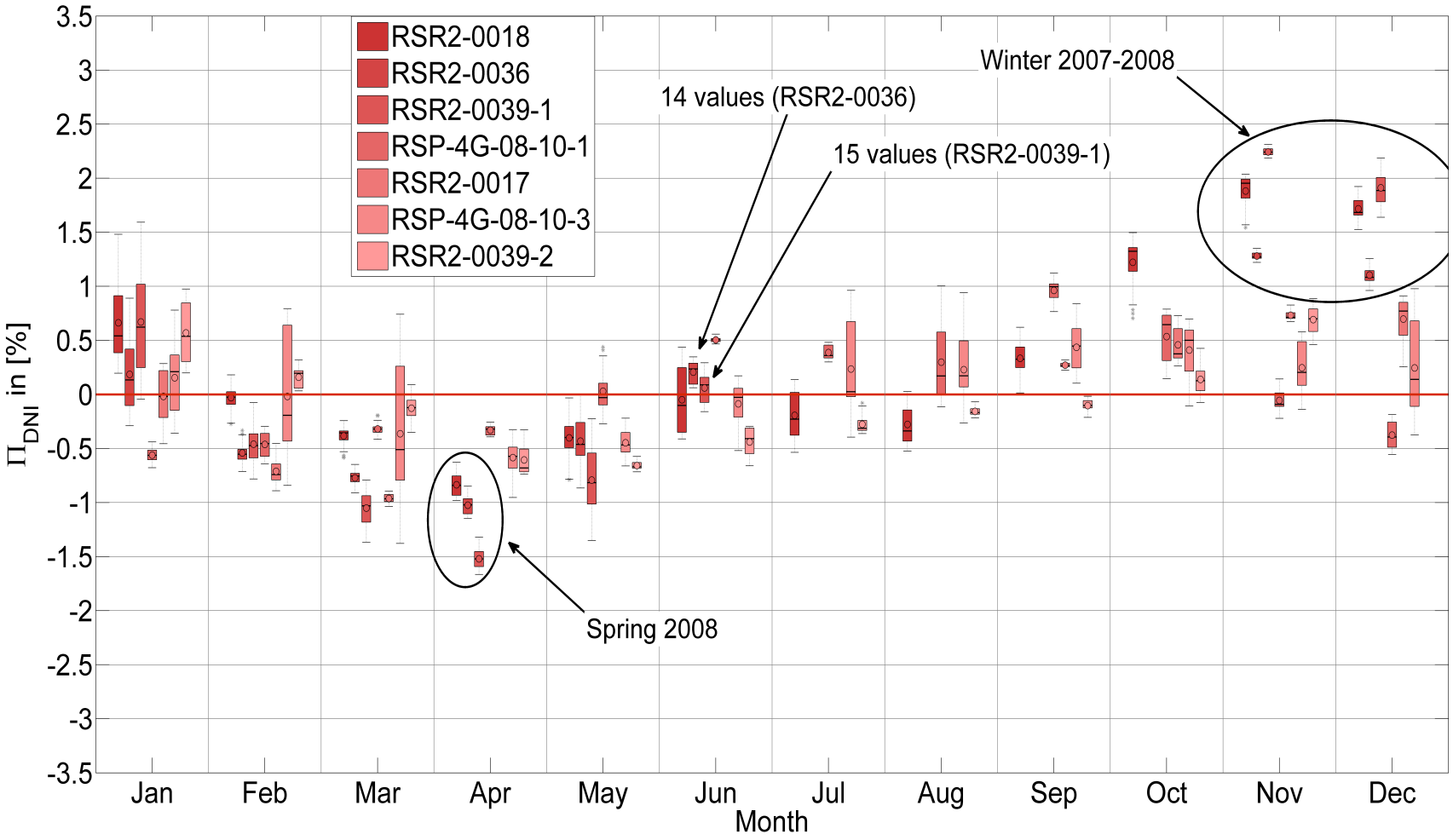

Figure 7.13: Π_{DNI} for $T = 60$ *days* by data set and starting month of calibration. Boxplots with 15 or less data points are marked as such.

Discussion of duration for specific starting months

The general observation in section 7.3.1 was that the longer the calibration duration the closer the outcome will be to a long-term calibration. While this is true in most cases, some exceptions were found.

In figure 7.10 for starting dates in November the Π_{DNI} with a duration of $T = 60$ days are distributed further from zero than with any other of the evaluated durations from $T = 14$ days to $T = 120$ days. This is true for all indicators the boxplot provides alike. However, a duration of T= 60 days exhibits a far better (in terms of coincidence with zero) distribution of Π_{DNI} than durations of 14 days and 30 days for starting dates in the following month of December. For starting dates in January the differences between the distribution of Π_{DNI} for 30 days and 60 days duration is further increased. This indicates that the meteorological conditions in November and February are generally more suitable for DLR2008 calibration than in December and January.

Furthermore, starting dates in January produced closer coincidence between Π_{DNI} and zero with a duration of $T = 90$ days than a duration of $T = 120$ days. The Π_{DNI} of starting dates in February exhibited the closest coincidence with zero for durations of $T = 60$ days along with $T = 30$ days. 90 days periods starting in January and 60 days periods starting in February have in common that they end in April while the respective longer periods include all of April and a part of May. Remarkably, the duration $T = 120$ days generated the greatest deviation of Π_{DNI} values from zero for starting dates in February. This is owed to its inclusion of the entire period of less suitable meteorological conditions in April and May.

However, out of all data visualized in figure 7.10 the Π_{DNI} distributions for starting dates in May and June with $T = 120$ days exhibited the smallest distance between upper and lower whiskers as well as the closest coincidence with 0 % since the respective periods of time are dominated by the more suitable conditions from June onward.

As shown by these examples the general rule that longer calibration durations yield better results does not always apply, due to the meteorological conditions (i.e. spectral composition of irradiance) at the time.

Recommendations for choice of calibration duration

In section 7.3.1 it was found that a calibration duration of $T = 60$ days is preferable in the case of using a constant duration throughout the year.

In consideration on the seasonal tendencies however, it appears to be more comprehensive to choose the calibration duration in dependence on the month in which measurements are commenced. This allows to keep the monthly maximum deviation of $M_{\mathrm{R,DNI}}$ from $L_{\mathrm{R,DNI}}$ within a given maximum Π_{DNI} ($\Pi_{DNI,max}$) and thus creates results of constant viability while minimizing calibration duration. Table 7.7 provides a summary of required minimum durations for varying $\Pi_{DNI,max}$.

Table 7.7: Minimum required calibration duration in days for given maximum Π_{DNI} and starting time - DLR2008

$\Pi_{DNI,max}$	Month											
	Jan	**Feb**	**Mar**	**Apr**	**May**	**Jun**	**Jul**	**Aug**	**Sep**	**Oct**	**Nov**	**Dec**
±2.5 %	30	14	14	14	14	14	14	14	14	14	14	60
±2.25 %	30	14	14	14	14	14	14	14	14	14	14[(1)]	60
±2 %	60	14	14	14	30	14	14	14	14	14	90	90
±1.5 %	60	14	14	90	60	30	30	30	14	30	120	120
±1 %	90	30[(2)]	120	90	60	30	60	30	90	90	-	120
±0.75 %	90	-	-	120	90	90	90	120	-	90	-	-
lowest	90	30	120	120	120	120	120	120	120	120	120	120

[(1)] 60 days is not suitable
[(2)] only 60 days and 30 days are suitable

Even if a constant calibration of $T = 60$ days is preferred to choosing the duration individually by month of the year, it should be considered to reduce the duration of calibration starting in November to $T = 30$ days only, since for this month a duration of $T = 60$ days exhibits the highest deviations of $M_{\mathrm{R,DNI}}$ from $L_{\mathrm{R,DNI}}$ in comparison to any other examined duration.

The evaluation of seasonal influences established the correlation between $\Pi_{DNI,max}$, calibration duration and the month in which a calibration is commenced. Π_{DNI} is also closely correlated with $\Pi_{\mathrm{cal,DNI}}$ as discussed in section 7.2.3. $\Pi_{\mathrm{cal,DNI}}$ on the other hand represents the deviation of calibration results from the result of a long-term calibration (section 7.10, equation 7.10). Therefore, $\Pi_{DNI,max}$ in combination with the relative uncertainty of the reference pyrheliometer (DNI_{Ref}) can be used for a conservative estimate of calibration uncertainty along equation 7.11.

$$\Delta DNI_{\mathrm{cal,rel}} \approx \sqrt{(\Delta DNI_{\mathrm{ref,rel}})^2 + (\Delta Soil_{\mathrm{ph}})^2 + (\Pi_{DNI,max})^2} \tag{7.11}$$

In accordance with [WMO, 2010] the relative uncertainty of the reference pyrheliometer is $\Delta DNI_{\mathrm{ref,rel}}$=1.8 %. Additionally, an error due to pyrheliometer soiling of $\Delta Soil_{\mathrm{ph}} \approx 0.2$ % can be estimated in respect of the findings in [Geuder and Quaschning, 2006].
An exemplary calculation for $\Pi_{DNI,max}$=2.25 % obtained an estimate of $\Delta DNI_{\mathrm{cal,rel}} \approx 3$ % for the calibration uncertainty.

7.3.3 Calibration duration - DLR-VigKing

The MAM was also applied to DLR-VigKing calibrations of the same data sets (table 7.1) as before for DLR2008.

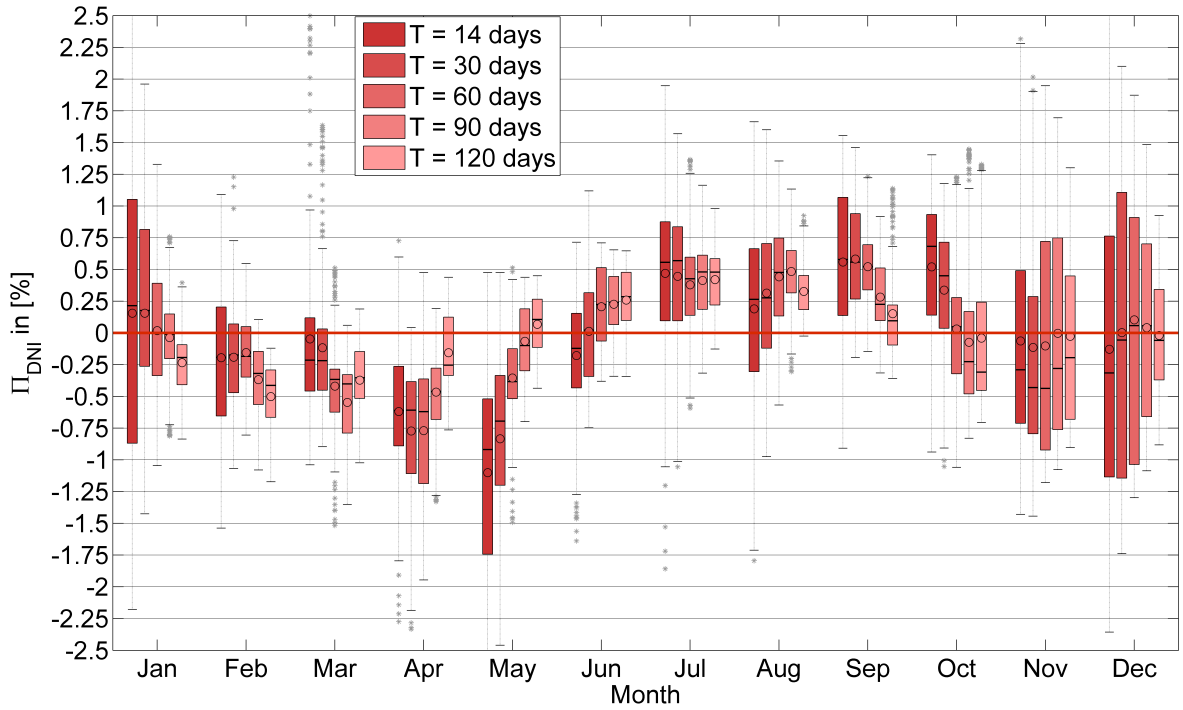

Figure 7.14: same as figure 7.10 for DLR-VigKing calibrations

Without discussing the results in the same detail as in the sections 7.3.1 and 7.3.2 pertaining to the DLR2008 the findings will be briefly outlined and presented in boxplots for the distribution of Π_{DNI} (figure 7.14) and a table for calibration duration (table 7.8). The equivalent plots for Π_{GHI} and Π_{DHI} can be found in the Appendix (figures D.4 and D.5). Plots for constant calibration duration throughout the year are depicted in the Appendix as well (figures D.1 to D.3). Drift correction was applied to the same data sets as previously for DLR2008 (see Appendix A).

In comparison to DLR2008 the DLR-VigKing method results in similar seasonal distributions of Π_{DNI}. However, in figure 7.14 it is noticeable that the DLR-VigKing produces wider IQRs of Π_{DNI}. This is especially true for starting dates during the time from November to January. During this period the distributions are exceptional symmetrically centered around zero but exhibit the widest range of Π_{DNI} values.

Similary as in DLR2008, also DLR-VigKing calibrations with durations of 60 days exhibited smaller maximum Π_{DNI} for starting dates in February than any other duration. In DLR-VigKing (figure 7.14) the Π_{DNI} distributions for starting dates in March where the closest to zero for durations of 30 days. Contrarily, in the following two months of April and May the distributions of Π_{DNI} for a duration of $T = 30$ days deviates further from zero than for other durations. This observation indicates that the meteorological conditions during April and May are not well suited for DLR-VigKing calibrations. In the case of calibrations which start

Table 7.8: Minimum required calibration duration for given maximum Π_{DNI} and starting time - DLR-VigKing

$\Pi_{DNI,max}$	Month											
	Jan	**Feb**	**Mar**	**Apr**	**May**	**Jun**	**Jul**	**Aug**	**Sep**	**Oct**	**Nov**	**Dec**
±2.25 %	30	14	14	14	60	14	14	14	14	14	30	30
±2 %	30	14	14	60	60	14	14	14	14	14	30	60
±1.5 %	60	30	14	90	60	14	60	60	30	14	120	90
±1 %	90	60[(1)]	30[(1)]	120	90	60	120	120	90	-	-	120
±0.75 %	90[(1)]	-	-	120	90	60	-	-	120	-	-	-
lowest	90	60	30	120	120	90[(2)]	120	120	120	90	120	120

[(1)] only this duration is suitable
[(2)] positioning of IQR better than 120 days

in April or May but reach well into the months of June or July a far closer coincidence of the Π_{DNI} with zero is achieved. This is caused by the more suitable conditions from June onward. A similar general tendency was observed in DLR2008.

In DLR2008 the duration (figure 7.10) of 60 days produced the highest upper Π_{DNI} whiskers among calibrations starting in November. This is not true for DLR-VigKing where only $T = 14$ days exhibits higher values than $T = 60$ days. On the other hand, in regard to maximum Π_{DNI} and IQR a duration of $T = 30$ days exhibits a more desirable distribution for this starting month than a duration of 60 days.

Measurements starting in October with 30 to 90 days duration resulted in smaller Π_{DNI} than 120 days duration due to the adverse conditions during the Winter months. In consideration of the IQRs of Π_{DNI} a duration of 90 days appears to perform best for calibration starting in the month of October.

Recommendations for choice of calibration duration

It is recommended to choose the calibration duration in accordance to table 7.8 in dependence on the month of the year and the desired $\Pi_{DNI,max}$.

If a constant calibration duration throughout the year is preferred, also for DLR-VigKing a duration of $T = 60$ days is advised as a compromise between producing results close to a long-term calibration and not consuming more time than reasonable. Similarly to DLR2008 one should resort to a shorter duration of $T = 30$ days for calibrations starting in November. In DLR-VigKing the same is true for calibrations starting in March. Figure 7.14 (also see figure D.1 in the Appendix) suggests a deviations from a long-term calibration below 2 % for $T = 60$ days throughout the year.

7.3.4 Conclusion

As shown in section 7.2.3 the course of Π_{DNI} closely coincides with $\Pi_{\mathrm{cal,DNI}}$ (the deviation of results of short-term calibrations from the result of a long-term calibration). Therefore, the examination of Π_{DNI} makes it possible to draw conclusions in regard to the effect of calibration duration on the fluctuation of calibration results.

While longer calibration durations generally yield smaller values for Π_{DNI} and therefore less fluctuation of results, seasonal influences need to be taken into consideration since the range of Π_{DNI} values differs considerably in dependence of the month of the year. Seasonal changes in meteorological conditions lead to seasonal tendencies of calibration results. For example, in DLR2008 calibrations a RSI calibrated at the PSA between September and January is likely to measure higher DNI values than if it was calibrated between February and June. In DLR-VigKing the same is true for the period from July to October in comparison to March to May.

In both calibration methods the evaluation indicated that measurements taken exclusively during the months of November, December, January, April and May have the tendency to lead to high fluctuation of calibration results and are more likely to produce strong deviations from a long-term calibrations.
However, by choosing a calibration duration which includes sufficient data from outside these particular periods the maximum occurring deviation from a long-term calibration can be reduced substantially. In some cases it is preferable to choose a shorter duration in order to avoid collecting too much data from these periods.
By using the tables 7.7 and 7.8 it is possible to choose the necessary calibration duration in dependence on the month of the year and the $\Pi_{DNI,max}$ which the operator deems desirable. A reasonable $\Pi_{DNI,max}$ should be chosen in regard to the overall uncertainty of the RSI.

While the results obtained here provide a basis on which to choose different calibration durations during different times of the year, there are limitations which need to be taken into consideration.
One limitation is the number of data sets. Seven data sets (table 7.1) were evaluated. They are a viable basis on which to draw conclusions of a general nature, but as the period from winter 2007 to April 2008 demonstrated some years can exhibit comparatively extreme fluctuations. Furthermore, some data sets were measured during the same period of time. Additionally, the validation of the MAM in section 7.2.3 did exhibit differences of up to 0.5 % between the ratios of actual calibrations and the Π_{DNI}. In respect to the above mentioned limitations a conservative estimate of the calibration uncertainty as discussed in section 7.3.2 has higher viability for generalization than the attempt of an exact determination of calibration error.

8 Conclusion and outlook

Calibration methods for thermopile irradiometers are similar to each other in their requirements and procedures. Measurement samples are taken during specific meteorological conditions. Clear sky conditions and a minimum cloud distance from the sun is required in many cases in order to ensure a high intensity of direct beam irradiance. The calibration factor is calculated as the mean of the ratios between measurements from the reference and the test instrument.

DLR's calibration methods for RSIs on the other hand have a different modus operandi. The most significant differences are found in the acquisition of test measurements and methods of data treatment. It is required to take measurements under a wide range of meteorological conditions and continuously during the entire measuring period. The data treatment includes application of a number of correctional functions for reduction of the sensor's systematic errors. After automatic and manual screening of data quality, the calibration factors are determined by an algorithm for minimization of RMSD of the test instrument from the reference. Furthermore, two or three (for DLR2008 and DLR-VigKing respectively) calibration factors are assigned to the different measurands instead of a single factor as in the calibration of thermopiles. Similarities between thermopile calibration and RSI calibration were found in regard to the setup of the measuring systems and the measuring site.

Calibration methods for thermopile irradiometers generally require measuring periods of less than 14 days. If the required conditions from the standards are fulfilled, as little as three days can be sufficient. Contrarily, RSI calibration by DLR presently uses data which is collected over a period from 30 to 120 days. Until the present day a duration of 60 days was most commonly used. Longer durations were chosen in dependence on the available time frame.

In this project it was found that the seasonal meteorological conditions at the PSA cause seasonal tendencies and fluctuation of RSI calibration results. Furthermore, the fluctuations are influenced by the calibration duration. Thus, it was possible to quantify correlations which can be used to optimize the calibration duration in dependence on the time of the year in which a calibration takes place.
However, one of the most important findings is the identification of seasons of adverse meteorological conditions. Test measurements from within the months November to January and April and May are less suitable for DLR2008 and DLR-VigKing than measurements during the remainder of the year. By including a sufficient amount of data from outside these periods

the adverse effects can be reduced.
Consequently, the duration of data acquisition for calibrations starting during these months should generally be longer than for calibrations starting during the rest of the year. In spring it is advantageous to limit the duration of calibrations starting before these periods. E.g. a DLR2008 or DLR-VigKing calibration starting in February with a duration of T=60 days has less tendency to deviate from a long-term calibration than a calibration with a duration of T=120 days or T=90 days.
Although longer durations are generally advisable during the winter months, one exception was found for DLR2008: Calibrations starting in November with a duration of T=60 days are more likely to exhibit deviations from a long-term calibration than with durations of T=30 days or even T=14 days. This seasonal effect is caused by the adverse meteorological conditions during the month of December.

In order to enable the reader to apply the results of this analysis, two tables where comprised which allow to choose the calibration duration for both DLR calibration methods in dependence on the month of the year in which measurements are commenced and the maximum tolerable value of $\Pi_{DNI,max}$ which represents the fluctuation of calibration results (tables 7.7 and 7.8). For DLR2008 a constant calibration duration of 30 days throughout the year with the exception of calibrations starting in December (60 days) is sufficient to keep $\Pi_{DNI,max}$ within 2.5%. In DLR-VigKing calibrations the same applies with the exception of using 60 days duration for calibrations starting in the month of May instead of December.

The data and methods presented in this report are suitable to examine the correlation between seasonal fluctuations and calibration duration. To make a final statement on the subject of calibration uncertainty is not within the scope of this work. However, a conservative estimate based on the presented findings can contribute to the ongoing studies of the overall accuracy of RSIs. Additionally, based on the observation that during certain times the deviation of calibration results exhibits one-sided tendencies towards the positive (November to January) or the negative (April and May) it could be investigated, if these seasonal effects can be compensated by functional corrections.

The amplitude of seasonal fluctuations as well as the month in which the amplitude is reached can vary to some extent among different years. If further investigations of seasonal fluctuations are carried out, it would be desirable to increase the total time span covered. Ideally, each long-term calibration would cover 12 months or multiple entire years. Even without using more data the accuracy of the evaluation method can be improved by using actual daily calibrations instead of moving averages. With a modification of the evaluation software which was created in the course of this project this is within the range of possibility.

The most recent calibration and correction method from [Vignola et al., 2017] could overcome

the complications of site dependence of calibration and calibration duration. Further studies of this new method are needed to proof this expectation.

Appendix

A Discussion of sensors drift in evaluated data

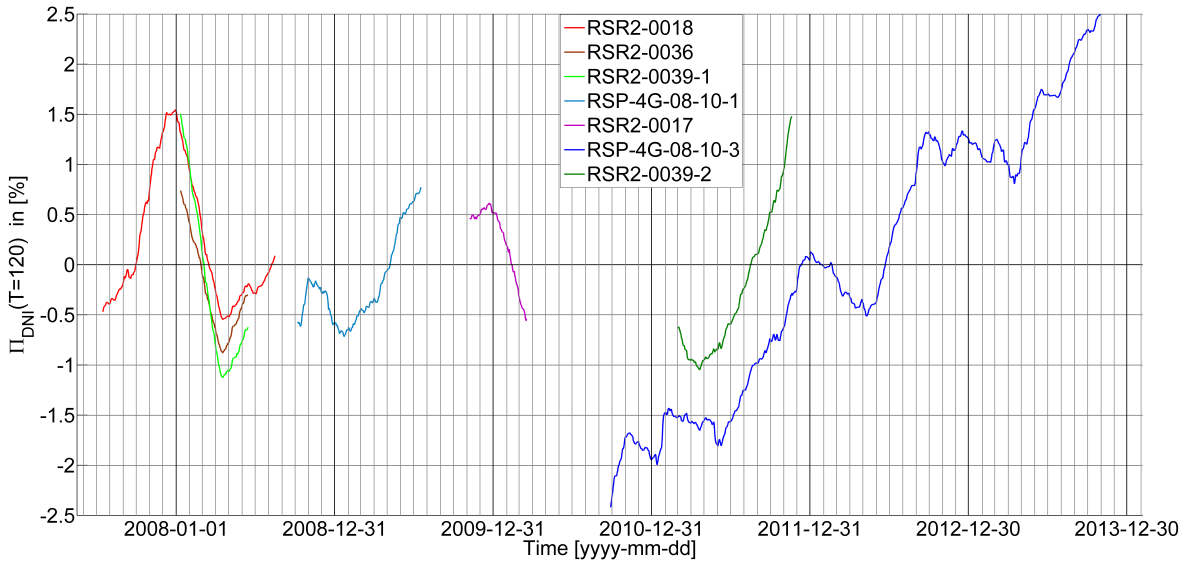

Figure A.1: Timeline for Π_{DNI}(T=120 days) from all data sets without removing drift

Before the final evaluation as presented in section 7.3.1 and 7.3.2 took place it was necessary to identify data sets in which significant drift is present. This was done after DLR2008 calibrations.

In data sets which cover a full year or multiple years drift can be recognized by comparing the same season in different years. However, even if drift is found to be present, the application of the drift correction as elaborated in section 7.2.2 can reduce the quality of the data. This will be discussed here on a case to case basis. For the drift removal procedure see section 7.2.2.

In the case of RSP-4G-08-10-3 the necessity of removing drift is apparent and doesn't need to be further elaborated (see figure A.1). In regard to RSR2-0018 the extend of drift can be estimated by comparing data of the same month in two different years. As already stated in [Geuder et al., 2014] the drift in this data set is negligible small. Similarly the data sets RSR2-0036 and RSR2-0039-1 match all three Π courses of RSR2-0018. The three data sets confirm each other. A slight drift is probable in RSR2-0039-1, but cannot be improved due to the nature of the drift removal algorithm.

The RSP-4G-08-10-1 data set is from the same sensor as the RSP-4G-08-10-3. It covers more than a year of measurements and exhibits similar drift (see figure A.2). Furthermore, after

correction of its drift a closer coincidence with the adjacent RSR2-0018 and RSR-0017 data sets was observed (see figures 7.9 and A.1).
RSR2-0039-2 covers slightly more than a year. Comparing the course of Π_{DNI}, Π_{GHI} and Π_{DHI} all three have similar drift over the period (see figure A.5). The drift corrected curve of RSR2-0039-2 seems to convey a better representation of the seasonal changes (see figures 7.9 and A.1).
The data sets RSR2-0036 and RSR2-0039-1 were used in their original state without drift correction. These data sets cover less than a year and make it difficult to differentiate between seasonal changes and drift. Comparison to the observed seasonal tendencies in the longer data set RSR2-0018 can help to reach a better understanding. However, regardless of drift being present or not the fitting functions (see section 7.2.2) are not suitable here, since the seasonal fluctuations are significantly stronger than any sensor drift.
In RSR2-0017 (see figure B.2 and A.4) the course of the Π_{DNI} curves is mostly seasonal. No apparent drift was recognized.

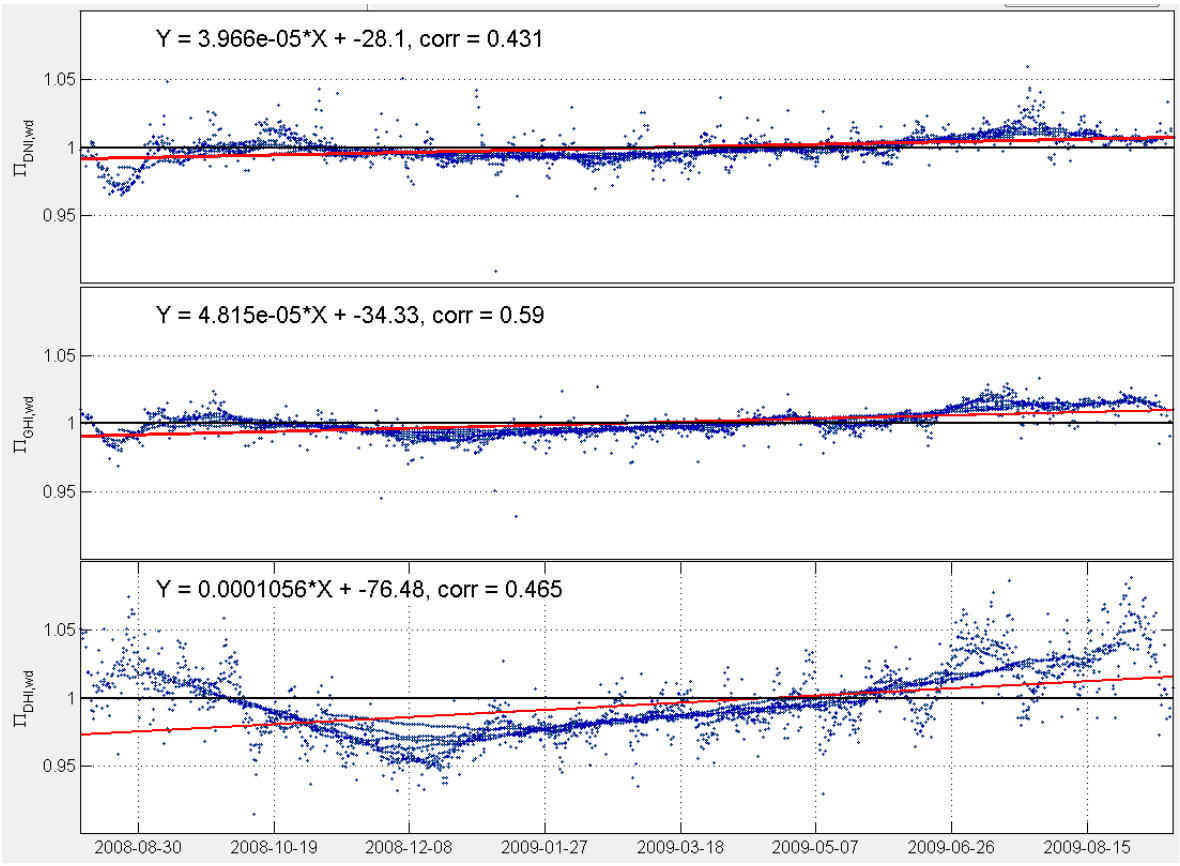

Figure A.2: Π for RSP-4G-08-10-1 without treatment for drift removal

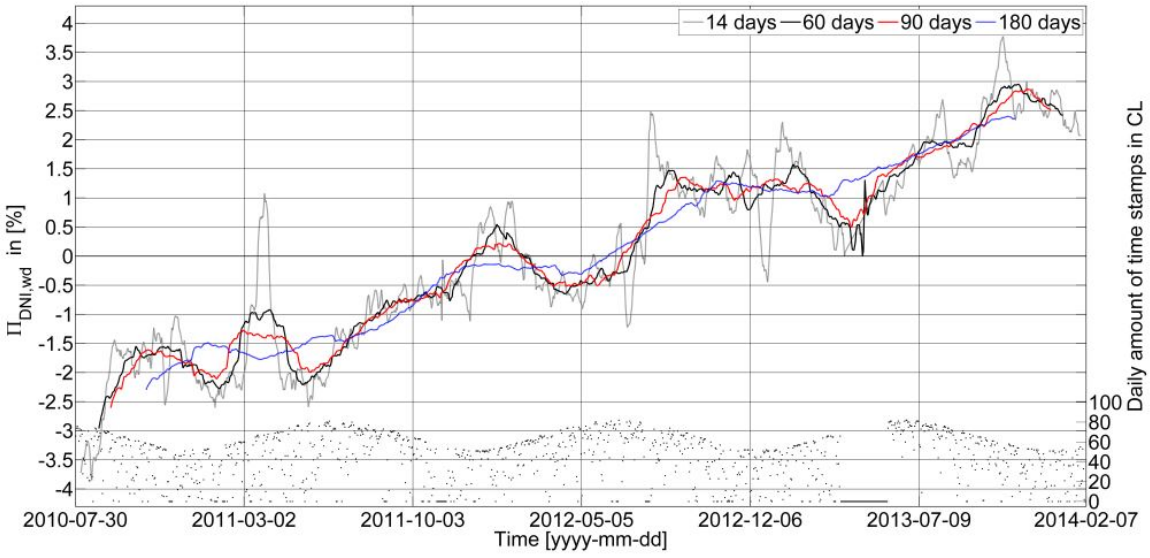

Figure A.3: Π_{DNI} for RSP-4G-08-10-3 without treatment for drift removal

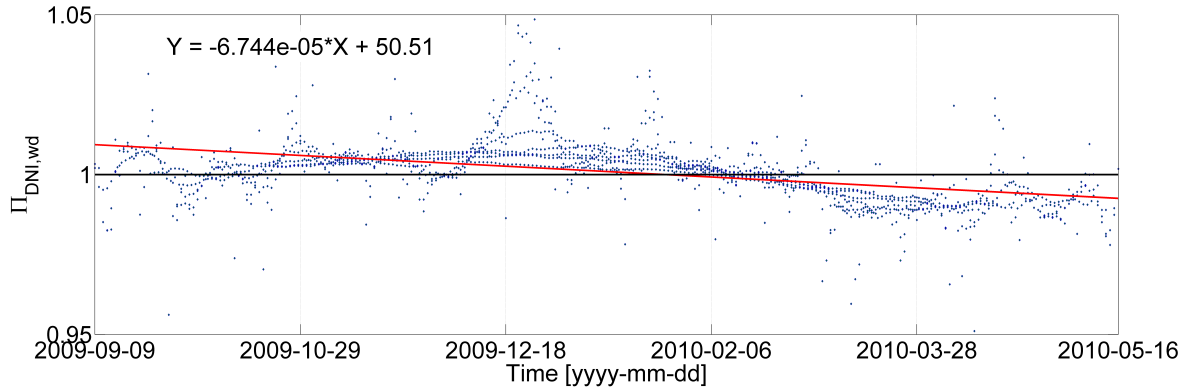

Figure A.4: Π_{DNI} with varying T for RSR2-0017 without drift removal treatment.

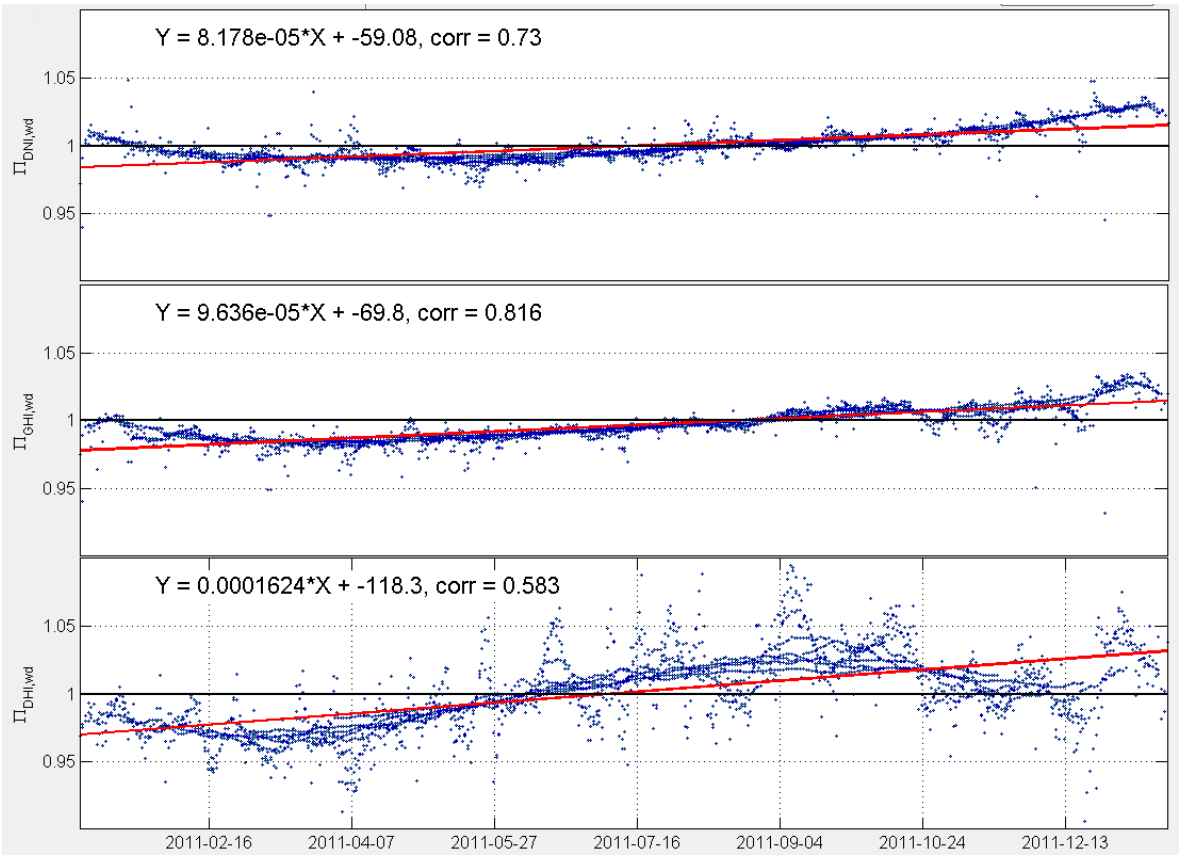

Figure A.5: Π with varying T for RSR2-0039-2 before treatment for drift removal

B Supplemental plots for discussion of calibration duration with DLR2008

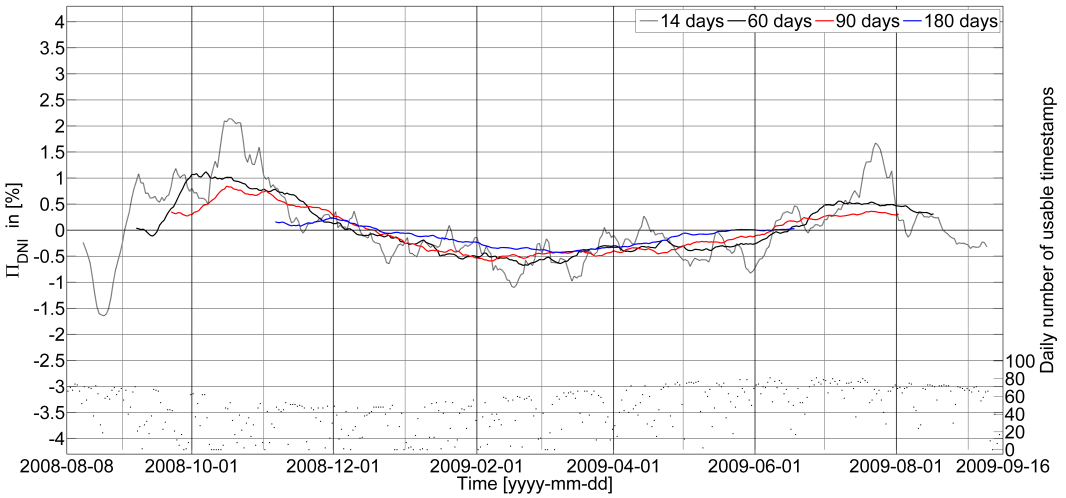

Figure B.1: Same as figure 7.8 for RSP-4G-08-10-1

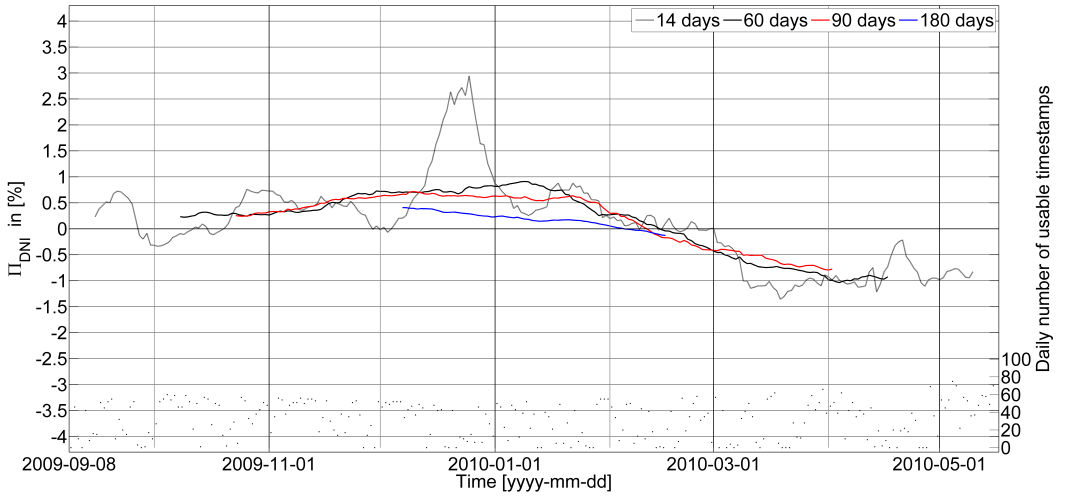

Figure B.2: Same as figure 7.8 for RSR2-0017

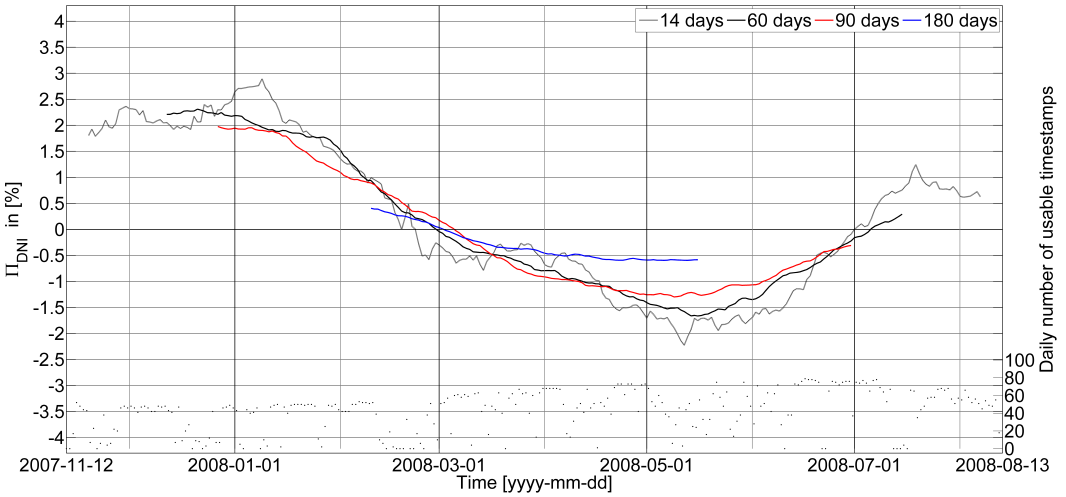

Figure B.3: same as figure 7.8 for RSR2-0039-1

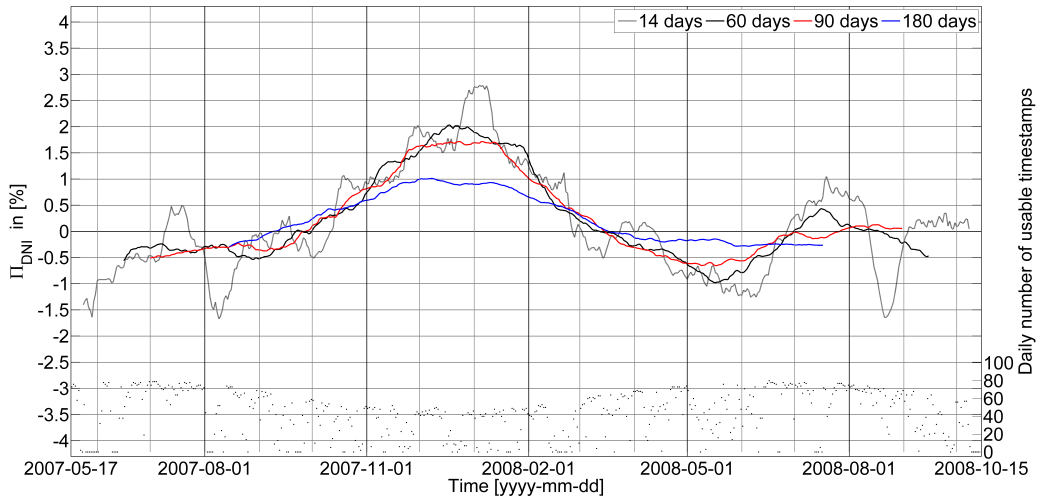

Figure B.4: same as figure 7.8 for RSR2-0018

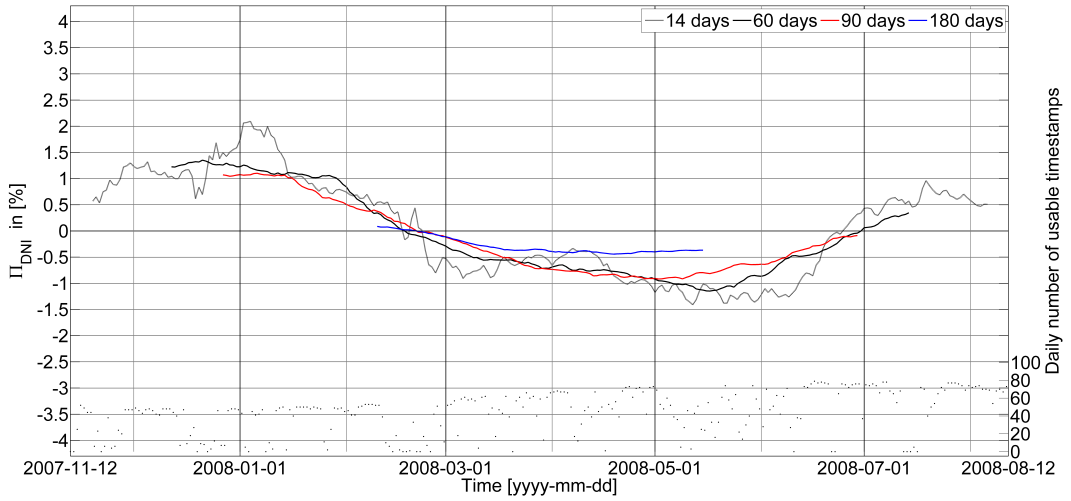

Figure B.5: same as figure 7.8 for RSR2-0036

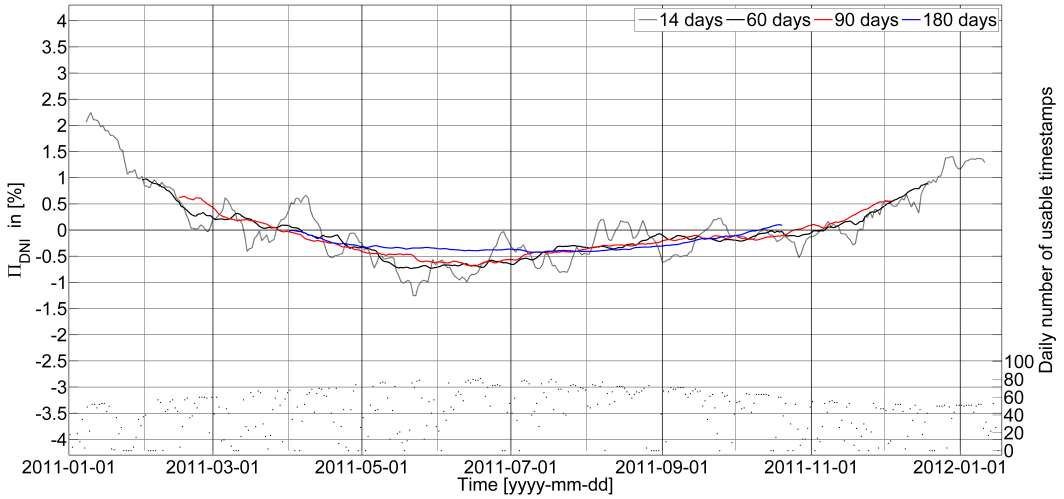

Figure B.6: same as figure 7.8 for RSR2-0039-2

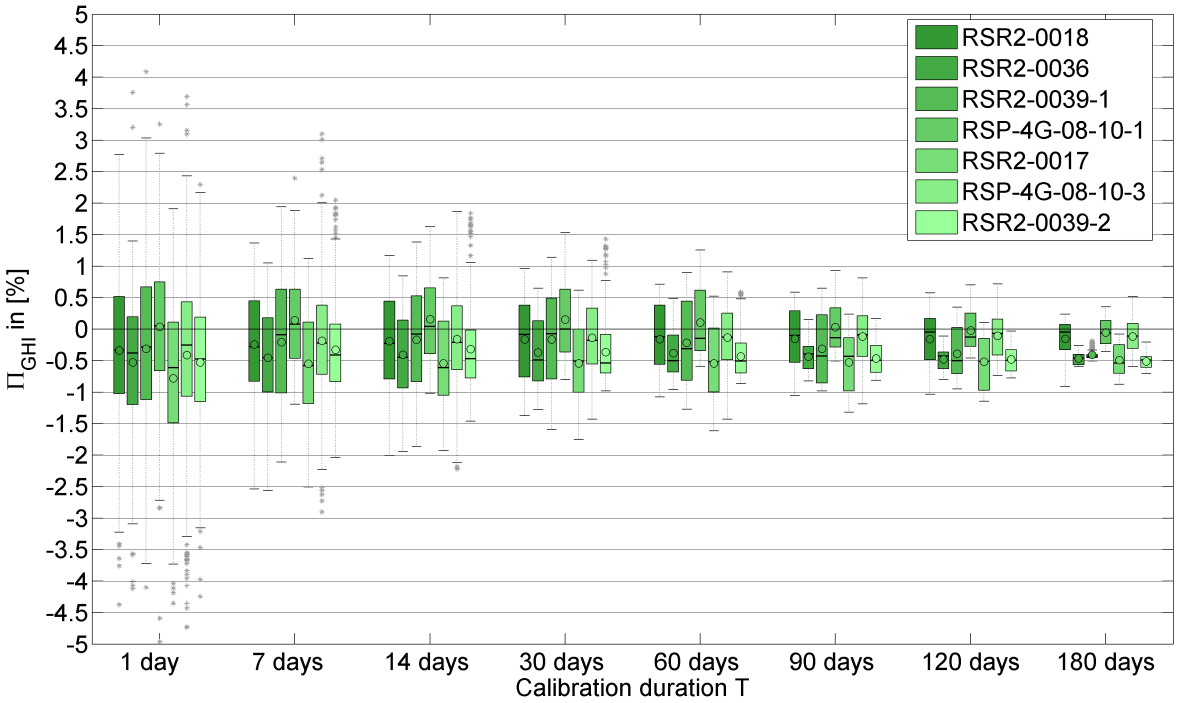

Figure B.7: Π_{GHI} in dependence on calibration duration for seven datasets - DLR2008

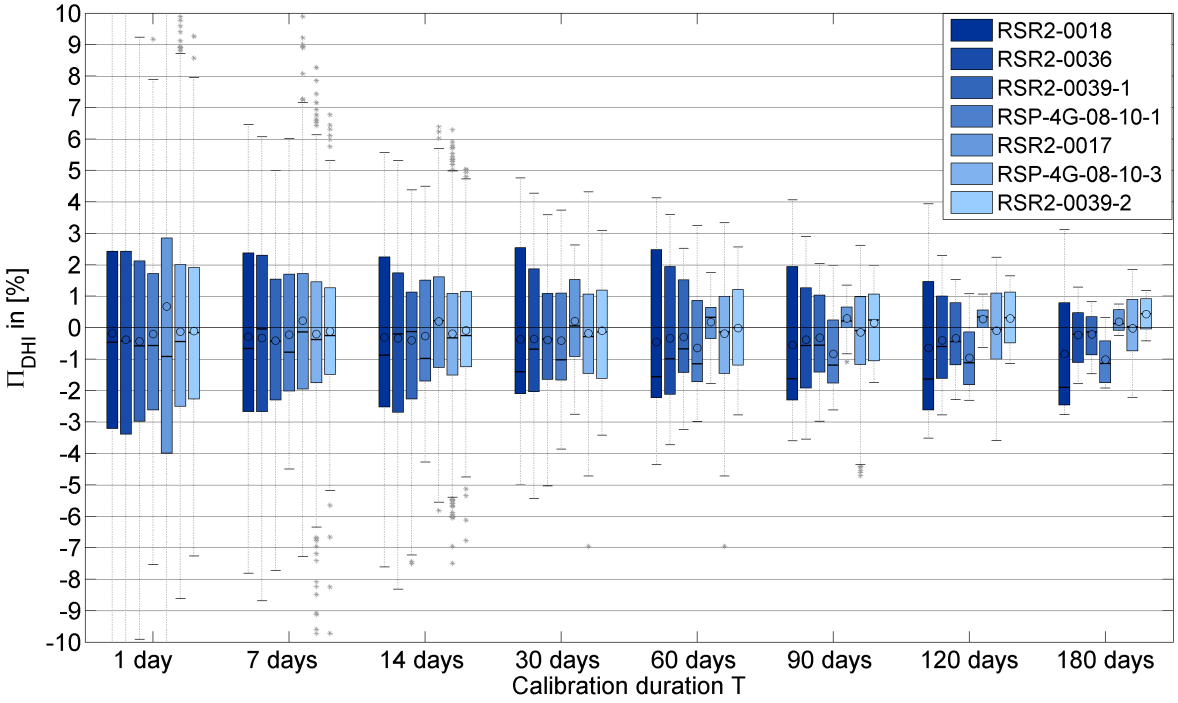

Figure B.8: Π_{DHI} in dependence on calibration duration for seven datasets - DLR2008

C Discussion of overlapping calibrations from different sensors with DLR2008

Some data sets were measured during the same time span (see figure 7.1). Comparison of their Π_{DNI} during the overlapping intervals leads to the following observations:

RSR2-0018, RSR2-0036 and RSR2-0039-1

These data sets can be seen figures B.4, B.3 and B.5. They overlap during the period from 2007-11-12 to 2008-08-12. There are differences in the values of Π_{DNI} but the general fluctuation of increase and decrease of the values during this period is common to all three. The course of Π_{DNI} of RSR2-0039-2 as seen in figure 7.9 crosses both other data sets while they are parallel to each other. This could be a sign of sensor drift as mentioned above. Further minor differences are attributed to the individually varying spectral sensitivity of each sensor.
A recalibration of the RSR2-0018 for only the overlapping period reduced the Π_{DNI} during the winter months (on 2008-01-01 by as much as 1 %) while its course during the summer only displayed minor changes. After recalibration the coincidence with the RSR2-0036 data set had increased significantly (see figure C.3).
By comparison of the data of both calibrations of RSR2-0018 during its MAM processing steps it was found that $L_{\mathrm{R,DNI}}$ had only changed by 0.06 % while the calibration factors CFG and CFD had changed by 0.18 % and 0.11 % respectively. This demonstrates that even among long-term calibrations with $T > 180$ days the measuring period has a noticeable influence on calibration results.
The recalibration included less summer months than the original longer calibration period. Thus the data collected during the winter months had a stronger influence on the calibration result than previously. Therefore, a reduced Π_{DNI} during winter was to be expected.

RSP-4G-08-10-3 and RSR2-0039-2

In opposition to the above observations a comparison of RSP-4G-08-10-3 to RSR2-0039-2 for the time span from 2011-01-01 to 2012-01-18 (figures B.6 and C.1) reveals only slight similarities. Few of the curve characteristics (e.g. the peaks of $\Pi_{\mathrm{DNI}}(T{=}14$ in August 2011) are similar in both data sets. Subsequently, the RSP-4G-08-10-3 was recalibrated for the same period as in the RSP2-0039-2. The Π_{DNI} of the recalibrated data set displayed the same characteristics as before recalibration (see figure C.2). Thus, in the case of RSP-4G-08-10-3 and RSP2-0039-2 the differences between both data set are owed to the individual

characteristics of each sensor instead of the time span of the data used for calibration.

Comparing recalibrations with the original calibrations

The RSIs RSR2-0039 and RSP-4G-08-10 have been used twice for long-term measurements and thus two separate data sets were available for each of the two sensors. However, comparing two data sets of the same sensor does not reveal any specific similarities apart from the presence of sensor drift in both RSP-4G-08-10 data sets. For RSR2-0039 see figures B.3 and B.6. For RSP-4G-08-10 see figures 7.8 and B.1.

Taking into account all of the above observations it can be stated that the meteorological conditions during the calibration period are the predominant factor in formation of Π_{DNI}. The same is the case for the determined calibration factors. Individual attributes of each sensor also play a role but the general tendencies clearly depend on the meteorological conditions.

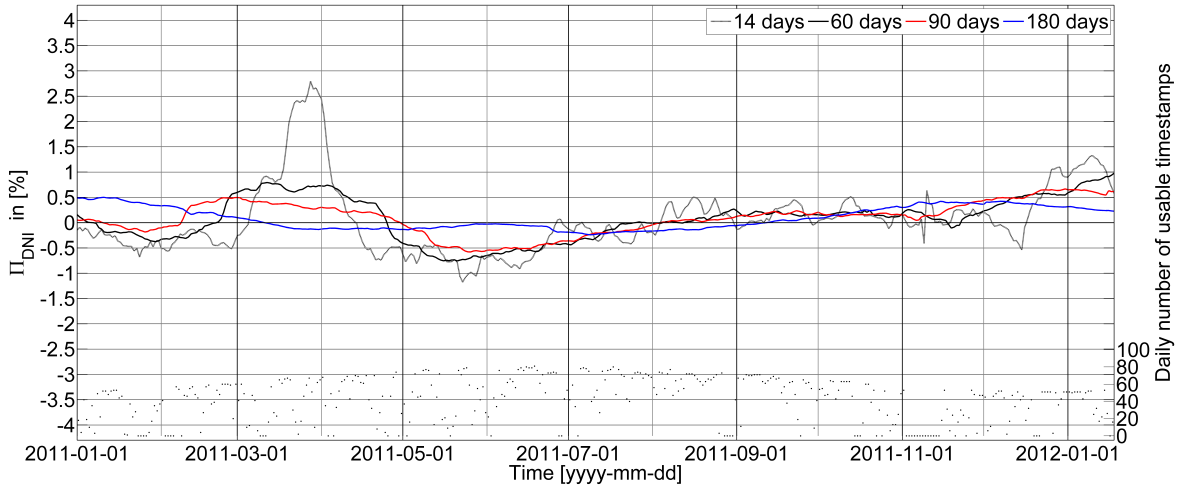

Figure C.1: same as figure 7.8. RSR-4G-08-10-3 for the period that matches RSR2-0039-2.

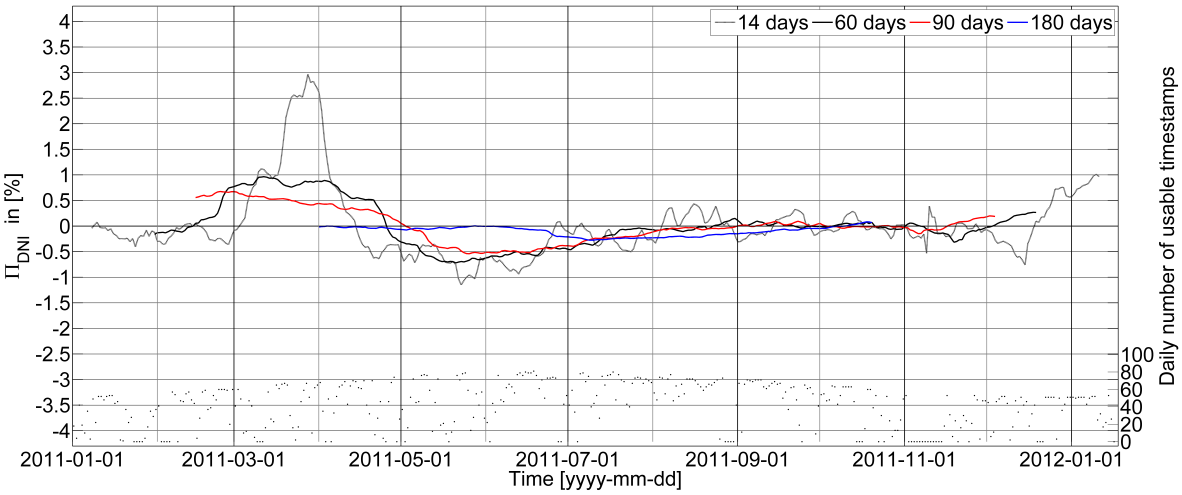

Figure C.2: Π_{DNI} for RSP-4G-08-10-3 calibration from 2011-01-01 to 2012-01-18

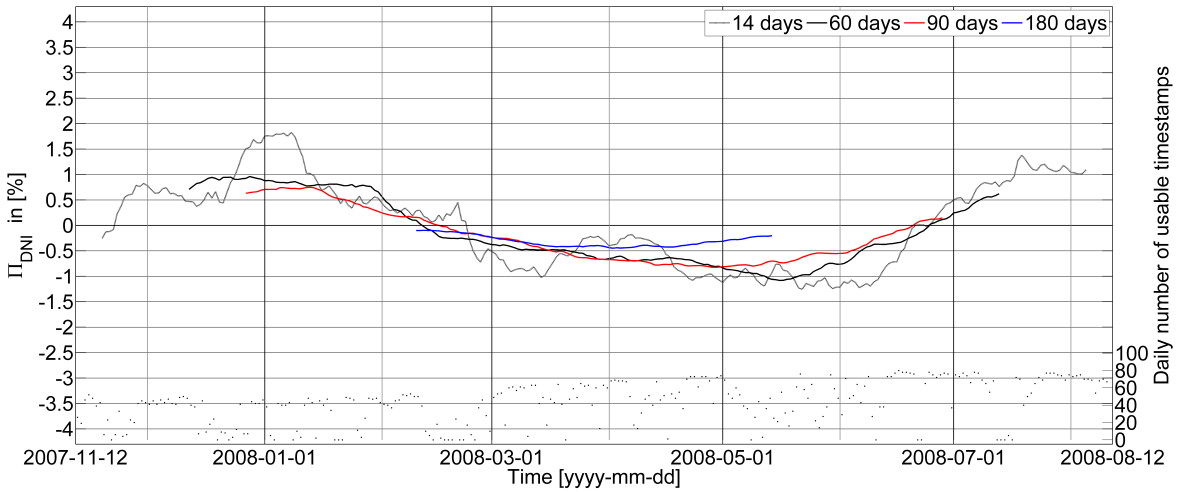

Figure C.3: Π_{DNI} for RSR2-0018 calibration from 2007-11-12 to 2012-08-12

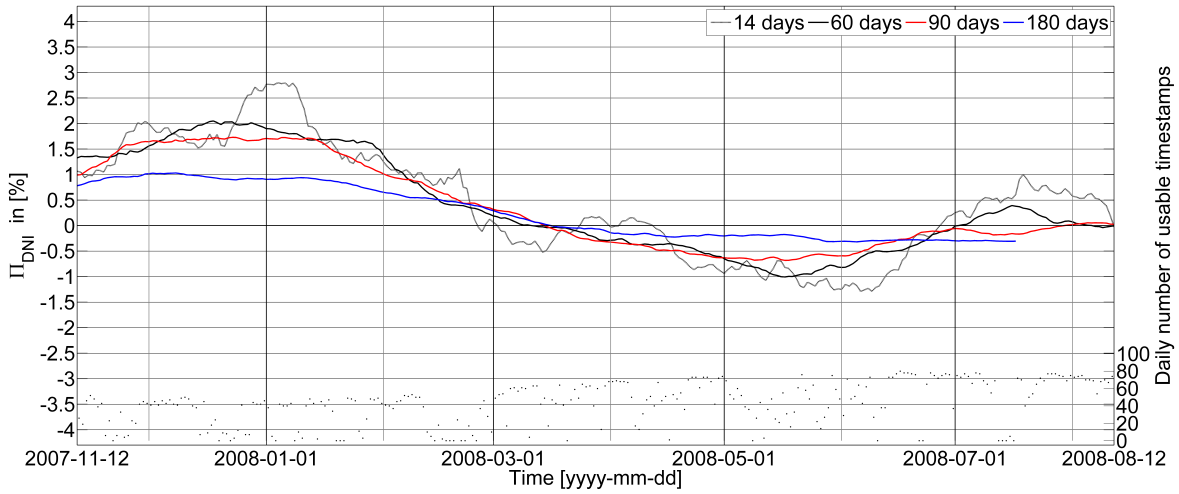

Figure C.4: Π_{DNI} for RSR2-0018 calibration from 2007-05-17 to 2012-10-15 plotted from 2007-11-12 to 2012-08-12

D Supplemental plots for discussion of calibration duration with DLR-VigKing

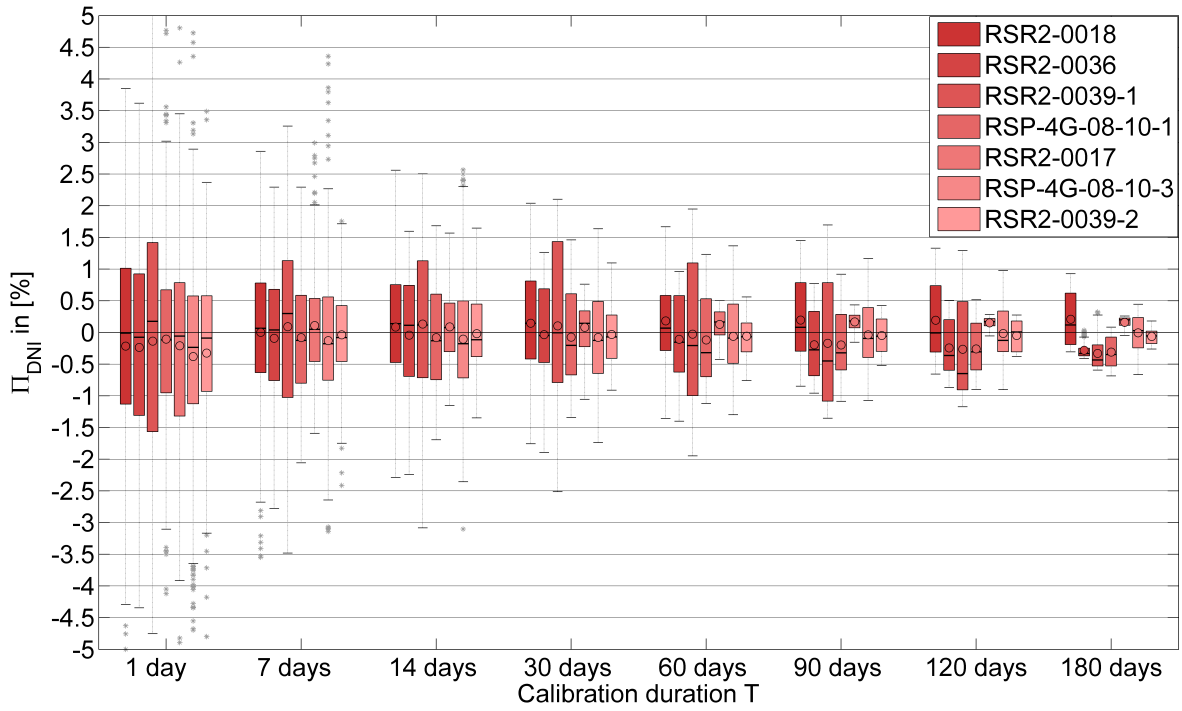

Figure D.1: Π_{DNI} in dependence on calibration duration for seven datasets - DLR-VigKing

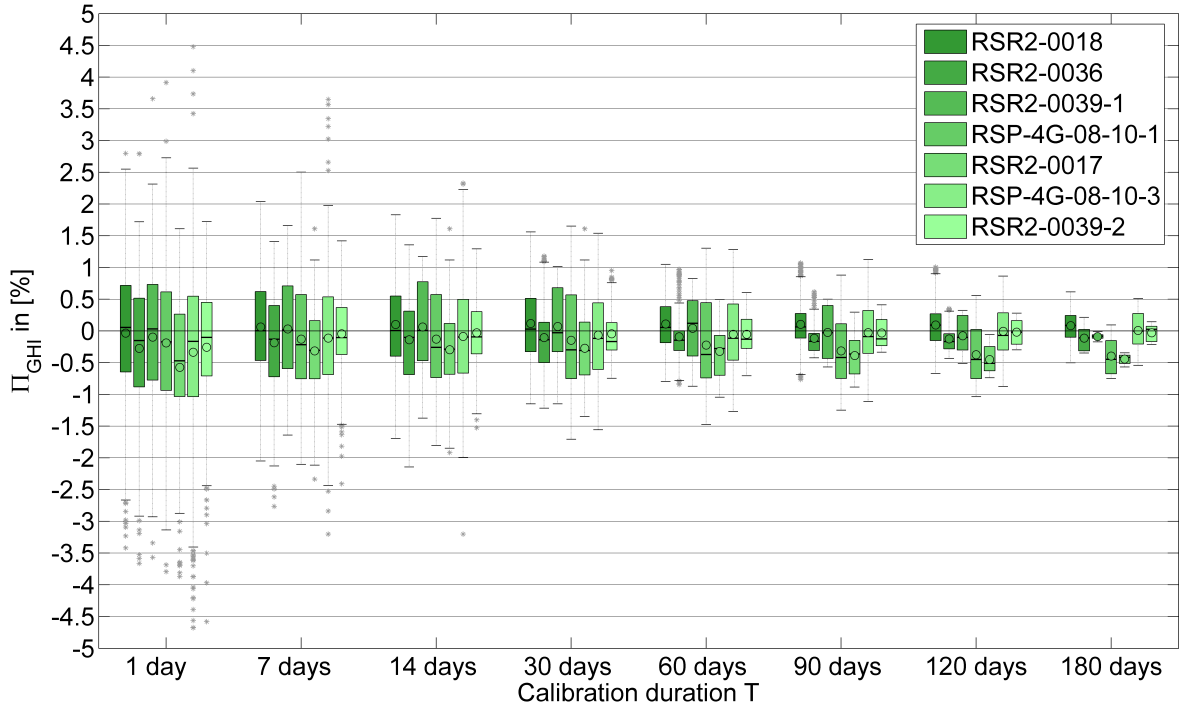

Figure D.2: Π_{GHI} in dependence on calibration duration for seven datasets - DLR-VigKing

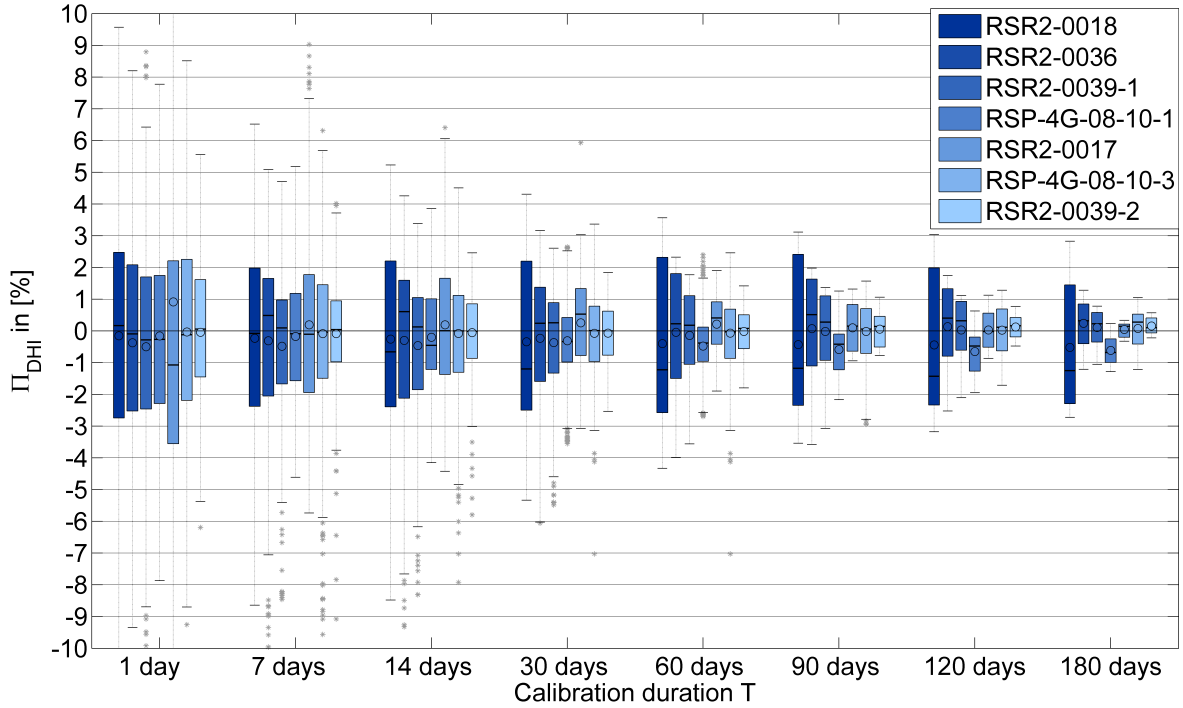

Figure D.3: Π_{DHI} in dependence on calibration duration for seven datasets - DLR-VigKing

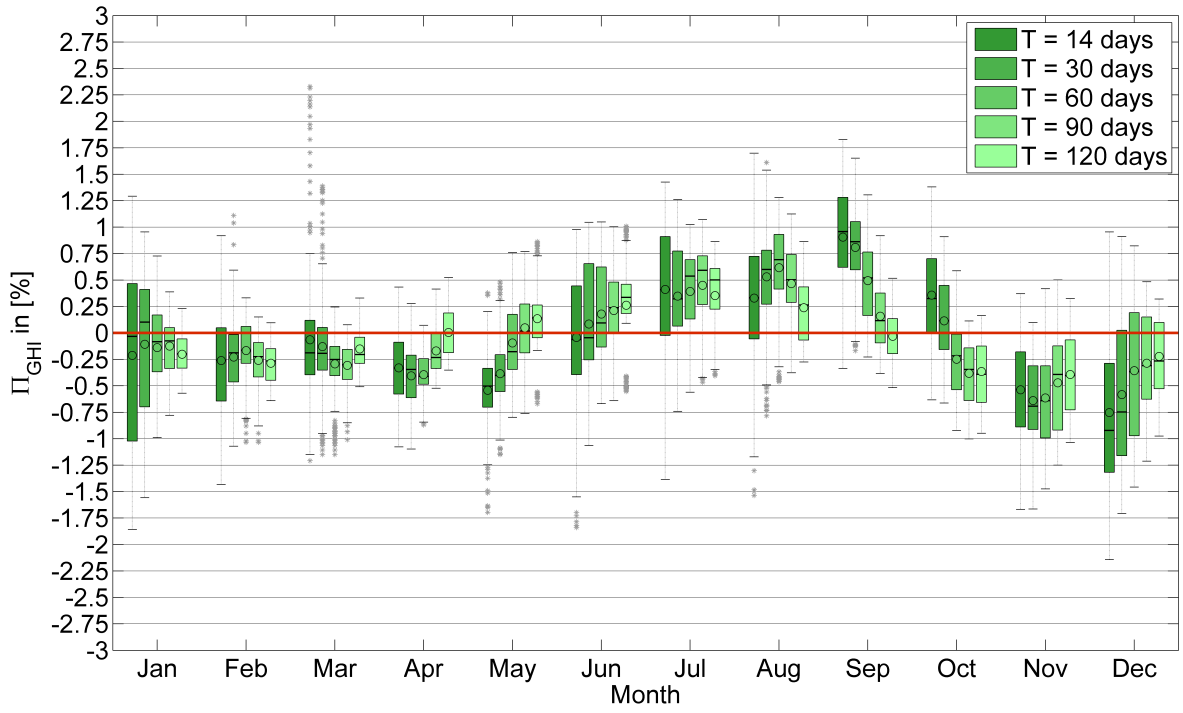

Figure D.4: Π_{GHI} by measurement starting month - DLR-VigKing

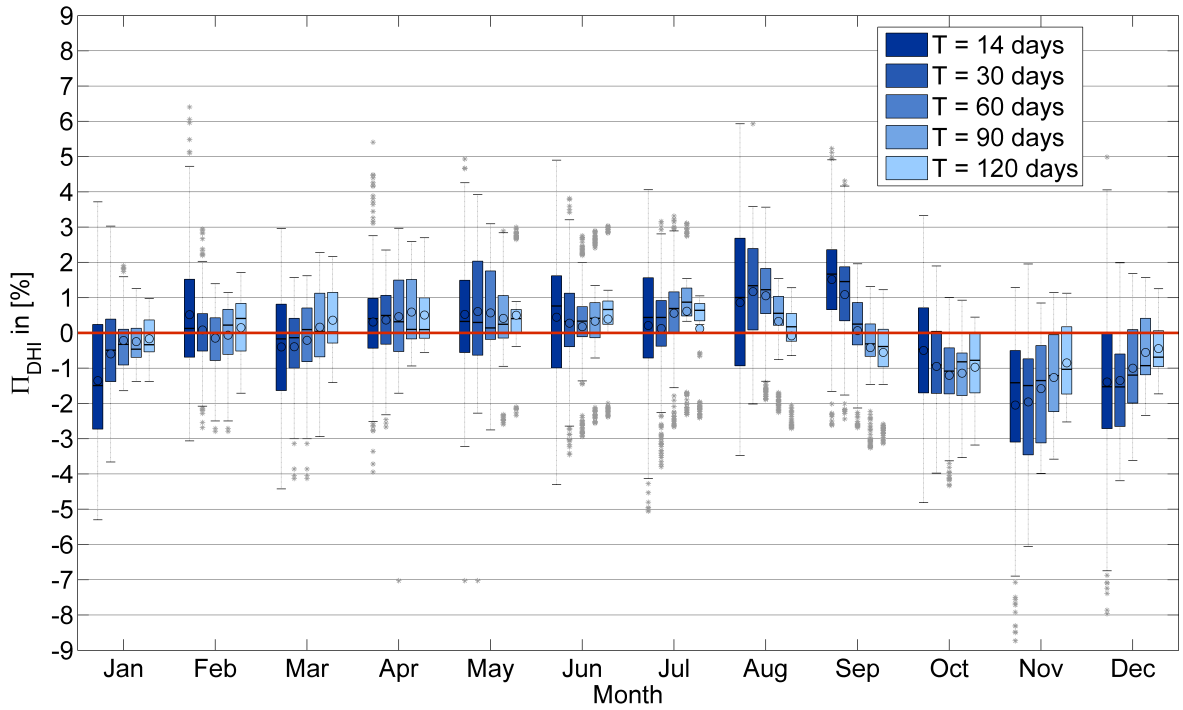

Figure D.5: Π_{DHI} by measurement starting month - DLR-VigKing

E Li-200 Si-pyranometer specifications

LI-200SA PYRANOMETER SENSOR

Total Solar Radiation

The LI-200SA Pyranometer is designed for field measurement of global solar radiation in agricultural, meteorological, and solar energy studies. In clear, unobstructed daylight conditions, the LI-COR pyranometer compares favorably with first class thermopile-type pyranometers (5, 11), but is priced at a fraction of the cost.

Patterned after the work of Kerr, Thurtell and Tanner (7), the LI-200SA features a silicon photovoltaic detector mounted in a fully cosine-corrected miniature head. Current output, which is directly proportional to solar radiation, is calibrated against an Eppley Precision Spectral Pyranometer (PSP) under natural daylight conditions in units of watts per square meter (W m^{-2}). Under most conditions of natural daylight, the error is <5% (7).

The spectral response of the LI-200SA does not include the entire solar spectrum, so it must be used in the same lighting conditions as those under which it was calibrated. ***Therefore, the LI-200SA should only be used to measure unobstructed daylight. It should not be used under vegetation, artificial lights, in a greenhouse, or for reflected solar radiation.***

LI-200SA Specifications

Calibration: Calibrated against an Eppley Precision Spectral Pyranometer (PSP) under natural daylight conditions. Typical error under these conditions is ± 5%.

Sensitivity: Typically 90 µA per 1000 W m^{-2}.

Linearity: Maximum deviation of 1% up to 3000 W m^{-2}.
Stability: < ± 2% change over a 1 year period.
Response Time: 10 µs.
Temperature Dependence: 0.15% per °C maximum.
Cosine Correction: Cosine corrected up to 80° angle of incidence.
Azimuth: < ± 1% error over 360° at 45° elevation.
Tilt: No error induced from orientation.
Operating Temperature: -40 to 65°C.
Relative Humidity: 0 to 100%.
Detector: High stability silicon photovoltaic detector (blue enhanced).
Sensor Housing: Weatherproof anodized aluminum case with acrylic diffuser and stainless steel hardware.
Size: 2.38 Dia. × 2.54 cm H (0.94″ × 1.0″).
Weight: 28 g (1 oz).
Cable Length: 3.0 m (10 ft).

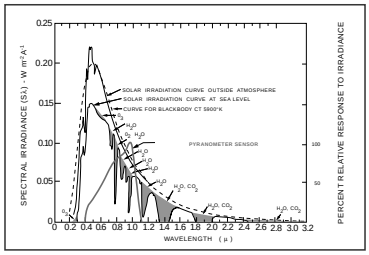

The LI-200SA Pyranometer spectral response is illustrated along with the energy distribution in the solar spectrum (8).

Ordering Information

The LI-200SA Pyranometer Sensor cable terminates with a BNC connector that connects directly to the LI-250A Light Meter or LI-1400 DataLogger. The 2220 Millivolt Adapter should be ordered if the LI-200SA will be used with a strip chart recorder or datalogger that measures millivolts. The 2220 uses a 147 ohm precision resistor to convert the LI-200SA output from microamps to millivolts. The sensor can also be ordered with bare leads (without the connector) designated LI-200SZ. Both are available with 50 foot cables, LI-200SA-50 or LI-200SZ-50. The 2003S Mounting and Leveling Fixture is recommended for each sensor unless other provisions for mounting are made. Other accessories are described on the Accessory Page.

LI-200SA Pyranometer
LI-200SZ Pyranometer
LI-200SA-50 Pyranometer
LI-200SZ-50 Pyranometer
2220 Millivolt Adapter
2003S Mounting and Leveling Fixture
2222SB-50 Extension Cable
2222SB-100 Extension Cable

LI-200SA Pyranometer Sensor

Figure E.1: LI-COR LI-200SA specifications (SA: with BNC connector) [LI-COR, 2011]

Bibliography

J. Augustyn, T. Geer, T. Stoffel, R. Kessler, E. Kern, R. Little, F. Vignola, and B. Boyson. Update of algorithm to correct direct normal irradiance measurements made with a rotating shadowband pyranometer. *Proc. Solar 2004, American Solar Energy Society*, 2004.

R.E. Bird. A simple, solar spectral model for direct-normal and diffuse horizontal irradiance. *Solar Energy, 1984. 32(4): p. 461-471.*, 1984.

N. Geuder, R. Affolter, B. Kraas, and S. Wilbert. Long-term Behavior, Accuracy and Drift of LI-200 Pyranometers as Radiation Sensors in Rotating Shadowband Irradiometers (RSI). *Energy Procedia*, 49:2330–2339, 2014.

N. Geuder, F. Wolfertstetter, S. Wilbert, D. Schueler, R. Affolter, B. Kraas, E. Lüpfert, and B. Espinar. Screening and Flagging of Solar Irradiation and Ancillary Meteorological Data. *Energy Procedia*, 69(0):1989–1998, 2015.

N. Geuder, R. Affolter, O. Goebel, B. Dahleh, M. Al Khawaja, S. Wilbert, B. Pape, and B. Pulvermueller. Validation of Direct Beam Irradiance Measurements From Rotating Shadowband Irradiometers in a Region With Different Atmospheric Conditions. *Journal of Solar Energy Engineering*, 138(5):051007–051007, 2016. none.

Norbert Geuder and Volker Quaschning. Soiling of irradiation sensors and method for soiling correction. *Solar Energy 80, no. 11 (2006): 1402-09*, 2006.

Norbert Geuder, W. Ortmanns, V. Quaschning, F. Trieb, C. Schillings, and R. Meyer. Determination of irradiation data for solar based energy generatiion. *ISES Solar World Congress, 2003 June 14-19, Göteborg, Sweden*, 2003.

Norbert Geuder, B. Pulvermueller, and O. Vorbrugg. Corrections for rotating shadowband pyranometers for solar resource assesment. *Solar Energy + Applications, part of SPIE Optics + Photonics 2008, 10-14 August, San Diego, USA*, 2008.

Norbert Geuder, M. Hanussek, J. Haller, R. Affolter, and S. Wilbert. Comparison of corrections and calibration procedures for rotating shadowband irradiance sensors. *SolarPACES 2011, 20-23 Sept. 2011, Granada, Spain*, 2011.

ISO 9059. *Solar energy - Calibration of field pyrheliometers by comparison to a reference pyrheliometer*. International Organization for Standardization, Geneva, Switzerland, 1990.

ISO 9060. *Solar energy - Specifiction and classification of instruments for measuring hemispherical solar and direct solar irradiation.* International Organization for Standardization, Geneva, Switzerland, 1990.

ISO 9846. *Solar energy - Calibration of a pyranometer using a pyrheliometer.* International Organization for Standardization, Geneva, Switzerland, 1993.

ISO 9847. *Solar energy - Calibration of field pyranometers by comparison to a reference pyranometer.* International Organization for Standardization, Geneva, Switzerland, 1992.

E Kern. Calibration methods for silicon photodiode pyranometers used in rotating shadowband radiometers. *SolarPACES 2010, 21-24. Sep 2010, Perpignan, France*, 2010.

D. L. King and D. R. Myers. Silicone photodiode pyranometers: Operational characteristics, historical experiences and new calibration procedures. *26th IEEE Photovoltaic specialists Conference*, 1997.

D. L. King, W. E. Boyson, B. R. Hansen, and W. I. Bower. Improved accuracy for low-cost solar irradiance sensors. *2nd World Conference and Exhibition on Photovoltaic Solar Energy Conversion Proceedings, 6-10 July 1998, Vienna, Austria*, 1998.

D.L. King, W.E. Boyson, and B.R. Hansen. *Improved accuracy for low-cost solar irradiance sensors.* Dec 1997. doi: 10.2172/661542. URL `http://www.osti.gov/scitech/servlets/purl/661542`.

Kipp&Zonen. *Instruction Manual - CHP 1 Pyrheliometer.* Kipp&Zonen, Delft, Netherlands, 2008.

Kipp&Zonen. *Instruction Manual - CMP series Pyranometer, CMA series Albedometer.* Kipp&Zonen, Delft, Netherlands, 2013.

LI-COR. *LI-COR Terrestrial Radiation Sensors - Instruction Manual.* LI-COR Biosciences, Lincoln, Nebraska, USA, 2005.

LI-COR. *Radiation Measurement Instruments.* LI-COR Biosciences, Lincoln, Nebraska, USA, 2011.

Keith Lovegrove and Wes Stein. *Concentrating Solar Power Technology: Principles, Developments and Applications.* Woodhead Publishing Limited, Cambridge, UK, 2012.

J. J. Michalsky. The astronomical almanac's algorithm for approximate solar positioning (1950-2050). *Solar Energy Vol. 40, No. 3, 227-235*, 1988.

H. Naumann, G. Schröder, and M. Löffler-Mang. *Handbuch Bauelemente der Optik.* Cal Hanser Verlag, München Wien, 2014.

F. Pedrotti, L. Pedritti, W. Bausch, and H. Schmidt. *Optik für Ingenieure - Grundlagen.* Springer, Berlin Heidelberg New York, 2008.

Volker Quaschning. *Regenerative Energiesysteme.* Hanser Verlag München, 2011.

T. Stoffel, D. Renne, D. Myers, S. Wilcox, M. Sengupta, R. George, and C. Turchi. Concentrating solar power - best practices handbook for the collection and use of solar resource data. *Technical Report NREL/TP-550-47465, September 2010*, 2010.

F. Vignola. Removing systematic errors from rotatng shadowband pytanometer data. *Solar 2006, American Solar Energy Society, 7th-13th July 2006, Denver, Colorado, USA*, 2006.

F. Vignola, J. Peterson, S. Wilbert, P. Blanc, N. , and C. Kern. New methodology for adjusting rotating shadowband irradiometer measurements. *AIP Conference Proceedings*, 1850(1):140021, 2017.

Laurent Vuilleumier, Christian Felix, Frank Vignola, Philippe Blanc, Jordi Badosa, Andreas Kazantzidis, and Bertrand Calpini. Performance evaluation of radiation sensors for the solar energy sector. *Meteorologische Zeitschrift*, 2017.

S. Wilbert. *Determination of Circumsolar Radiation and its Effect on Concentrating Solar Power.* PhD thesis, Rheinisch-Westfälische Technische Hochschule Aachen, 2014.

S. Wilbert, N. , M. Schwandt, B. Kraas, W. Jessen, R. Meyer, and B. Nouri. Best practices for solar irradiance measurements with rotating shadowband irradiometers. *Technical Report IEA Task 46, Subtask B1 and INS project 1268, October, 2014*, 2014.

WMO. *Guide to Meteorological Instruments and Methods of Observation. WMO-No. 8, 2010 Update. (Seventh ed.).* World Meteorological Organization, 2010.

WRC. *PMO6-CC Operating Manual.* World Radiation Center, Davos, Switzerland, 2001.

A. T. Young. Air mass and refraction. *Applied Optics Vol.33 No.6*, 1994.